2010-12-15

Chemical Vapor Deposition of Silanes and Patterning on Silicon

Feng Zhang
Brigham Young University - Provo

Chemical Vapor Deposition of Silanes and Patterning on Silicon

Feng Zhang

A dissertation submitted to the faculty of
Brigham Young University
In partial fulfillment of the requirements for the degree of

Doctor of Philosophy

Matthew R. Linford
Milton L. Lee
Matthew C. Asplund
Daniel E. Austin
Robert C. Davis

Department of Chemistry and Biochemistry

Brigham Young University

April 2011

ABSTRACT

Chemical Vapor Deposition of Silanes and Patterning on Silicon

Feng Zhang

Department of Chemistry and Biochemistry

Doctor of Philosophy

Self assembled monolayers (SAMs) are widely used for surface modification. Alkylsilane monolayers are one of the most widely deposited and studied SAMs. My work focuses on the preparation, patterning, and application of alkysilane monolayers.

3-aminopropyltriethoxysilane (APTES) is one of the most popular silanes used to make active surfaces for surface modification. To possibly improve the surface physical properties and increase options for processing this material, I prepared and studied a series of amino silane surfaces on silicon/silicon dioxide from APTES and two other related silanes by chemical vapor deposition (CVD). I also explored CVD of 3-mercaptopropyltrimethoxysilane on silicon and quartz. Several deposition conditions were investigated. Results show that properties of silane monolayers are quite consistent under different conditions.

For monolayer patterning, I developed a new and extremely rapid technique, which we termed laser activation modification of semiconductor surfaces or LAMSS. This method consists of wetting a semiconductor surface with a reactive compound and then firing a highly focused nanosecond pulse of laser light through the transparent liquid onto the surface. The high peak power of the pulse at the surface activates the surface so that it reacts with the liquid with which it is in contact.

I also developed a new application for monolayer patterning. I built a technologically viable platform for producing protein arrays on silicon that appears to meet all requirements for industrial application including automation, low cost, and high throughput. This method used microlens array (MA) patterning with a laser to pattern the surface, which was followed by protein deposition.

Stencil lithography is a good patterning technique compatible with monolayer modification. Here, I added a new patterning method and accordingly present a simple, straightforward procedure for patterning silicon based on plasma oxidation through a stencil mask. We termed this method subsurface oxidation for micropatterning silicon (SOMS).

Keywords: protein arrays, micropatterning, chemical vapor deposition, silane, polyaniline

ACKNOWLEDGEMENTS

I want to express my great gratitude to my advisor, Dr. Matthew R. Linford. His instructions, patience, and encouragement helped me build a deep understanding of chemistry and finish my PhD work smoothly. I appreciate the opportunity to work in his group during the past few years and this experience will be the most valuable memory of my life.

I would also like to give many thanks to my committee members: Dr. Milton L. Lee, Dr. Matthew C. Asplund, Dr. Daniel E. Austin and Dr. Robert C. Davis. They gave me valuable suggestions to help drive my projects forward. I also want to thank all the other members of the BYU faculty who taught and trained me.

I wish to thank all the Linford group members for their collaboration and support: Dr. Li Yang, Dr. Guilin Jiang, Dr. Michael Lee, Lei Pei, Gaurav Sani, *etc*. I thank Diane Colebeck for her warm smile and delicious food.

I would like to thank the Department of Chemistry and Biochemistry at Brigham Young University for the opportunity to study and also those who funded my research.

I also wish to thank my friends in or from other groups in the Chemistry Department: Dr. Weichun Yang, Dr. Renmao Liu, Dr. Quan Shi, Dr. Haibin Ma, Miao Wang, *etc*. Their friendship added unlimited fun and happiness to my time as a PhD candidate.

I would like to give my endless gratitude to my parents and three sisters for their love, support, and selfless contributions to our family.

Last but not least, I want to thank my wife, Mengfei. Her deep love and strong support did and will motivate me to overcome any difficulties. It is my honor to live with her throughout my whole life.

Table of Contents

List of Tables

List of Figures

List of Abbreviations and Symbols

AFM	Atomic force microscopy
AMPSA	2-Acrylamido-2-methyl-1-propanesulfonic acid
APTES	3-Aminopropyltriethoxysilane
APDMES	3-Aminopropyldimethylethoxysilane
APDIPES	3-Aminopropyldiisopropylethoxysilane
CSA	Camphorsulfonic acid
CVD	Chemical vapor deposition
DCA	Dichloroacetic acid
ELISA	Enzyme-linked immunosorbent assays
KOH	Potassium hydroxide
ICRs	Intrinsically conducting polymers
MA	Microlens array
MCR	Multivariate curve resolution
PAH	Poly(allylamine hydrochloride)
PANi	Polyaniline
PBS	Phosphate buffered saline
PDADMAC	Poly(diallyldimethylammonium chloride)
PEG	Polyethylene glycol
PSS	Poly(sodium 4-styrenesulfonate)
SEM	Scanning electron microscopy
SOMS	Subsurface oxidation for micropatterning of silicon
TEM	Transmission electron microscopy

ToF-SIMS	Time-of-flight secondary ion mass spectrometry
XPS	X-ray photoelectron spectroscopy

Å	Angstrom
µ	Micron
M	Molar
ml	Milliliter
nm	Nanometer
θ_a	Advancing contact angle
W	Watt

Chapter 1. Background Information*

Self-assembled monolayers (SAMs) are monomolecular layers spontaneously adsorbed onto surfaces. Alkylsilane monolayers on silicon surfaces are one of the most common SAMs. The reactive group of alkylsilanes is often a SiCl, $SiCl_2$, $SiCl_3$, $SiOCH_3$, $Si(OCH_3)_2$, $Si(OCH_3)_3$, $SiOCH_2CH_3$, $Si(OCH_2CH_3)_2$, or $Si(OCH_2CH_3)_3$ moiety, which is used to attach silanes to oxide surfaces. In particular, alkylsilane monolayers are of great importance for the modification of silicon oxide. Strong covalent bonds between the monolayer and the silicon surface provide a solid platform for subsequent surface modification. Diverse chemical groups on monolayer surfaces available from the precursor silanes offer many choices for further chemical reaction and attachment. For example, amino- and epoxy-terminated monolayers can effectively bind DNA, proteins, and even cells, and, accordingly, these monolayers have been applied widely in biosensors.[1-3] Mercapto groups can function as adhesion promoters for gold mirrors.[4] Fluorosilane monolayers yield good hydrophobic and even oleophobic films.[5] Combined with some sort of silicon patterning technique, alkylsilane monolayers are used rather widely in optics and materials science.[6-8]

Laser pattering and stencil lithography are patterning techniques compatible with alkylsilane monolayer preparation and modification. These techniques are clean, low cost, and fast, which helps retain the integrity of silane monolayers after patterning. The combination of these patterning techniques with functional silane monolayers produces desirable surface modifications for a variety of applications.

---

* Some parts of this chapter were taken from the introductory sections of Chapters 2-7 of this dissertation.

1.1. Alkylsilane monolayers

1.1.1 Synthesis of alkylsilanes

There are several methods for synthesizing silanes. For example, tetrachlorosilane reacts with Grignard reagents as follows:[9]

$$CH_3(CH_2)_{11}MgBr \xrightarrow{SiCl_4,\ benzene} CH_3(CH_2)_{11}SiCl_3$$

Another method is the hydrosilylation of an alkene with $HSiCl_3$ in the present of a platinum catalyst:[10]

$$RCH=CH_2 + HSiCl_3 \xrightarrow{Pt\ cat.,\ e.g.,\ H_2PtCl_6} RCH_2 - CH_2SiCl_3$$

After hydrosilylation, trichlorosilanes can be transformed into trimethoxysilanes or triethoxysilanes as follows:

$$RSiCl_3 + 3R'OH \rightarrow RSi(OR')_3 + 3HCl$$

This reaction can be reversed as follows:[11]

$$RSi(OR')_3 + 3HCl\ (concentrated) \rightarrow RSiCl_3 + 3R'OH$$

Triethoxysilanes or trimethoxysilanes can also be synthesized using an alumina catalyst and an alcohol at 700 K:[12]

$$RSiH_3 + 3R'OH \xrightarrow{alumina\ catalyst,\ e.g.,\ KF/Al_2O_3} RSi(OR)_3$$

1.1.2 Alkylsilane monolayer formation

There are many papers that report and describe the attachment process between the reactive groups of alkylsilanes and oxide surfaces. Sagiv and coworkers were pioneers in this regard.[13-15] They concluded that after hydrolysis, octadecyltrichlorosilane (OTS) initially interacts with the surface through hydrogen bonds. Then, after a condensation process, OTS binds to the surface to form a polymerized network. Since their initial work, the formation of

silane monolayers has been widely explored, where one universal opinion seems to be that a water film is necessary on the surface for monolayers to form. In the case of a trichlorosilane precursor, the three chlorine groups are first hydrolyzed and become silanol groups. After that, the silanol groups react with –OH groups on the surface to produce Si-O-Si linkages. The remaining silanol groups in the film react with each other to form a cross-linked network. The integrity of this network mainly depends on the concentration of water on the substrate and in the solvent, the solvent used to prepare the film, and the reaction temperature. Angst and Simmons systematically compared the OTS monolayer with the dimethyloctadecylchlorosilane (DMODCS) monolayer.[16] They found that neither silanes can form monolayers on dry SiO_2 surfaces, but that both form good monolayers on hydrated surfaces. OTS forms well ordered monolayers because of its $–SiCl_3$ moieties, but the steric hindrance of the methyl groups of DMODCS affect the order of the monolayer. They also found that water adsorption into OTS monolayers is significant after film formation, even for very closed packed OTS monolayers, but small for DMODCS monolayers. However, after high temperature curing, water adsorption into the OTS monolayer decreased substantially. Therefore, they concluded that after curing, unreacted silanol groups react with each other and decrease the number of free silanols. Through IR, Allara et al. also demonstrated that some level of hydration of a surface is necessary for quality (desnsely packed and well ordered) monolayers to form.[17] They too could not get OTS monolayers to grow on dry surfaces. Using Raman spectroscopy, Wunder illustrated that the order and quality of OTS monolayers increased with increasing hydration of the substrates.[18] Kato studied the transition temperature for monolayer growth.[19] Below 20ºC, OTS forms a well-ordered monolayer from hexane solution, but above this temperature, the monolayer is disordered and has a low density. Grange found that dehydrated surfaces can be easily rehydrated with atmospheric water at room

temperature to form well ordered OTS monolayers.[20] They also found that a completely hydrolyzed surface is not necessary for full coverage of the monolayer and estimated that only about 20% percent of the silanol groups in the monolayers bind to the surfaces. Silberzan et al. confirmed Grange's work by illustrating that the surface becomes much smoother after OTS monolayer deposition on very rough silica surfaces. That is, if each silane molecule in the monolayer bonded to the surface, the morphology of the surface would not change much.[21] They also studied the effect of water content and temperature on monolayer formation. They found that trace water is necessary to form high quality films, but too much water will cause the silanes to polymerize and form aggregates on the surface. They found the best conditions for OTS deposition out of hexadecane and CCl_4 to be 2 min and below 18ºC, i.e., high reaction temperature and long times did not lead to high quality monolayers. Silvia et al. discussed solvent effects in OTS monolayer formation.[22] They found that from hexane solution, the surface is not fully covered with the OTS network. Smirnov et al. suggested a two step monolayer deposition process to get closer packed monolayers of trimethoxysilane.[23] The silane was introduced onto hydrated surfaces first. Then, a little water was introduced to hydrolyze the methoxy groups on the silanes. After that, more silane was introduced and additional condensation took place.

Although the solution-phase deposition of silanes is the most widely studied method, this approach is neither environmentally friendly nor is it typically industrially viable because it generates significant amounts of solvent waste. In addition, it is often irreproducible and/or produces poor quality films. In many cases, self-polymerization of silanes in solution, which is difficult to control, remains a major obstacle for production of clean homogeneous silane films.[24] In most cases, silane films prepared from solution show irregularities in their morphologies,

which limits the effectiveness of the films' potential technological applications. Compared to solution phase deposition, vapor phase deposition provides more uniform monolayers and uses lower quantities of reagents.[25-26] Moreover, the vapor phase approach provides for control of the amount of moisture in the deposition chamber, which limits or eliminates self polymerization (or dimerization) of the silane.[18] Lab scale vapor phase deposition may take place in a desiccator. For example, samples may be cleaned first with piranha solution and then put in a descicator and exposed to the vapor of a silane.[27-28] However, it is often time consuming to let silanes evaporate by themselves. Vacuum and or elevated temperature may effectively shorten deposition times and provide better film quality.

1.1.3. Stability of alkylsilane monlayers

Wang et al. investigated the stability of several alkylsilane monolayers.[29] Their results showed that the alkyl chains of amino sliane monolayers play an important role. For example, the short alkyl chains of aminopropylsilane monolayers provide little stability to the monolayer. Indeed, 92% of an aminopropyltrimethoxysilane (APTMS) monolayer decomposed in saline solution (0.9% NaCl in DI water) after 10 days at 37ºC. However, a longer alkyl chain amino silane made from aminounidecyltrimethoxysilane was almost unchanged under the same conditions. For an alkylsilane monolayer without any active end group, both a short chain silane (propyltrimethoxysilane) and OTS showed good stability. Only 5% of these silane monolayers were lost in the saline solution. Although glycidoxypropyltrimethoxy silane has the same alkyl chain as APTMS, it shows better stability, where 77% of the monolayer was retained after 10 days in saline solution. Sugimura and coworkers explored the stability of n-octadecyltrimethoxysilane (ODS) monolayers under vacuum ultraviolet (VUV) light of 172

nm.[30-31] They found that under atmospheric conditions, after a 100 s exposure to the VUV light, the ODS monolayer contained carboxyl groups. 200 s later, the surface was completely hydrophilic, indicating complete removal of the ODS monolayer. They also compared the etching rate of VUV on the monolayer under different pressures. They found that the rate of etching increased with an increase in pressure. At low pressure (< 0.1 atm), they did not observe signals from carboxyl groups during monolayer degradation. Kato systematically researched the stability of several silane monolayers including OTS, dichloro(methyl)(octadecyl)silane (DCMOS), and chloro(dimethyl)(octadecyl)silane (CDMOS).[32] They found that OTS monolayers retain 50% of their integrity after 15 min at 200ºC, while CDMOS monolayers were completely destroyed at 140ºC. OTS also showed good stability for 8 days in ethanol, benzene, chloroform, hexane, and in pH 1 aqueous sulfuric acid, but it was etched slowly by pH 13 aqueous KOH solutions. DCMOS and CDMOS were unstable in these organic solvents or aqueous solutions and were etched very quickly in KOH solutions. OTS also had a lower coefficient of friction than DCMOS or CDMOS. They concluded in their study that the number of reactive groups on the silanes determined the strength of covalent binding to the surfaces. Chandekar found that 4-aminobutyltriethoxysilane (ABTES) is not stable at 250ºC, but perfluorodecyltriethoxysilane (PFDS) is stable up to 350ºC.[33] Kim demonstrated that plasma treatment of the substrate prior to monolayer formation can substantially improve the stability of OTS monolayers.[34]

1.1.4. Common alkylsilane monolayers

Amino terminated silane monolayers have been widely used for biological applications, including biosensors with attached biomolecules. The compound 3-aminopropyltriethoxysilane

(APTES) is one of the most frequently used of such silanes. Among the applications of APTES and similar amino silanes are 1) to serve as the foundation layer in biosensors and bioarrays,[35-38] 2) to increase adhesion in fiberglass-epoxy composites on silica surfaces,[39-41] 3) to suppress polymer film dewetting,[38] 4) to produce arrays of metal nanoparticles on silica substrates,[42] 5) to help probe protein and cell adhesion.[43-46] Tana used 3-aminopropyltriethoxysilane (APTES) to fabricate electrodes for the diagnosis of dengue infection.[47] Ramrus investigated the adhesion effects of APTES and OTS between poly(vinyl butyral) (PVB) and glass.[48] APTES led to good adhesion, while OTS showed insignificant improvements. A mixed monolayer of APTES and OTS could be used to adjust the adhesion strength. Suemori successfully assembled antenna core complexes onto APTES modified ITO electrodes.[49] Rahman patterned APTES lines for DNA attachment to make biosensors.[50] Mercaptosilanes have been widely used for metal attachment/binding because of the strong interaction between sulfhydryl groups and metals. Perona packed gold nano particles onto quartz surfaces modified with 3-mercaptopropyltrimethoxysilane (MCPTMS) monolayers and used this gold particle film to enhance the signals from surface-enhanced Raman measurements.[51] Liu deposited copper by CVD onto an MCPTMS pattern prepared by UV irradiation of an MCPTMS monolayer.[52] Yuan modified surfaces of gold nanoparticles with double layers of MCPTMS to make biosensors for DNA detection.[53] Epoxysilane monolayers have also been used in biosensors for the attachment of biomolecules.[54-56] Poly(ethylene glycol) silane monolayers have been widely used for resistance of biomolecules, more particularly proteins.[57-60]

1.2. Patterning techniques

There are many patterning techniques compatible with alkylsilane monolayer formation including microcontact printing[61-62] and photolithography.[63-64] However, these techniques have some limitations, including the chemicals or temperatures used in the methods, contamination issues, need for expensive instrumentation, etc. Because of their cleanness, laser patterning and stencil lithography are promising techniques for maintaining monolayer integrity after patterning. They are also low cost patterning techniques.

1.2.1 Laser direct writing

Laser direct writing uses a laser to deposit organic monolayers,[65-66] metals,[67-68] polymers,[69-70] or biomaterials[71-72] without a mask or lithographic methods. This technique was first used at the Lawrence Livermore National Laboratory and the AT&T Bell Laboratories to fabricate micro-electronic circuits. Currently, this technique is widely applied in materials modification and bioengineering.

Meunier and coworkers used an Ar ion laser beam (488 nm) to deposit a series of metals or metal compounds.[73] They focused the laser on a 2 μm spot, and WF_6/H_2 and WF/SiH_4 were used as the precursor gas mixtures to deposit lines of pure tungsten and WSi_x on silicon, TiN, and polyimide surfaces. They used a KrF excimer laser and a precursor gas mixture of WF_6, H_2, and Ar to deposit smooth and uniform W films of high purity on GaAs substrates. With the KrF excimer laser, they deposited copper on TiN and fluoropolymer substrates with a gaseous precursor of copper (hexafluoroacetylacetonate trimethylvinylsilane) [Cu(hfac)(TMVS)]. Carbon nanotubes can also be deposited with gaseous precursors under laser assistance. Jeonga et al.

deposited single-walled carbon nanotubes (SWCNTS) with a Nd:YVO_4 laser (532nm).[74] They used a gaseous mixture of ethylene and hydrogen as precursors. The diameter of the SWCNTS spots ranged from 0.8 to 2 nm.

Maruo mixed a silver nitrate solution into polyvinylpyrrolidone (PVP) and made PVP films containing silver ions.[75] Light from a Ti:sapphire laser (752 nm) was focused into this PVP film. Accordingly, they obtained different three dimensional silver shapes by controlling the exposure time of the film to the laser and the movement of the samples. Wee et al. used a two-electrode system to deposit copper onto stainless steel.[76] In this simple system, a stainless steel cathode, a copper anode, and a $CuSO_4$ electrolyte solution were used. A Nd:YO_4 laser was focused onto the stainless steel cathode. Upon illumination, $CuSO_4$ was reduced to copper and formed 400-600 μm copper lines, where the line width varied with laser exposure time. Kordas deposited copper lines on polyimide surfaces from a solution containing $CuSO_4$, KNa-tartarate, NaOH and HCOH, by exposure of an Ar ion laser (488 nm).[77] Li used a Ti:Sapphire laser and a solution of zinc nitrate and hexamethyltetramine to prepare flower-like nanostructures of ZnO.[78]

Lasers can also be used to transfer small droplets, including from biomolecule-containing solutions, onto substrates to make patterns. This method is called laser induced forward transfer (LIFT). In this method, a solution forms a thin film at the bottom of a transparent substrate that has been precoated with a material such as titanium to absorb laser energy. Upon laser exposure, a tiny droplet of solution is ejected from the bottom surface of the substrate to a parallel receptor substrate 100 μm beneath the liquid film. Serra et al. patterned a protein array with LIFT.[79] They used a Nd: YAG laser beam (355 nm) to burn a 40 μm hole in the Ti film and obtained a protein array with 80 μm diameter spots on nylon coated slides. They also patterned antibody IgG arrays

using this method.[80] Colina similarly patterned a DNA array.[81] Kafetzopoulos patterned enzyme spots with *ca.* 10 µm diameter KrF laser.[82]

Laser direct patterning has also been used to pattern monolayers. Hartmann made an OTS monolayer and then patterned the monolayer by laser ablation.[83] Gong modified silicon substrates by laser irradiation to remove silanol groups.[84]

1.2.2 Microlens array patterning

Laser direct writing can only pattern one spot at a time. With microlens arrays (MLA), a laser can pattern thousands of spots at the same time. An MLA consists of thousands of miniaturized lenses on the same optical element. These lenses are usually spherical or cylindrical, where the spherical lenses are typically in a hexagonal or square pattern. Compared with regular, single lenses, an MLA can focus a series of parallel light spots on a surface.

Hong et al. used a Ti:Sapphire laser (400 nm) and an MLA made of quartz to pattern a silicon substrate.[85] Their MLA was hexagonally packed, and the diameter of each microlens was 23 µm. The output of their process was a 401×401 spot/cm^2 array, where their laser created small holes in the silicon surfaces. (A laser shot of 12.6 mJ/cm^2 created 72 nm deep holes with diameters of approximately 635 nm. A laser shot of 4.1 mJ/cm^2 made 40 nm deep holes that were 340 nm wide.) Kato fabricated an MLA by reactive ion etching and a photoresist reflow technique.[86] The diameters of their spherical microlenses were 200 µm, which were squarely packed with a pitch of 250 µm. The total size of their MLA was 1 cm × 1 cm. A Ti:sapphire laser was used with this MLA, which yielded 200 nm polymerized spots in a resin on glass substrates.

Microlens arrays are typically made of glass, fused silica, or even plastic. Tsai fabricated microlens arrays with a photosensitive glass by laser direct writing and wet etching to make both

cylindrical and spherical MLAs.[87] A thermal reflow process is also widely used to make glass microlens arrays.[88] A glassy carbon mold is fabricated with photolithography and RIE etching. With this mold, and after thermal reflow, spherical lens can be made on glass. Polymers including PDMS and PMMA can also be used to make microlens arrays.[89-90] In addition to photolithography,[91] ink-jet printing can be used to make polymer microlens arrays.[92]

1.2.3 Stencil lithography

Grey and Weimer invented stencil lithography in 1959.[93] Stencil lithography transfers patterns from stencil masks to create patterns on substrates by selectively masking regions of a substrate. Various materials are used as stencil masks including silicon,[94] silicon nitride,[95] and polymers.[96-97]

The process of stencil lithography is simple. As Figure 1.1 shows, a stencil mask is placed on top of a substrate, and particles, e.g., ions, from a source pass through the stencil mask leading to deposition or etching of substrates. Depending on the source, stencil lithography can be used for deposition, etching, or ion implantation. In the case of deposition, physical vapor deposition is the main method compatible with stencil lithography and includes e-beam deposition, thermal evaporation, and sputtering.[98] Because stencil masks can be made from flexible polymers, stencil lithography can be used to deposit materials on flexible substrates. Silicon and boron can be implanted through stencil masks.[99-102] Different materials can be plasma etched by stencil lithography including polymers and silicon.[103-104] Villanueva used silicon stencil masks coated with silicon nitride for plasma etching to pattern different substrates including silicon, silicon dioxide, and polyimide.[105-106] Viallet used silicon nitride membranes as a mask and an oxygen plasma to make patterns on silicon substrates for wet etching.[105]

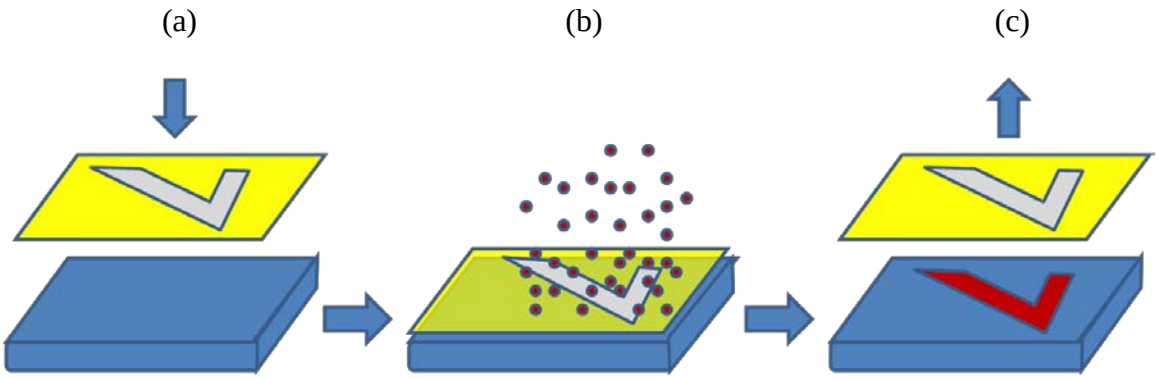

Figure 1.1. Process of stencil lithography. (a) Stencil mask is aligned on a substrate; (b) deposition, etching, or implantation; and (c) stencil mask is lifted off, leaving a patterned substrate.

There are two modes for stencil lithography: static and dynamic.[107-108] In the static mode, the positions of the stencil mask and substrate are fixed after alignment of the stencil mask on top of the substrate. In the dynamic mode, the stencil mask or the substrate can be moved. By controlling the direction and speed of the mask and/or substrate, different patterns, depositions or etching densities can be obtained.

Stencil lithography is a clean and simple technique. However, it faces two major challenges. First, any deposition also occurs on the stencil mask and may ultimately clog the apertures or damage the mask. Another problem is diffusion, referred to as blurring. Because of the distance between the mask and substrate, ions will diffuse in this space so that the pattern width on the substrate will be larger than the stencil mask pattern. Proper cleaning can remove the materials deposited on a stencil mask to recover the original pattern. Va'zquez-Mena et al. washed their silicon nitride mask with an aluminum wet etching solution [CH_3COOH (100%), HNO_3 (70%) and H_3PO_4 (85%) in proportions of 5:3:75] to remove aluminum deposited on the mask.[109]

1.3. Analytical techniques

For the surface modification of silicon, surface analytical tools are crucial for obtaining accurate information regarding a desired modification. Currently, there are a number of important surface analytical methods including X-ray photoelectron spectrometry (XPS), time of flight secondary ions mass spectrometry (ToF-SIMS), and atomic force microscopy (AFM). I used these three techniques extensively in my research.

1.3.1. XPS

XPS is also called electron spectroscopy for chemical analysis (ESCA). Since it was invented in the mid 1960s by Siegbahn, XPS has been widely applied for analysis of many materials including metals,[110-111] polymers,[112-113] semiconductors,[114] and ceramics.[115-116]

As Figure 1.2 (a) shows, atoms at surfaces absorb the energy of X-rays and release photoelectrons. The kinetic energies of these photoelectrons are measured with an electron analyzer. The fundamental equation of XPS is:

$$BE = h\nu - KE - \omega \quad (1.1)$$

where BE is the Binding energy, $h\nu$ is the energy of the incident X-ray, KE is the kinetic energy, and ω is the work function of the spectrometer, which is the difference between the vacuum level and the Fermi level. The value of $h\nu$ is known from the X-ray source, and KE is measured at the analyzer.

The vacuum level is the energy level of free electrons. The Fermi level of a conducting sample will align with that of the instrument. Binding energies of photoelectrons are calculated using the fundamental equation of XPS, which are generally unique to specific atoms. Therefore, the surface chemical components can be deduced. For example, a binding energy at *ca.* 285 eV corresponds to the C1s orbital. Because XPS signals are related to many parameters, including sensitivity factors of elements, chemical states of atom, transition efficiencies (probabilities that electrons absorb the energies of incident X-rays), and the instruments themselves, XPS cannot provide absolute quantitative information. XPS is a quasi-quantitative method and can provide relative amounts of elements in the form of percentages. Nevertheless, in spite of these limitations, it remains one of the most important surface analytical techniques in existence.

(a)

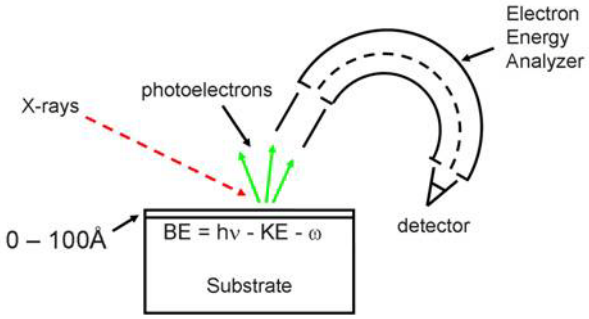

(b)

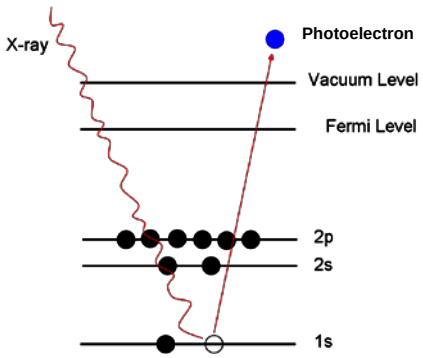

(c)

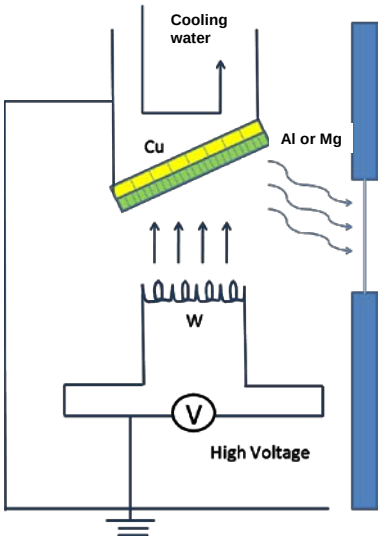

Figure 1.2. XPS instrument structure and principles. (a) XPS instrument, (b) removal of a core electron from an element, and (c) structure of an X-ray source.

Because the binding energies of core electrons of an element are related to the chemical states of atoms, shifts in binding energy can be used to measure the chemical (oxidation) states of atoms. These changes are called chemical shifts. For example, silicon bonded only to silicon, e.g., in a silicon wafer, has a binding energy of 99 eV for its 2p electrons. For silicon in silicon dioxide, the binding energy of an Si2p electron is 102.3 eV. Clearly, oxidation of an element increases binding energy. Negative charge (additional electron density) will cause the binding energy to decrease.

Because electrons are unable to travel very far in solids without losing energy, the depth XPS can probe into a sample is only *ca.* 10 nm. In other words, 3 nm is a typical mean free path of photoelectrons at the kinetic energies of electrons encountered in XPS. Their means free paths are about 10 nm in solids. Angle-resolved XPS for depth profiling can be used to measure the distribution of different chemical components in this upper 10 nm.[117-118] In this process, the sample is first measured with high incident angle of the X-rays. This XPS spectrum contains chemical component information of the deepest parts of the layer. Then, the sample is tilted to obtain a lower incidence angle of X-rays. The spectrum contains more information about the chemical components of the elements nearer the surface. Comparing a series of spectra obtained in this way, chemical information at different depths into the samples can be obtained. Another way to obtain information about buried layers in a material is through destructive profiling.[119-120] Ar^+ may be used to sputter the sample to remove surface layers. XPS data can then be taken after each sputtering cycle. This method can be used to measure chemical changes in surfaces by comparing surface spectra to bulk spectra. Small spot XPS has developed considerably in the last few decades.[121-122] This technique can be used to scan surfaces and provide images/maps of

elements/oxidation states. Of course, imaging might be combined with depth profiling, although the resulting scans might be very long.

Usually, XPS uses an X-ray tube as an X-ray source. As Figure 1.2 (c) shows, a high voltage is applied to a filament, such as tungsten. Electrons from the filament cross a gap between the filament and a target, usually aluminum or magnesium. Core electrons from target atoms are ejected and X-rays are released when other electrons drop into the holes created by ejection of the first electrons. There are two universal X-ray sources: Mg Kα(1254eV) and Al Kα(1487eV), with Al Kα being the more common.

XPS cannot detect hydrogen or helium. First, hydrogen has a binding energy of 13.6 eV for its 1s electron; helium has a 1s electron binding energy of 24.6 eV. The noise in this area of the spectrum is high because of instrumental noise, free electrons in the chamber, and small overlapping valence band peaks of different elements. Therefore, it is hard to pick out the hydrogen and helium signals. Second, because the binding energies of hydrogen and helium are very far from the X-ray energy (1245 or 1487 eV), the cross section, the probability that these electrons absorb X-ray energy, is very low. Therefore, the signal of photoelectrons of hydrogen and helium is also very low. For both of these reasons, hydrogen and helium cannot be detected with XPS.

1.3.2. ToF-SIMS

ToF-SIMS is a very sensitive surface characterization method, and Honig, Liebl and Slodzian did pioneering work in this area.[123-125] After fifty years of development, ToF-SIMS has become widely applied for the surface analysis of diverse materials including semiconductors, metals, polymers, and biological samples.

As Figure 1.3 (a) shows, primary ions with high energy, e.g., 25 eV, bombard surfaces, which are destroyed/damaged at the point of ion impact and release secondary particles including ions, electrons and neutrals. Ions are only a small fraction of these secondary particles. These ions are detected using ToF mass spectrometry. Because these ions may be molecular fragments, ToF-SIMS can provide important structural information about surfaces.

There are three basic ionization sources. Electron impact ion sources are used for gases, including Ar, Xe, O_2, SF_6, and C_{60}. Gas molecules are struck by energetic electrons and yield ions, which are extracted by an electrical field. This ion source is easy to operate and maintain. The nature of the ion can be easily changed, simply by changing the gas. The duoplasmatron ion source is suitable for oxygen, where the oxygen gas is ionized in a plasma and ions are extracted by an electrical field. This ion source can also be used for other gases, but oxygen ions typically show the best ionization efficiencies. Both negative and positive oxygen ions can be extracted. Surface ionization ion sources gently heat a metal or alloy and extract positive ions with a high electrical field. The common metals for this type of source are gallium and indium. Both are low melting point metals. As Figure 1.3 (b) shows, the metal is heated to melting so that it can wet a tungsten needle. Under high electrical fields (5-25 kV), the positive ions are extracted. Gallium is the most common liquid metal for this ion source because of its very low melting point 29.8ºC.

Quadrupole detectors were first used in SIMS. However, the low throughput (*ca.* 1%) created problems for surface analysis because, in general, only small amounts of material are initially present at the surface. Quadrupoles are also unable to detect fragments with high masses. ToF analyzers overcome these drawbacks and can detect both low mass fragments and high mass fragments, which is important in analysis of organic materials. The ToF detector has been the major detector for SIMS.

(a)

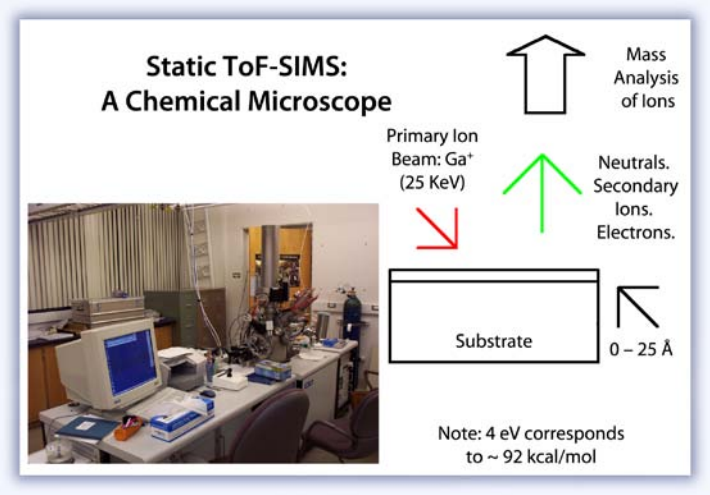

(b)

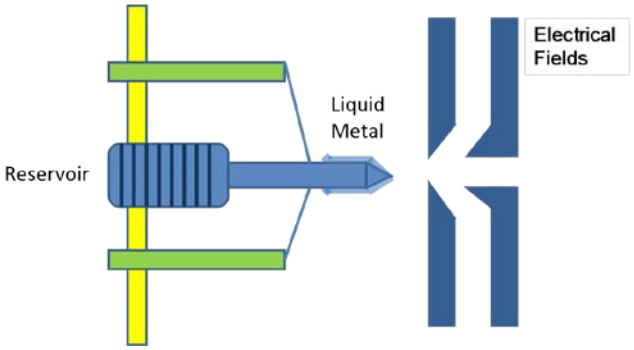

Figure 1.3. (a) SIMS instrument and schematic, (b) liquid metal primary ion source.

There are two modes for ToF-SIMS: static and dynamic.[126-128] The static mode employs a low primary ion dose of about 10^{12} atoms/cm^2. Therefore, the static mode usually shows negligible contributions from damaged surface areas (places that have been hit twice by primary ions). This mode only senses the upper *ca.* 2.5 nm of surfaces. The dynamic mode employs ion bombardment, or sputtering, to gradually remove surface layers. Therefore, deeper regions in a sample can be probed. Thus, ToF-SIMS can provide multiple levels of surface information including surface spectra, spectra from depth profiling, surface imaging, and three dimensional analysis or profiles built from surface spectra and depth profiling.

1.3.3. AFM

Binning et al. invented AFM in 1986.[129] AFM maps the morphology of surfaces by rastering the surface with a tip.[130] Because AFM only measures atomic forces, and does not rely on conductivity, nonconductive samples can be probed. Using proper instrumental conditions, AFM can measure very soft surfaces, and the tip can operate in vacuum, ambient, or liquid environments.[131-132] Because of its ability to measure soft surfaces, AFM has been widely applied to biological samples.[133] Because of its high resolution and possibility of low forces on surfaces, under proper conditions AFM has also been widely used to study the morphology and patterning of monolayers.[134-135]

The AFM tip is about 3-15 μm tall with an end radius of 10-50 nm. Tips are usually made from silicon or silicon nitride. The atomic force between the tip and surface can be calculated from the deflection of the cantilever and spring constant of the tip:[136]

$$F = S_{tip} \times Z_{deflection} \quad (1.2)$$

where F is the force, S_{tip} is the spring constant of the tip, and $Z_{deflection}$ is the deflection of the cantilever.

As Figure 1.4 shows, when the tip scans the surface, a diode laser on the top of the cantilever reflects the movement and deflection of the cantilever to a detector. Using this information, the instrument can then map the surface morphology. Piezoelectric scanners in a feedback loop adjust the position of the tip to keep it in contact with the surface. This adjustment is also used to determine the morphology of the surface.

There are two common AFM modes: contact mode and tapping mode.[137-138] Contact mode operates by scanning the tip across the surface.[139] A low force (about 10^{-9} N) is maintained between the tip and the surface. The instrument determines the surface morphology according the atomic force and cantilever deflection. The resolution of AFM in contact mode is very high: down to 0.1 nm. However, contact mode has some drawbacks. Because the tip is consistently in contact with the surface, it may damage soft surfaces, and even silicon.[130, 140-141] The tip can also move small particles on samples, and may generate inaccurate surface information. Another AFM mode, tapping mode solves many of these problems.[142-143] In tapping mode, the tip oscillates above a surface. Therefore, the tip only contacts surfaces for a very short time. This limits lateral force damage to soft surfaces and avoids moving small particles. Tapping mode is widely used to measure biological and liquid samples.

Although AFM has advantages for probing insulators and biological samples, AFM also has its disadvantages. Because of size limitations, the tip may not be able to make contact with every feature on the surface. Another issue is tip-sample convolution. Therefore AFM images do not always reflect the real morphology of the surfaces. In addition, images are typically convolutions of the shape of surface features with the shape of the tip. Tip modification with

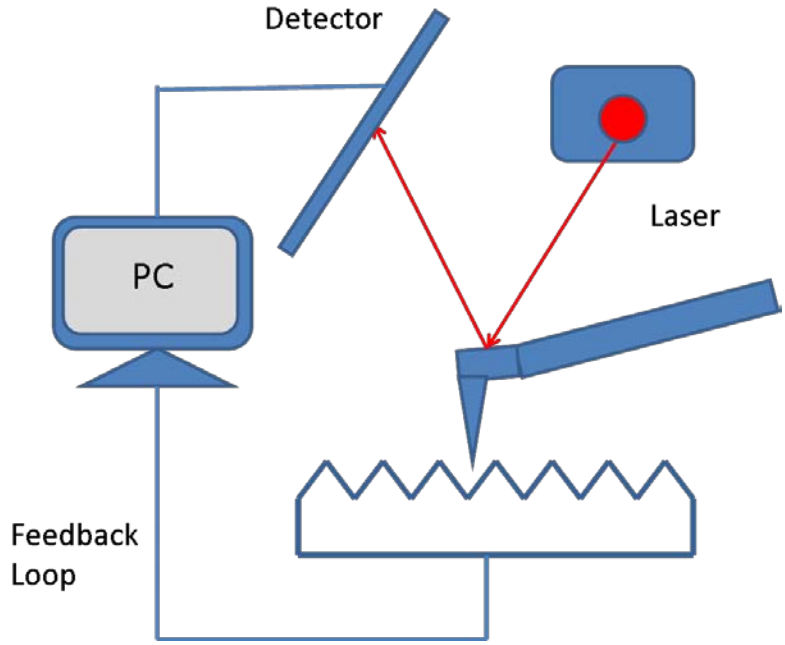

Figure 1.4. Atomic force microscopy (AFM).

carbon nanotubes to produce extremely sharp tips has been researched to help overcome these disadvantages but this type of tip has not been commercialized.[144]

1.3.4. Other surface analytical techniques

Spectroscopic ellipsometry is a sensitive optical technique used to measure film thicknesses. One of its most important advantages is that it is a non-contact method that does not damage surfaces. Thickness measurements are achieved by measuring differences between incident and reflected light. In a simple embodiment of ellipsometry, the light from a source is first polarized by an analyzer, which can be resolved into its components p and s. Then, the light, which contains both p and s components, is reflected off a surface into a detector. Differences between the p and s components of the incident and reflected light can then be used to calculate the amplitude ratio and phase shift, which yield the film thickness and optical constants. The measurement process simply utilizes the difference between incident and reflected light so that spectroscopic ellipsometry is insensitive to the beam intensity and measurement conditions.

Contact angle goniometry is a method for measuring the contact angles of probe liquids on surfaces to probe surface hydrophobicity, i.e., surface energies. A droplet of water or another liquid, such as an alkane, e.g., hexadecane, is placed on a surface. The contact angle of the droplet is measured as the angle of the tangent of the droplet and the plane of the surface. If the liquid has a lower surface energy than the surface, it will spread over the surface. Otherwise, the liquid will form a droplet with a contact angle that reflects the difference in surface energies of the probe liquid and surface.

Scanning electron microscopy (SEM) scans surfaces using a high energy beam of primary electrons. The energy of these primary electrons is typically 0.1-40 keV. The primary

electrons are focused and collide with surfaces. Some electrons penetrate into the samples and are not detected. However, a large number of electrons are reflected as backscattered electrons through elastic scattering. This signal includes secondary electrons, which are generated by the collision between incident electrons and sample electrons. The detection depth of electrons with an energy of 20 keV is approximately 1.5 μm. The incident spot diameter is 5-200 nm.

1.4. Overview of my work

My work focused on the preparation, patterning, and applications of self-assembled monolayers, especially alkylsilane monolayers. I explored new methods for preparing alkysilane monolayers, investigated patterning techniques for monolayers, and developed new applications for these monolayers. This work provides new surface functionalization methods for microchips, optical devices, and semiconductor fabrication. Chapters 2 and 3 describe the preparation and properties of alkylsilane monolayers. In Chapters 4, 5, and 6, I describe new pattering methods and applications of monolayers. In Chapter 7, I show a new application of monolayers for synthesis of conductive polymers.

1.4.1. Content of Chapter 2

Compared to solution phase deposition, vapor phase deposition is by far the most effective, simple, and potentially reproducible method for producing homogeneous, covalently bonded, high density, functionalized silane films on silicon and glass surfaces. Vapor phase deposition is much cleaner than the liquid phase approach because the surface is not exposed to impurities that may be in the solvent, and no surface rinsing or cleaning is required after deposition. However, not all vapor phase surface preparation methods produce the same quality

films. For example, the vapor phase coating procedure in a desiccator described by Fiorilli et.al., minimizes, but does not entirely eliminate, the size of the aggregates deposited on the surface of the silane films compared to films prepared from solution.[145] In contrast, with chemical vapor deposition (CVD) at high temperature and under vacuum conditions, I prepared high quality and reproducible ultrathin aminosilane monolayers on silicon substrates with roughnesses (rms) of 0.1 nm, including 3-aminopropyltriethoxysilane (APTES), 3-aminopropyldimethylethoxysilane (APDMES), and 3-aminopropyldiisopropylethoxysilane (APDIPES). Characterization of these films indicated that monolayer quality is quite insensitive to the amount of reagent. Surface properties of these three amino silane films were investigated. Stability tests showed that APDIPES had the best stability in basic solutions.

1.4.2. Content of Chapter 3

The film uniformity of mercaptosilane monolayers is especially critical for optical devices.[146] Here, vapor phase deposition is again advantageous over solution phase deposition because vapor phase deposition can provide more uniform monolayers. There have been several reports of the vapor phase deposition on mercaptosilanes using lab scale desiccators.[147] Here, I prepared uniform 3-mercaptopropyltrimethoxysilane (MCPTMS) monolayers at 150ºC and under vacuum with a commercial chemical vapor deposition system. Results illustrated that this CVD method is robust, and monolayer quality was little affected by deposition conditions. This silane monolayer can effectively improve the adhesion of gold.

1.4.3. Content of Chapter 4

Laser direct writing is often used to deposit metals. Organic monolayer deposition with

lasers or other light has been less frequently reported. Here, I explored a method to directly deposit organic monolayers by laser activation on semiconductor substrates, i.e., silicon or germanium. This deposition was implemented under atmospheric conditions and the surfaces did not need special pretreatment. As an extremely fast process, laser activation can functionalize and pattern surfaces simultaneously.

1.4.4. Content of Chapter 5

The use of DNA microarrays constitutes an important technique for studying human DNA and other genome sequences. This technique has been applied to determine outcomes in disease studies at many levels, including diagnosis, prognosis, and drug therapy.[148] However, DNA arrays are unable to provide information regarding the functions and changes in protein levels, which could include characterization of every protein encoded by the human genome, *i.e.*, the proteome. The appearance of protein arrays presented an opportunity to advance proteomics through exploration of protein interactions.[149]

To prepare a protein array, proteins are attached to a solid support such as glass, silicon, or a polymer substrate, and the interacting partner that is to be detected is applied from solution. The means of protein attachment can be physical adsorption, covalent bonding, or affinity interaction. To reduce non-specific adsorption of proteins outside of control areas, which may contain, for example, poly-L-lysine or epoxides, silane-grafted polyethylene glycol (PEG) slides have been used to prevent direct contact between the proteins in solution and the glass or silicon surface because of the well-known resistance of PEG to proteins.[150]

I developed a high throughput protein array technology. A silicon substrate coated with a PEG silane monolayer was patterned using a laser and a microlens array (MLA) to form

micrometer-sized spots with densities of 10,000 spots/cm^2. Proteins were deposited using a microfludic spotter. I also applied this technology to the detection of iron in ferritin.

1.4.5. Content of Chapter 6

Plasma etching is the main method by which stencil lithography is used to make deep patterns. However, this method still requires expensive plasma etching instruments. I developed a straightforward method to create deep patterns on silicon substrates using a stencil mask and plasma oxidation. A silicon dioxide pattern could be obtained after plasma oxidation through the stencil mask. HF and KOH etching created shallow and deep features, respectively. This patterning process can be implemented in laboratories that have relatively basic equipment.

1.4.6. Content of Chapter 7

In 2000, the Nobel Prize in chemistry was awarded to Heeger, MacDiarmid, and Shirakawa for their pioneering work on conductive polymers, including polyaniline (PANi).[151-152] As Figure 1.5 shows, PANi has three forms: the fully reduced leucoemeraldine base state (LB), the fully oxidized pernigraniline base state (PNB), and the half oxidized emeraldine base state (EB).[153] The LB and PNB forms do not show conductivity. The EB state has low conductivity.[154] Doping delocalizes the charges of each unit of the EB to the whole polymer chain and increases the conductivity of PANi dramatically from 10^{-5} S/cm to more than 10^3 S/cm.[155] There are two common doping methods: redox doping and non-redox doping. In the redox doping methods, PANi is oxidized with reagents such as iodine, and the conductivity increases up to 10^3 S/cm. Non-redox doping uses dopant ions to protonate PANi, including hydrochloric acid.[156]

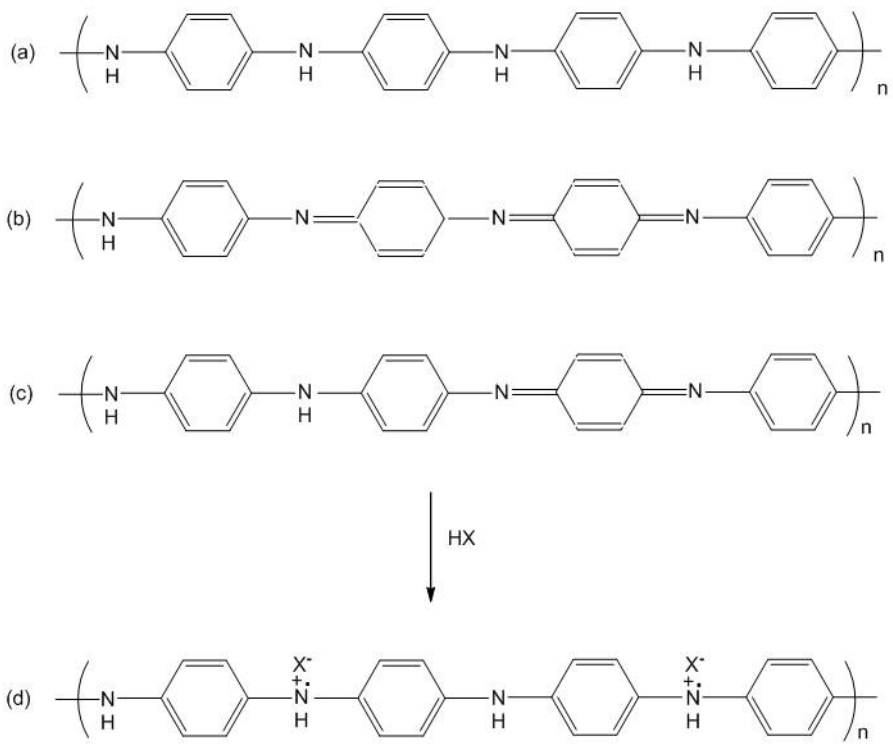

Figure 1.5. Structures of PANi. (a) Leucoemeraldine base state, (b) Pernigraniline base state, (c) Emeraldine base state, and (d) doped emeraldine base state with acid.[153]

Camphorsulfonic acid (CSA) and 2-acrylamido-2-methylpropanesulfonic acid (AMPSA) have been used as dopants, and this method has yielded stable PANi fibers.[157-159] However, previous work to spin fibers used organic solvents as coagulation solutions. I developed a method that uses much safer aqueous solutions without significantly altering fiber conductivity. PANi fibers with unlimited length can be spun into polyanion aqueous solutions. Characterization showed that polyanions stabilize the fiber by forming a polyelectrolyte film.

1.5. References

1. Jang, L.-S.; Liu, H.-J., *Biomed. Microdevices* **2009,** *11*, 331-338.
2. Dong, H.; CM, L.; Zhou, Q.; Sun, J.; Miao, J., *Biosens. Bioelectron.* **2006,** *22*, 621-626.
3. Nam, Y.; Branch, D. W.; Wheeler, B. C., *Biosens. Bioelectron.* **2006,** *22*, 589-597.
4. Oleksandrov, S.; Lee, J.; Lee, S.; Lee, M.-G.; Choi, H. Y.; Chung, C.-H., *J. Nanosci. Nanotechnol.* **2009,** *9*, 7481-7484.
5. Bauermann, L. P.; Gerstel, P.; Bill, J.; Walheim, S.; Huang, C.; Pfeifer, J.; Schimmel, T., *Langmuir* **2010**, 3774-3778.
6. Imae, T., *Advanced Chemistry of Monolayers at Interfaces: Trends in Methodology and Technology*. Academic Press: Amsterdam, Netherlands, 2007.
7. Onclin, S.; Ravoo, B. J.; Reinhoudt, D. N., *Angew. Chem. Int. Ed.* **2005,** *44*, 6282-6304.
8. Ruckenstein, E.; Li, Z. F., *Adv. Colloid Interface Sci.* **2005,** *113*, 43-63.
9. Maoz, R.; Sagiv, J., *Langmuir* **1987,** *3*, 1045-1051.
10. Wasserman, S. R.; Tao, Y.-T.; Whitesides, G. M., *Langmuir* **1989,** *5*, 1074-1087.
11. Masaoka, S.; Banno, T.; Ishikawa, M., *J. Organomet. Chem.* **2006,** *691*, 174-181.
12. Baba, T.; Kawanami, Y.; Yuasa, H.; Yoshida, S., *Catal. Lett.* **2003,** *91*, 31-34.

13. Sagiv, J., *J. Am. Chem. Soc.* **1989,** *102*, 92-98.

14. Rubinstein, I.; Steinberg, S.; Tor, Y.; Shanzer, A.; Sagiv, J., *Nature* **1988,** *332*, 426-429.

15. Netzer, L.; Sagiv, J., *J. Am. Chem. Soc.* **1983,** *105*, 674-676.

16. Angst, D. L.; Simmons, G. W., *Langmuir* **1991,** *7*, 2236-2242.

17. Allara, D. L.; Parikh, A. N.; Rondelez, F., *Langmuir* **1995**, 2357-2360.

18. Wang, R.; Guo, J.; Baran, G.; Wunder, S. L., *langmuir* **2000,** *16*, 568-576.

19. Iimura, K.-i.; Nakajima, Y.; Kato, T., *Thin Solid Films* **2000,** *379*, 230-239.

20. Grange, J. D. L.; Markham, J. L.; Kurkjian, C. R., *Langmuir* **1993,** *9*, 1749-1753.

21. Silberzan, P.; Leger, L.; Ausserre; Benattar, J. J., *Langmuir* **1991,** *7*, 1647-1651.

22. Manifar, T.; Rezaee, A.; Sheikhzadeh, M.; Mittler, S., *Appl. Surf. Sci.* **2008,** *254*, 4611-4619.

23. Krasnoslobodtsev, A. V.; Smirnov, S. N., *Langmuir* **2002,** *18*, 3181-3184.

24. Zheng-Zheng, L.; Qi, W.; Xin, L.; Jie-Qiong, B., *Thin Solid Films* **2008,** *517*, 635-640.

25. Hozumi, A.; Yokogawa, Y.; Kameyama, T.; Sugimura, H.; Hayashi, K.; Shirayama, H.; Takai, O., *J. Vac. Sci. Technol. A* **2001,** *19*, 1812-1816.

26. Crampton, N.; Bonass, W. A.; Kirkham, J.; N.H, T., *Langmuir* **2005,** *21*, 7884-7891.

27. Du, Y.; George, S. M., *J. Phys. Chem. C* **2007,** *111*, 8509-8517.

28. Kurth, D. G.; Bein, T., *Langmuir* **1995,** *11*, 3061-3067.

29. Wang, A.; Tang, H.; Cao, T.; Salley, S. O.; Ng, K. Y. S., *J. Colloid Interface Sci.* **2005,** *291*, 438-447.

30. Hong, L.; Sugimura, H.; Furukawa, T.; Takai, O., *Langmuir* **2003,** *19*, 1966-1969.

31. Sugimura, H.; Hayashi, K.; Amano, Y.; Takai, O., *J. Vac. Sci. Technol. A* **2001,** *19*, 1261-1265.

32. Iimura, K.-i.; Kato, T., *Colloid Surface A* **2000,** *171*, 249-264.

33. Chandekar, A.; Sengupta, S. K.; Whitten, J. E., *Appl. Surf. Sci.* **2010,** *256*, 2742-2749.

34. Kim, S.; Sohn, H.; Boo, J.-H.; Lee, J., *Thin Solid Films* **2008,** *516*, 940-947.

35. Kamisetty, N. K.; Pack, S. P.; Nonogawa, M.; Devarayapalli, K. C.; Kodaki, T.; Makino, K., *Anal. Bioanal. Chem.* **2006,** *386*, 1649-1655.

36. Sun, Y.; HaiyingWang; Sun, C., *Biosens. Bioelectron.* **2008,** *24*, 22-28.

37. Tessier, D. C.; Boughaba, S.; Roos, P.; Pan, G., *Sens. Actuators, B* **2006,** *120*, 220-230.

38. Shang, Y.; Zhao, W.; Xu, E.; Wu, J., *Biosens. Bioelectron.* **2010,** *25*, 1056-1063.

39. Olmos, D.; Aznar, A. J.; Baselga, J., *J. Colloid Interface Sci.* **2003,** *267*, 117-126.

40. Albala, R.; Olmos, D.; Aznar, A. J.; Baselga, J.; Gonzalez-Benito, J., *J. Colloid Interface Sci.* **2004,** *277*, 71-78.

41. Wang, B.; Huang, Y.; Liu, L., *J. Mater. Sci.* **2006,** *41*, 1243-1246.

42. Kang, E. T.; Neoh, K. G.; Tan, K. L., *Prog. Polym. Sci.* **1998,** *23*, 277-324.

43. Sapsford, K. E.; Ligler, F. S., *Biosens. Bioelectron.* **2004,** *19*, 1045-1055.

44. El-Ghannam, A. R.; Ducheyne, P.; Risbud, M.; Adams, C. S.; Shapiro, I. M.; Castner, D.; Golledge, S.; Composto, R. J., *J. Biomed. Mater. Res. Part A* **2004,** *68*, 615-627.

45. Balasundaram, G.; Sato, M.; Webster, T., *Biomaterials* **2006,** *27*, 2798-2805.

46. Filippini, P.; Rainaldi, G.; Ferrante, A.; Mecheri, B.; Gabrielli, G.; Bombace, M.; Indovina, P. L.; Santini, M. T., *J. Biomed. Mater. Res. Part A* **2001,** *55*, 338-349.

47. Fang, X.; Tan, O. K.; Tse, M. S.; Ooi, E. E., *Biosens. Bioelectron.* **2010,** *25*, 1137-1142.

48. Ramrus, D. A.; Berg, J. C., *J. Adhesion Sci. Technol.* **2004,** *18*, 1395-1414.

49. Suemori, Y.; Nagata, M.; Nakamura, Y., *Photosynth Res* **2006,** *90*, 17-21.

50. Rahman, M.; Norton, M. L., *IEEE Trans. Nanotechnol.* **2010,** *9*, 539-542.

51. Pérona, O.; Rinnert, E.; Lehaitre, M.; Crassous, P.; Compère, C., *Talanta* **2009,** *79*, 199-204.

52. Liu, X.; Wang, Q.; Chen, L.-P., *Appl. Surf. Sci.* **2009,** *255*, 3789-3794.

53. Fu, Y.; Yuan, R.; Xu, L.; Chai, Y.; Tang, D., *Biochem. Eng. J.* **2005,** *23*, 37-44.

54. Pan, J.; Yang, Q., *Anal. Bioanal. Chem.* **2007,** *288*, 279-286.

55. Ruan, C.; Yang, L.; Li, Y., *Anal. Chem.* **2002,** *74*, 4814-4820.

56. Cloarec, J.; Deligianis, N.; Martin, J.; Lawrence, I.; Souteyrand, E.; Polychronakos, C.; Lawrence, M., *Biosens. Bioelectron.* **2002,** *17*, 405-412.

57. Das, J.; Huh, C.-H.; Kwon, K.; Park, S.; Jon, S.; Kim, K., *Langmuir* **2009,** *25*, 235-241.

58. Cerruti, M.; Fissolo, S.; Carraro, C.; Ricciardi, C., *Langmuir* **2008,** *24*, 10646-10653.

59. Yue, M.; Stachowiak, J. C.; Lin, H.; Datar, R.; Cote, R.; Majumdar, A., *Nano Lett.* **2008,** *8*, 520-524.

60. Cai, Y.; Newby, B.-m. Z., *Langmuir* **2008,** *24*, 5202-5208.

61. Perl, A. s.; Reinhoudt, D. N.; Huskens, J., *Adv. Mater.* **2009,** *21*, 2257-2268.

62. Ruizab, S. A.; Chen, C. S., *Soft Matter* **2007,** *3*, 168-177.

63. Sugimura, H.; Hozumi, A.; Takai, O., *IEICE Trans. Electron.* **2000,** *E83C*, 1099-1103.

64. Mooney, J.; Hunt, A.; McIntosh, J.; Liberko, C.; Walba, D.; Rogers, C., *Proc. Natl. Acad. Sci. U. S. A.* **1996,** *93*, 12287-12291.

65. Pena, A.; Wang, Z.; Whitehead, D.; Li, L., *Appl. Phys. A: Mater. Sci. Process.* **2010,** *101*, 287-295.

66. Scheres, L.; Klingebiel, B.; ter Maat, J.; Giesbers, M.; de Jong, H.; Hartmann, N.; Zuilhof, H., *Small* **2010,** *6*, 1918-1926.

67. Lee, H.; Shin, H.; Lee, M., *Opt Laser Eng* **2010,** *48*, 380-384.

68. Hullavarad, S.; Hullavarad, N.; Vispute, R.; Venkatesan, T.; Kilpatrick, S.; Ervin, M.; Nichols, B., *J. Electron. Mater.* **2010,** *39*, 1209-1217.

69. Tsouti, V.; Boutopoulos, C.; Goustouridis, D.; Zergioti, I.; Normand, P.; Tsoukalas, D., *Sensor Actuat. B-Chem.* **2010,** *150*, 148-153.

70. Boutopoulos, C.; Pandis, C.; Giannakopoulos, K.; Pissis, P.; Zergioti, I., *Appl. Phys. Lett.* **2010,** *96*, 041104.

71. Serra, P.; Fernandez-Pradas, J.; Berthet, F.; Colina, M.; Elvira, J.; Morenza, J., *Appl Phys A-Mater* **2004,** *79*, 949-952.

72. Xu, J.; Grant, S.; Pastel, R., *IEEE Trans. Biomed. Eng.* **2003,** *50*, 126-128.

73. Meunier, M.; Izquierdo, R.; Tabbal, M.; Stephane Evoy; Desjardins, P.; Bernier, M.-H., *Mater. Sci. Eng., B* **1997,** *45*, 200-207.

74. Park, J. B.; Jeong, S. H.; Jeong, M. S., *Appl. Surf. Sci.* **2010,** *257*, 641-649.

75. Maruo, S.; Saeki, T., *Opt. Express* **2008,** *16*, 1174-1179.

76. Wee, L. M.; Li, L., *Appl. Surf. Sci.* **2005,** *247*, 285-293.

77. Kord´as, K.; Na´nai, L.; Galba´cs, G.; Uusim¨aki, A.; Leppa¨vuori, S.; Bali, K., *Appl. Surf. Sci.* **2000,** *158*, 127-133.

78. Guo, X.; Zhao, Q.; Li, R.; Pan, H.; Guo, X.; Yin, A.; Dai, W., *Opt. Express* **2010,** *18*, 18401-18406.

79. Serra, P.; Duocastella, M.; Ferna´ndez-Pradas, J. M.; Morenza, J. L., *Appl. Surf. Sci.* **2009,** *255*, 5342-5345.

80. Serra, P.; Fern´andez-pradas, J. M.; Berthet, F. X.; Colina, M.; Elvira, J.; Morenza, J. I., *Appl. Phys. A* **2004,** *79*, 949-952.

81. Colina, M.; Serraa, P.; Fern´andez-Pradasa, J. M.; Sevillab, L.; Morenzaa, J. L., *Biosens. Bioelectron.* **2005,** *20*, 1638-1642.

82. Dinca, V.; Ranella, A.; Farsari, M.; Kafetzopoulos, D.; Dinescu, M.; Popescu, A.; Fotakis, C., *Biomed. Microdevices* **2008,** *10*, 719-725.

83. Hartmann, N.; Balgar, T.; Bautista, R.; Franzka, S., *Surf. Sci.* **2006,** *600*, 4034-4038.

84. Halfpenny, D. R.; Kane, D. M.; Lamb, R. N.; Gong, B., *Appl. Phys. A* **2000,** *71*, 147-151.

85. Lima, C. S.; Hongb, M. H.; Lin, Y.; Chend, G. X.; Kumar, A. S.; Rahman, M.; Tan, L. S.; Fuh, J. Y. H.; Lim, G. C., *J. Mater. Process. Technol.* **2007,** *192-193*, 328-333.

86. Kato, J.-i.; Takeyasu, N.; Adachi, Y.; Sun, H.-B.; Kawata, S., *Appl. Phys. Lett.* **2005,** *86*, 044102.

87. Lin, C. H.; Jiang, L.; Chai, Y. H.; Xiao, H.; ·, S. J. C.; Tsai, H. L., *Appl Phys A* **2009,** *97*, 751-757.

88. Chen, Y.; Yi, A. Y.; Yao, D.; Klocke, F.; Pongs, G., *J. Micromech. Microeng.* **2008,** *18*, 055022.

89. Wu, J.; Yang, S., *J. Micromech. Microeng.* **2010,** *20*, 085038.

90. Zeng, X.; Jiang, H., *J. Microelectromech. Syst.* **2008,** *17*, 1210-1217.

91. Chou, M.-C.; Pan, C. T.; Shen, S. C.; Chen, M.-F.; Lin, K. L.; Wu, S.-T., *Sens. Actuators, A* **2005,** *118*, 398-306.

92. Lu, J.; Huang, W.; Chen, F., *Opt Eng* **2009,** *48*, 073606.

93. Gray, S.; Weimer, P. K., *RCA Rev.* **1959,** *20*, 413-425.

94. Fostner, S.; Burke, S. A.; Topple, J.; Mativetsky, J. M.; Beerens, J.; Grutter, P., *Microelectron. Eng.* **2010,** *87*, 652-657.

95. Kim, J.-W.; Yamagata, Y.; Higuchi, T., *J. Micromech. Microeng.* **2009,** *19*, 025021.

96. Racz, Z.; He, J.; Srinivasan, S.; Zhao, W.; Seabaugh, A.; Han, K.; Ruchhoeft, P.; Wolfe, J., *J. Vac. Sci Technol. B* **2004,** *22*, 74-76.

97. Tourovskaia, A.; Barber, T.; Wickes, B. T.; Hirdes, D.; Grin, B.; Castner, D. G.; Healy, K. E.; Folch, A., *Langmuir* **2003,** *19*, 4754-4764.

98. Mena, O. V.; Villanueva, G.; Savu, V.; Sidler, K.; Boogaart, M. A. F. v. d.; Brugger, J., *Nano Lett.* **2008,** *8*, 3675-3682.

99. Dumas, C.; Grisolia, J.; Ressier, L.; Arbouet, A.; Paillard, V.; Ben Assayag, G.; Claverie, A.; Brugger, J., *Phys. Status Solidi A* **2007,** *204*, 487-491.

100. Nishihashi, T.; Kashimoto, K.; Fujiyama, J.; Sakurada, Y.; Shibata, T.; Suguro, K.; Sugihara, K.; Okumura, K.; Gotou, T.; Saji, N.; Tsunoda, M., *IEEE Trans. Semicond. Manuf.* **2002,** *15*, 464-469.

101. Shibata, T.; Suguro, K.; Sugihara, K.; Nishihashi, T.; Fujiyama, J.; Sakurada, Y., *IEEE Trans. Semicond. Manuf.* **2002,** *15*, 183-188.

102. von Borany, J.; Friedrich, M.; Rub, M.; Deboy, G.; Butschke, J.; Letzkus, F., *Nucl. Instrum. Methods Phys. Res., Sect. B* **2005,** *237*, 62-67.

103. Kim, G.; Maf, v. d. B.; Brugger, J., *Microelectron. Eng.* **2003,** *67-8*, 609-614.

104. Cho, B.; Ryu, J.; Hwang, S.; Moon, S., *J. Vac. Sci Technol. B* **2000,** *18*, 2769-2773.

105. Viallet, B.; Grisolia, J.; Ressier, L.; Boogaart, M. A. F. V. D.; Brugger, J.; Lebraud, T., *Microelectron. Eng.* **2008,** *85*, 1705-1708.

106. Villanueva, G.; Vazquez-Mena, O.; Boogaart, M. A. F. v. d.; Sidler, K.; Pataky, K.; V. Savu, J. B., *Microelectron. Eng.* **2008,** *85*, 1010-1014.

107. Savu, V.; Boogaart, M. A. F. v. d.; Brugger, J.; Arcamone, J.; Sansa, M.; Perez-Murano, F., *J. Vac. Sci Technol. B* **2008,** *26*, 2054-2058.

108. Guo, H.; Martrou, D.; Zambelli, T.; van den Boogaart, M. A. F.; Brugger, J., *Appl. Phys. Lett.* **2007,** *90*, 093113.

109. Va´zquez-Mena, O.; Villanueva, G.; M.a.f. Van den, B.; Savu, V.; Brugger, J., *Microelectron. Eng.* **2008,** *85*, 1237-1240.

110. Fan, C.-h.; Zhang, Y.-c.; Zhang , Y.; Han, X.; Chefetz, B., *Spectrosc. Spect. Anal.* **2010,** *30*, 2752-2757.

111. Custodio, J. V.; Agostinho, S. M. L.; Simoes, A. M. P., *Electrochim. Acta* **2010,** *55*, 5523-5531.

112. Hook, A. L.; Anderson, D. G.; Alexander, M. R., *Biomaterials* **2010,** *31*, 187-198.

113. Mishra, A.; Chattopadhyay, D.; Sreedhar, B., *Pro Org Coat* **2006,** *55*, 231-243.

114. Hajati, S.; Tougaard, S., *Anal. Bioanal. Chem.* **2010,** *396*, 2741-2755.

115. Grosvenor, A. P.; Cavell, R. G.; Mar, A., *Controlled Assembly and Modification of Inorganic Systems*. SPRINGER-VERLAG: Berlin, Germany, 2009; Vol. 133, p 41-92.

116. Chen, R.; Korotcov, A.; Huang, Y.; Tsai, D., *Nanotechnology* **2006,** *17*, R67-R87.

117. Herrera-Gomez, A.; Grant, J. T.; Cumpson, P. J., *Surf. Interface Anal.* **2009,** *41*, 840-857.

118. Turner, N. H., *Anal. Chem.* **1996,** *68*, 309-332.

119. Artyushkova, K., *J. Electron Spectrosc. Relat. Phenom.* **2010,** *178*, 292-302.

120. Escobar Galindo, R.; Gago, R.; Duday, D.; Palacio, C., *Anal. Bioanal. Chem.* **2010,** *396*, 2725-2740.

121. Vohrer, U.; Blomfield, C.; Page, S.; Roberts, A., *Appl. Surf. Sci.* **2005,** *252*, 61-65.

122. Blomfield, C., *J. Electron Spectrosc. Relat. Phenom.* **2005,** *143*, 241-249.

123. Honig, R., *Int. J. Mass Spectrom. Ion Processes* **1985,** *66*, 31-54.

124. Liebl, H., *J. Vac. Sci. Technol.* **1975,** *12*, 385-391.

125. Lorin, J.; Slodzian, G.; Dennebouy, R., *Meteoritics* **1989,** *24*, 294-295.

126. Vickerman, J.; Oakes, A.; Gamble, H., *Surf. Interface Anal.* **2000,** *29*, 349-361.

127. Van Vaeck, L.; Adriaens, A.; Gijbels, R., *Mass Spectrom. Rev.* **1999,** *18*, 1-47.

128. Boxer, S. G.; Kraft, M. L.; Weber, P. K., *Annu. Rev. Biophys.* **2009,** *38*, 53-74.

129. Binnig, G.; Quate, C.; Gerber, C., *Phys. Rev. Lett.* **1986,** *56*, 930-933.

130. García, R.; Pérez, R., *Surf. Sci. Rep.* **2002,** *47*, 197-301.

131. Hodges, C., *Adv. Colloid Interface Sci.* **2002,** *99*, 13-75.

132. Custance, O.; Perez, R.; Morita, S., *Nature Nanotech* **2009,** *4*, 803-810.

133. Connell, S.; Smith, D., *Mol. Membr. Biol.* **2006,** *23*, 17-28.

134. Smith, R. K.; Lewis, P. A.; Weiss, P. S., *Prog. Surf. Sci.* **2004,** *75*, 1-68.

135. Lin, Y.; Huck, W. T. S.; Whitesides, G. M., *J. Macromol. Sci., Polym. Rev.* **2004,** *C44*, 175-206.

136. Maganov, S. N.; Whangbo, M.-H., *Surface Analysis with STM and AFM: Experimental and Theoretical Aspects of Image Analysis* Wiley-VCH: 2008.

137. Garcia, R.; Perez, R., *Surf. Sci. Rep.* **2002,** *47*, 197-301.

138. Gan, Y., *Surf. Sci. Rep.* **2009,** *64*, 99-121.

139. Rugan, D.; Hansma, P., *Phys. Today* **1990,** *43*, 23-30.

140. Solares, S. D., *Meas. Sci. Technol.* **2007,** *18*, 592-600.

141. Kitamura, S.; Iwatsuki, M., *Jpn. J. Appl. Phys., Part 2* **1996,** *35*, L668-L671.

142. Jalili, N.; Laxminarayana, K., *Meteoritics* **2004,** *14*, 907-945.

143. Zhong, Q.; Inniss, D.; Kjoller, K.; Ellings, V., *Surf. Sci.* **1993,** *290*, L688-L692.

144. Wilson, N. R.; Macpherson, J. V., *Nature Nanotech* **2009,** *4*, 483-491.

145. Fiorilli, S.; Rivolo, P.; Descrovi, E.; Ricciardi, C.; Pasquardini, L.; Lunelli, L.; Vanzetti, L.; Pederzolli, C.; Onida, B.; Garrone, E., *J. Colloid Interface Sci.* **2008,** *321*, 235-241.

146. Goss, C. A.; Charych, D. H.; Majda, M., *Anal. Chem.* **1991,** *63*, 85-88.

147. Mahapatro, A. K.; Scott, A.; Janes, D. B., *Appl. Phys. Lett.* **2006,** *88*, 151917.

148. Dharmadi; R, Y. a.; Gonzalez, *Biotechnol. Prog.* **2004,** *20*, 1309-1324.

149. Sakanyana, V., *J. Chromatogr., B* **2005,** *8015*, 77-95.

150. Prime, K. L.; Whitesides, G. M., *J. Am. Chem. Soc.* **1993,** *115*, 10714-10721.

151. Kohlman, R. S.; Zibold, A.; Tanner, D. B.; Ihas, G. G.; Ishiguro, T.; Min, Y. G.; MacDiarmid, A. G.; Epstein, A. J., *Phys. Rev. Lett.* **1997,** *78*, 3915-3918

152. Shimano, J. Y.; MacDiarmid, A. G., *Synth. Met.* **2001,** *123*, 251-262.

153. Wan, M., *Conducting Polymers with Micro or Nanometer Structure*. Springer Berlin Herdelberg: New York, 2008.

154. Kahol, P. K.; Perera, R. P.; Geetha, S., *Solid State Commun.* **2003,** *125*, 369-372.

155. Skotheim, T. A.; Dekker, M., *Handbook of Conductiing Polymers*. New York, 1986;

156. Kand, E. T.; Neoh, K. G.; Tan, K. L., *Prog. Polym. Sci.* **1998,** *23*, 277-324.

157. Cao, Y.; Smith, P.; Heeger, A. J., *Synth. Met.* **1992,** *48*, 91-97.

158. Pratt, F. L.; Blundell, S. J.; Hayes, W. A.; Nagamine, K.; Ishida, K.; Monkman, A. P., *Phys. Rev. Lett.* **1997,** *79*, 2855-2858.

159. Pomfret, S. J.; Adams, P. N.; Monkman, A. P., *Adv. Mater.* **1998,** *10*, 1351-1353.

Chapter 2. Chemical Vapor Deposition (CVD) of Three Amino Silanes on Silicon Dioxide: Surface Characterization, Stability, Effects of Silane Concentration, and Cyanine Dye Adsorption*

2.1. Introduction

Although liquid phase deposition is still widely used for silane film deposition, chemical vapor deposition (CVD) shows significant advantages because it is much more effective, simple, and potentially reproducible. In the CVD process, surfaces are exposed to the pure chemical in vapor form so that impurities that are often present in solution deposition are excluded. In addition, more even surface deposition is often observed. Therefore, CVD appears to be a viable method for producing homogeneous, covalently bonded, high density, functionalized silane films on silicon and glass surfaces.

There have been relatively few reports on the gas phase deposition of silanes, which includes reports of the deposition of alkyl silanes, fluoroalkyl silanes, and aminosilanes.[1-11] However, we are not aware of any study exploring the effects of steric hindrance on these monolayers, or the use of cyanine dyes as a probe for these monolayers.

Here, I explore conditions for CVD to make aminosilane monolayers of APTES, APDMES, and APDIPES (see Scheme 2.1) on silicon substrates. One important purpose of this study is to determine the gas phase concentration of silane that is needed to saturate the surface of a silicon oxide surface. The three silanes were chosen to have obvious structural differences and corresponding reactivities and stabilities on bonded surfaces. That is, APTES has three potential attachment points to the surface or other silane molecules, while APDMES and

*Taken from (Feng Zhang, Ken Sautter, Adam M. Larsen, Daniel A. Findley, Robert C. Davis, Hussein Samha, and Matthew R. Linford) *Langmuir*, **2010**, *26(18)*, 14648-114654. Copyright 2010 American Chemical Society.

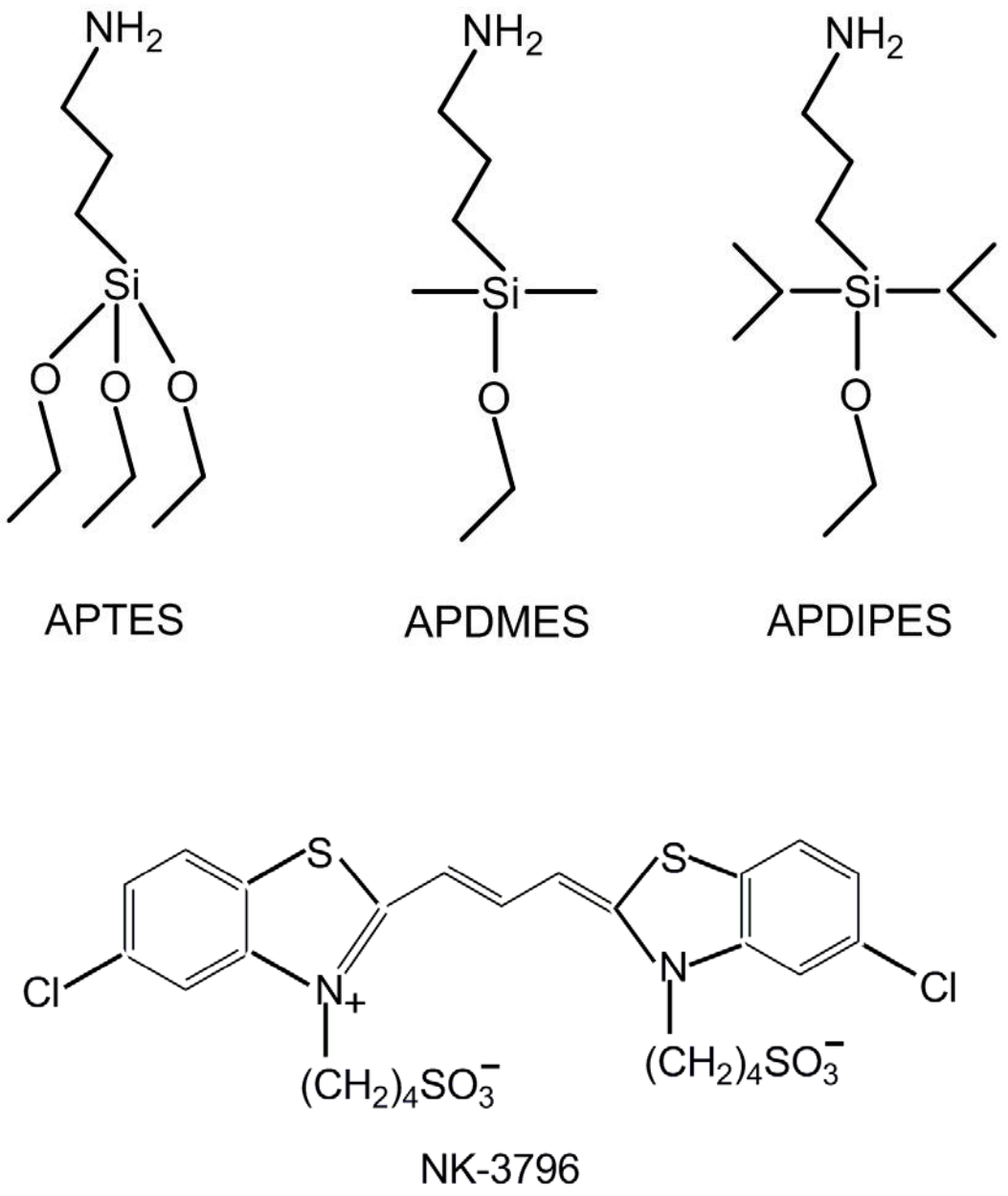

Scheme 2.1. Structures of 3-aminopropyltriethoxysilane (APTES), 3-aminopropyldimethylethoxysilane (APDMES), 3-aminopropyldiisopropylethoxysilane (APDIPES), and 5-chloro-2-[3-[5-chloro-3-(4-sulfobutyl)-2(3H)-benzothiazolylidene]-1-propenyl]-3-(4-sulfobutyl)-benzothiazolium hydroxide triethylamine salt (NK-3796).

have only one. Therefore APTES may polymerize, but APDMES and APDIPES are more simple molecules that can only dimerize (of course if they dimerize they cannot covalently bind to the surface). The two methyl groups on APDMES provide some steric hindrance around its silicon atom, and should also give the adsorbed species some measure of hydrophobicity. The two isopropyl groups on APDIPES provide its silicon atom with even greater steric hindrance and more hydrophobic character in the adsorbed state. This additional steric hindrance and hydrophobicity should increase the stability of APDIPES films under extreme pH conditions. This approach has been used to produce chromatographic stationary phases with improved stability.[12] In addition to these observations, I show the morphology and functionality of the prepared films with regards to adsorption of a cyanine dye.

2.2. Experimental

2.2.1. Materials and chemicals

Si(100) wafers, polished on one side, were obtained from Montco Silicon Technologies (Spring City, PA, USA). 2-Propanol (99.9%, Sigma, USA), acetone (> 99.5%, Sigma), potassium hydroxide (> 90%, Sigma), and oxygen gas (99.994%, Airgas) were used as received. APTES, APDMES, and APDIPES were purchased from Gelest (Morrisville, PA, USA) and the cyanine dye (NK-3796) was purchased from Hayashibara Biochemical Laboratory, Okayama, Japan, and used as received.

2.2.2. Surface cleaning

Native oxide-terminated silicon wafers and glass substrates were washed successively with soap and water, 2-propanol, and acetone, and then dried under a stream of pure nitrogen gas.

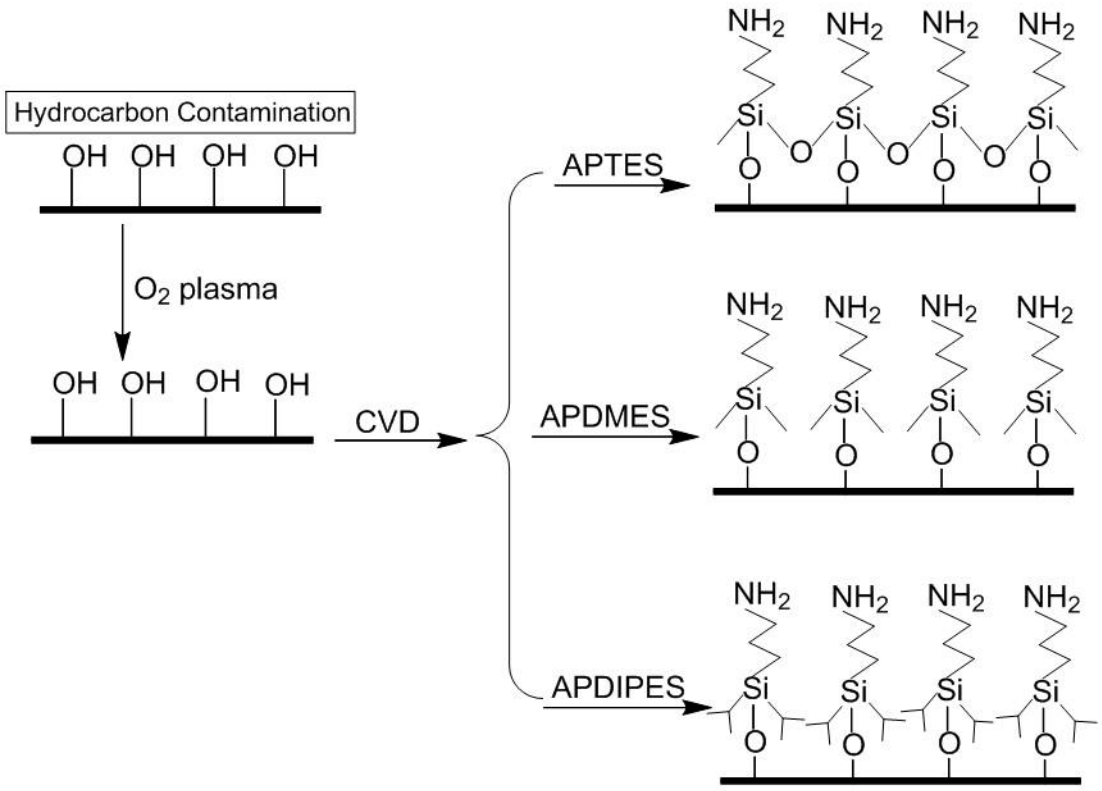

Scheme 2.2. Idealized representation of surface cleaning followed by surface modification with APTES, APDMES, and APDIPES.

Plasma cleaning of the washed slides was performed with a plasma cleaner model PDC-32G from Harrick Plasma (Ithaca, NY, USA) at medium power (10.5 W applied to the rf coil) for *ca*. 3 min using an air plasma. The thickness of the native oxide was then measured by ellipsometry, after which the surfaces were introduced into the silane deposition system.

2.2.3. CVD system

The YES-1224P chemical vapor deposition System from Yield Engineering Systems (Livermore, CA, USA) incorporates a plasma cleaning/modification capability into a heated vacuum deposition chamber where the internal dimensions of this deposition chamber are 16" (width) × 18" (depth) ×16" (height). Reactive chemicals are vaporized in temperature-controlled flasks and introduced via heated lines to the main chamber. The system allows precise control of chemical volume, reaction temperature, and exposure time. Plasma cleaning can prepare substrates for consistent, repeatable surface reaction, where three types of plates may be used in the YES-1224P including active, ground, and float. Voltages are applied to active plates vis-à-vis any ground plates and/or the walls of the chamber, which are grounded. Therefore, active plates generally have somewhat higher concentrations of plasma species than do ground plates, and float plates generally have much lower concentrations of such active species.[13]

2.2.4. CVD of the aminosilanes

The entire cleaning, dehydration, and deposition process was performed at 150°C. Surfaces were first plasma cleaned in the YES-1224P (200 W with high purity O_2 (99.994%) at *ca*. 0.5 Torr) using a three-plate configuration (active, ground, and float), with the substrates on the float plate. This surface cleaning, which did not increase the thickness of the native oxide,[13]

was followed by a dehydration purge to remove residual water from the surfaces. The dehydration purge consisted of evacuating the system to 5 Torr, refilling with N_2 gas to 500 Torr, and evacuating to the base pressure (1 Torr). An aminosilane was then introduced into the sealed chamber, raising the pressure of the deposition chamber to 2 – 3 Torr. The reaction time of the surface with the gas phase adsorbate was 5 min. After deposition, three purge cycles were performed, which consisted of addition of N_2 gas, followed by evacuation. These purge cycles were performed for both safety reasons and also to improve the quality of the deposition – they were used to remove residual silane from the chamber before it was opened, and they aided in removing any unreacted silane from the surfaces of the substrates.

2.2.5. Contact angle analysis

Water contact angles were measured with a Ramé-Hart (model 100-00) contact angle goniometer (Ramé-hart Instrument Co., Netcong, NJ, USA). The water contact angles, thicknesses (*vide infra*), and XPS N/Si ratios (*vide infra*) reported for the aminosilane surfaces are the averages of measurements obtained from multiple surfaces (sometimes as many as 15 – 20) prepared over a period of months.

2.2.6. Spectroscopic ellipsometry

Thicknesses of silane films, as well as films doped with adsorbed cyanine dye, were obtained using an M-2000D instrument from the J.A. Woollam Co. (Lincoln, NE, USA), Inc. The wavelength range was 190.5 - 989.4 nm, and the angle of incidence was fixed at 75°. The native oxide of silicon dioxide, aminosilane films, and cyanine dye films were modeled using the optical constants of silicon dioxide that were found in the instrument software. This is a valid and

widely used approach for ellipsometry of ultrathin organic films,[3, 14-16] where part of the justification for this approach stems from the similarity of the optical constants of SiO_2 and many other organic materials over a wide range of wavelengths (see, for example, Table 2.1). Note also that all of the silanes deposited in this study will be bonded through at least one Si-O bond, which obviously resembles SiO_2.

2.2.7. X-ray photoelectron spectroscopy

XPS was performed with an SSX-100 instrument from Surface Sciences using a monochromatic Al Kα source and a hemispherical analyzer.

2.2.8. Time-of-flight secondary ion mass spectrometry

ToF-SIMS was performed in spectroscopy mode using an ION-TOF TOF-SIMS IV instrument with a two-lens $^{69}Ga^+$ gun. Both positive and negative ion spectra were acquired.

2.2.9. UV-Vis measurements of the cyanine dye adsorbed on aminosilane films

Glass substrates modified with APTES, APDMES, and APDIPES were analyzed spectrophotometrically using an Agilent 8453 UV-Vis spectrophotometer (Lexington, MA, USA) after exposure to an aqueous solution of the cyanine dye.

2.2.10. AFM measurements

Atomic force microscopy (AFM) was performed with a Veeco Dimension V Scanning Probe Microscope (Plainview, NY, USA).

Table 2.1. Optical constants at 300 nm, 500 nm, and 700 nm of SiO_2, polymethylmethacrylate (PMMA), and polyethylene.

Material	n_{300}, k_{300}	n_{500}, k_{500}	n_{700}, k_{700}
SiO_2	1.49, 0	1.47, 0	1.46, 0
PMMA	1.51, 1.5×10^{-4}	1.49, 0	1.49, 0
Polyethylene	1.50, 0	1.49, 0	1.48, 0

2.2.11. Stability tests

Experiment 1 consisted of immersing aminosilane-coated silicon wafers in a pH 10.0 buffer (potassium carbonate-potassium borate-potassium hydroxide) for either 2h, 2h followed by another 2h, or 4h. The loss of any aminosilane was determined by the change in the N/Si ratio by XPS. Experiment 2 consisted of 6 months of storage of the aminosilane-coated surfaces in the laboratory, after which the samples underwent sonication for 3 min in isopropyl alcohol and then for 3 min in acetone, after which they were rinsed with water and dried with a jet of N_2. The samples were then recharacterized by spectroscopic ellipsometry and water contact angle goniometry (both advancing and receding angles were measured). These samples were also probed by ToF-SIMS.

2.2.12. Cyanine dye adsorption

Glass slides were immersed in an aqueous solution of the cyanine dye (see Scheme 2.1) for 10 min, removed, rinsed with deionized water, and then dried with a jet of nitrogen gas. The treatment of silicon wafers with the dye solution was accomplished by adding a few drops of the dye solution to the polished surface of a silicon shard (enough to cover the surface), after which it was allowed to stand for 10 min before the excess solution was rinsed away with deionized water, and the slides were again dried with nitrogen gas.

2.3. Results and discussion

2.3.1. Thin film characterization and stability

AFM and XPS were performed on silicon substrates prior to and following aminosilane CVD with 3-aminopropyltriethoxysilane (APTES), 3-aminopropyldimethylethoxysilane

(APDMES), and 3-aminopropyldiisopropylethoxysilane (APDIPES) (see Scheme 2.1). As expected, the silicon substrates were initially very smooth, with an rms roughness value of 0.103 ± 0.009 nm. Only a small increase in film roughness was observed after CVD of the aminosilanes. That is, the roughness (root mean square, rms) of the APTES, APDMES, and APDIPES films were 0.152 ± 0.005 nm, 0.104 ± 0.004 nm, and 0.122 ± 0.006 nm, respectively. The films appeared flat and monotonous by AFM; neither the control surface, nor the aminosilane surfaces showed any substantial features in this analysis. Indeed, AFM images of the films of these three silanes suggested complete coverage of their silicon substrates without any indication of rough morphologies. Anderson and coworkers similarly found that vapor phase deposition of an aminosilane (a molecule with two attachment points; i.e., 3'-aminopropylmethyldiethoxysilane) produced very smooth surfaces, which were much flatter than those made by solution deposition.[1] Figure 2.1 is a representative XPS survey scan of the surfaces modified with the three aminosilanes. These survey scans show the expected elemental composition of the surfaces: the presence of silicon, carbon, nitrogen, and oxygen. No N1s signal is present on the bare Si/SiO_2 substrates.

One key purpose of this study was to determine the amount of aminosilane that would be necessary to saturate the surface of an oxidized silicon wafer with a monolayer of an aminosilane. Accordingly, each of the three aminosilanes was deposited at different concentrations, *i.e.*, 0.1 mL to 5 mL of the silanes were injected into the chamber, which corresponds to concentrations (in the gas phase) of (0.1 - 5) × 5.7× 10^{-5} mol/L, (0.1 - 5) × 7.1× 10^{-5} mol/L, and (0.1 - 5) × 5.3× 10^{-5} mol/L of APTES, APDMES, and APDIPES, respectively. Interestingly, even the lowest concentration of the silanes appeared to saturate the surfaces, and this degree of surface saturation did not seem to increase with increasing silane concentration.

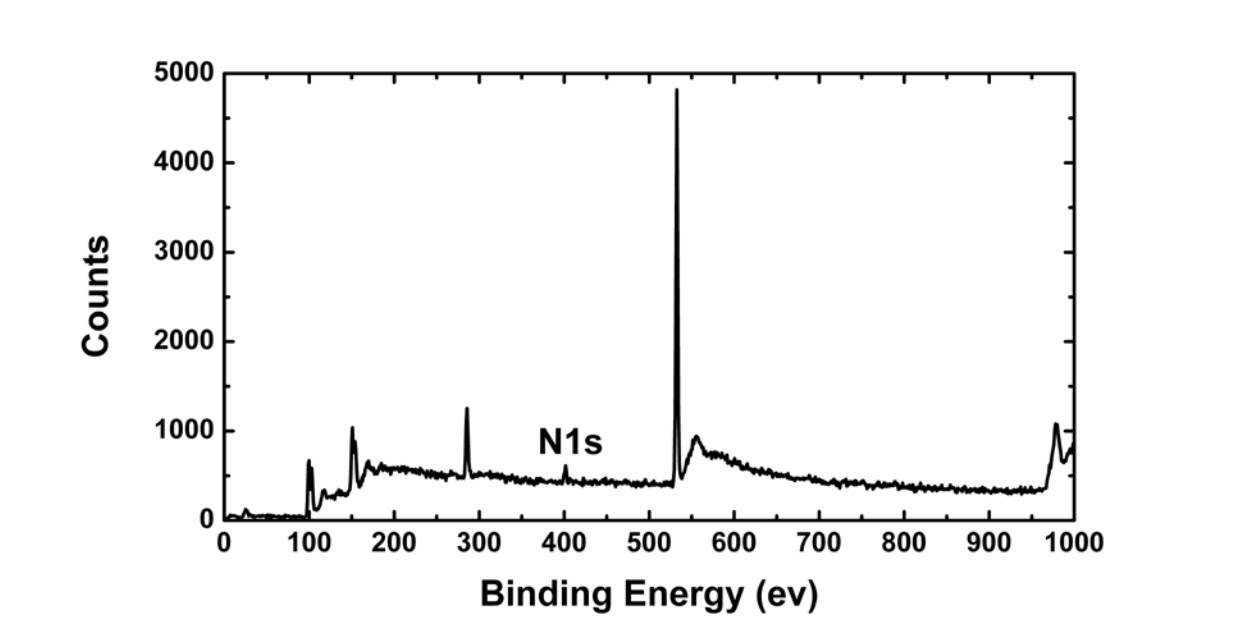

Figure 2.1. A representative XPS survey spectrum of one of our aminosilane (APTES) films on silicon oxide showing the expected signals due to nitrogen (N1s), silicon (Si2p and Si2s), carbon (1s), and oxygen (O1s and Auger signals). There are no unexpected peaks.

For example, Figure 2.2 shows the essentially constant advancing water contact angles of surfaces treated with different concentrations of the three aminosilanes. Clearly, for each of the silanes, the resulting water contact angle does not depend on the concentration of the gas phase reagent. Also, the trend in water contact angles reflects the chemistry of the adsorbates. APTES, with its three ethoxy groups, shows the lowest water contact angles, where unreacted ethoxy groups are expected to be subject to hydrolysis to silanols after the substrates are removed from the oven. APDMES, with its two methyl groups, produces surfaces with substantially higher water contact angles, and there is yet another increase in the water contact angles when two isopropyl groups are present on the silane (APDIPES).

XPS confirmed the wetting results, showing approximately the same surface coverage for deposition of a given aminosilane at different concentrations. However, the total amount of surface nitrogen does appear to depend on the nature of the adsorbate; the average N1s/Si2p XPS ratios of APTES, APDMES, and APDIPES are 0.074 ± 0.010, 0.058 ± 0.010, and 0.050 ± 0.005, respectively. APTES shows the highest coverage of amine groups, followed by APDMES, which only has one possible attachment point to the surface and some steric hindrance to this site, finally followed by APDIPES, which also has only one possible attachment point and even greater steric hindrance around this point. Interestingly, ellipsometry shows what appears to be the opposite trend. The thicknesses of the APTES, APDMES, and APDIPES surfaces were 6.6 ± 0.5, 6.5 ± 0.9, and 8.3 ± 1.0 Å, respectively. These results may be a reflection of condensation of APTES molecules at the surface with loss of water versus the permanent methyl and isopropyl groups of APDMES and APDIPES, where especially the isopropyl groups might contribute to the apparent thickness of the film. (Consider that APTES only has three carbon atoms in its alkyl chain bonded to silicon, but APDIPES has nine carbon atoms so bonded.)

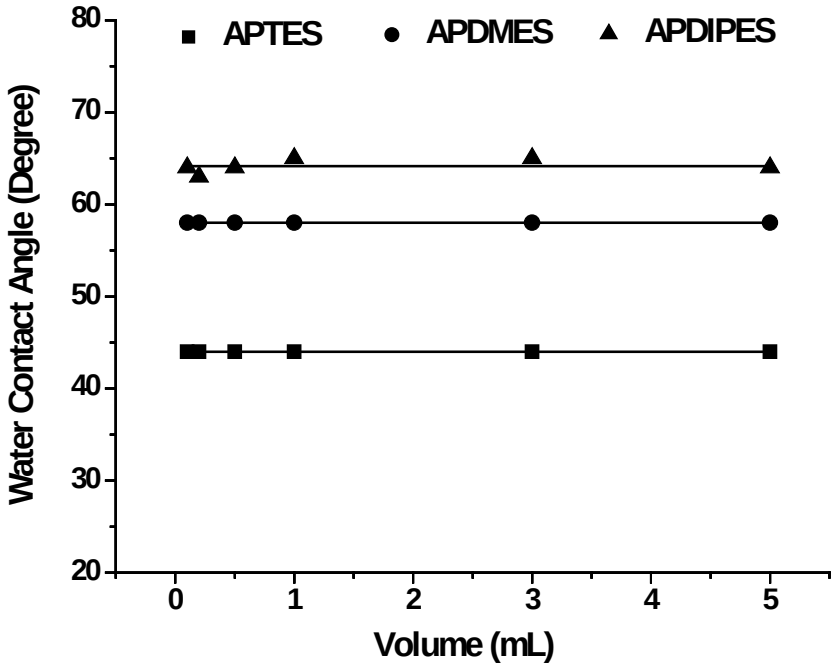

Figure 2.2. The advancing water contact angle vs. the volume of silane reagent introduced into the deposition chamber for surfaces coated with APTES, APDMES, and APDIPES.

Two stability tests were performed on aminosilane films. Experiment 1 consisted of immersing aminosilane coated surfaces in a pH 10 buffer for different periods of time, after which surface characterization was performed (see Table 2.2). In this experiment, it was expected a *priori* that the relatively high pH buffer would challenge the SiO_2 substrates along with any covalently attached adsorbates, and that APDIPES would have the greatest stability of the three silanes because of the steric hindrance and hydrophobicity of its isopropyl groups.[12] In the first trial of the experiment, which was repeated, aminosilane films were immersed in the pH 10 buffer for 2 h. As expected, there was very little loss in the nitrogen content of the APDIPES surfaces (*ca*. 1 – 4%), as measured by XPS. These losses are probably not statistically significant; it seems reasonable to state that the APDIPES surface was stable, or almost entirely stable, under these conditions. However, the APTES surface showed a significant loss of nitrogen (*ca*. 20%), and the APDMES surface suffered an even greater loss (*ca*. 40%). These results suggest that APTES' three reactive groups, which could form a network or attach at more than one place to the surface, are harder to hydrolyze than the singly bonded APDMES molecules. In the second trial, aminosilane surfaces that had been immersed in the pH 10 buffer for 2h, and then characterized, were again immersed in the pH 10 buffer for an additional 2h. These results are similar to those obtained in the third trial in which aminosilane surfaces were immersed continuously in the pH 10 buffer for 4h. In the results from these longer exposures, the APDIPES surfaces began to show real loss of nitrogen (*ca.* 5 – 20%), but not as great as APTES (*ca.* 30 – 35%) or APDMES (*ca.* 60 – 65%).

The second stability test consisted of simply storing aminosilane-coated surfaces in the laboratory for 6 months. Accordingly, three APTES, three APDMES, and three APDIPES surfaces were stored for 6 months and then cleaned and reanalyzed by spectroscopic ellipsometry

Table 2.2. Change in XPS N1s/Si2p ratios for APTES, APDMES, and APDIPES surfaces after immersion in a pH 10 buffer.

Time	APTES	APDMES	APDIPES
2 h	-22%	-45%	-4%
2 h	-18%	-35%	-1%
2 h + 2 h	-36%	-68%	-19%
4 h continuous	-31%	-58%	-6%

and contact angle goniometry (see Table 2.3). The thicknesses of the APTES, APDMES, and APDIPES layers increased by 1.5, 1.8, and 0.4 Å, respectively. These results suggest a small amount of irreversible contamination of the APTES and APDMES surfaces, but little or no contamination of the APDIPES surface. These results are consistent with the greater hydrophobicity (lower surface free energy) of the APDIPES surface contributing to a greater resistance to contamination. The advancing water contact angles of these surfaces were found to be essentially unchanged after 6 months of storage. Receding water contact angles were also measured and are reported in Table 2.3. In addition, ToF-SIMS was performed on these surfaces to further characterize them, where peaks corresponding to the following atomic and molecular fragments were found in all the negative ion ToF-SIMS spectra: H^-, C^-, CH^-, CH_2^-, O^-, OH^-, C_2^-, C_2H^-, CN^-, CNO^-, SiO_2^-, SiO_2H^-, SiO_3^-, and SiO_3H^-. It is significant that the CN^- peak was present for all the aminosilanes, as it is characteristically found in the ToF-SIMS spectra of materials that have C-N containing moieties.[17] Interestingly, the CNO^- ion, which was also present in all the spectra, may have resulted from amino groups ionically bonded to silanols through $NH_2^+/^-OSi$ interactions.

2.3.2. Cyanine dye adsorption

Freshly deposited silane films on glass slides and silicon wafers were treated with a 0.1 mM aqueous solution of the cyanine dye shown in Scheme 1. Glass slides were used for UV-VIS absorption measurements (Figure 2.3) and silicon wafers were used for water contact angle and ellipsometry measurements (Table 2.4). The UV-VIS results obtained in Figure 2.3 are typical of those found in these experiments; the most intense signals come from the APTES surface, followed by the APDMES surface, and finally by the APDIPES surface. Note that dye did not

Table 2.3. Sample wetting and thickness properties after six months of storage.

Property	APTES	APDMES	APDIPES
$\theta_a(H_2O)$	No change[a]	No change[a]	No change[a]
$\theta_r(H_2O)$	31 ± 1°	42 ± 0°	43 ± 1°
Film thickness	8.1 ± 0.2 Å	8.3 ± 1.0 Å	8.7 ± 0.6 Å

[a]Indicates that there was essentially no change in the advancing water contact angle ($\theta_a(H_2O)$) of the surfaces after 6 months of storage in the laboratory.

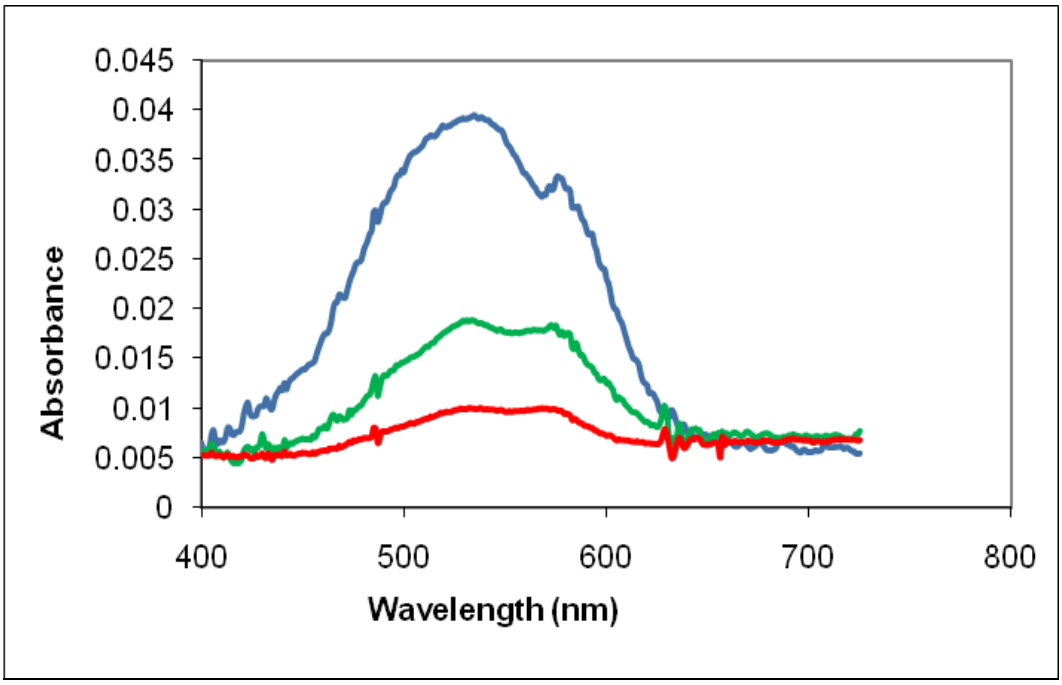

Figure 2.3. UV-Vis absorbance spectra of the cyanine dye adsorbed on APTES (blue), APDMES (green), and APDIPES (red) surfaces.

Table 2.4. Ellipsometry and water contact angle data obtained after dye treatment. These data were obtained from three separate experiments.

Aminosilane	Contact angle after dye adsorption	Adsorbed dye thickness (Å)
APTES	32.3 ± 2.3	14.5 ± 1.2
APDMES	51.3 ± 0.6	11.7 ± 0.8
APDIPES	63 ± 2	7 ± 1

adsorb onto clean glass surfaces, *i.e.*, those that were not coated with an aminosilane. The broad absorbance band centered around 520 nm is attributable to the dimer of the dye, while the monomer absorbs at 563 nm.[18] That is, the dimer and monomer peaks have roughly the same height for the APDIPES and APDMES surfaces, but the dimer peak dominates on the APTES surface. These results seem reasonable in light of both the structure of the dye (*vide infra*) and also the higher number of amine groups on the APTES surface, followed by APDMES, and finally APDIPES (*vide supra*).

During deposition, the glass slides lay flat on the surface of one of the plates. Because there are holes in the plates, and we have two hard surfaces placed against each other, there was some question as to whether the silane would primarily deposit on the upper surface of the slide, or on both sides. The top curve (blue) in Figure 2.4 shows the adsorbance of an APTES-coated glass slide after immersion in the cyanine dye solution. The middle curve shows the absorbance of the slide after one side was wiped and rubbed with a wet tissue. The bottom curve shows the absorbance after both sides of the glass slide were rubbed with the wet tissue. We conclude that both sides of the glass slides were coated during silane deposition.

Thicknesses of films and water contact angle measurements after dye adsorption are compared in Table 2.4, where the water contact angles on the dye-coated surfaces decrease going from APDIPES to APDMES to APTES, *i.e.*, the more dye that is adsorbed, the lower the water contact angle. This decrease in water contact angle with increase in dye adsorption seems reasonable in light of the quaternary amine on the dye, which is extremely hydrophilic. In addition, one might expect the dye to adsorb through ionic interactions between its two sulfonate groups and two protonated amine groups on an aminosilane surface. If a dye were attached in this manner, one might imagine the dye film thickness to be that of a chain of atoms running

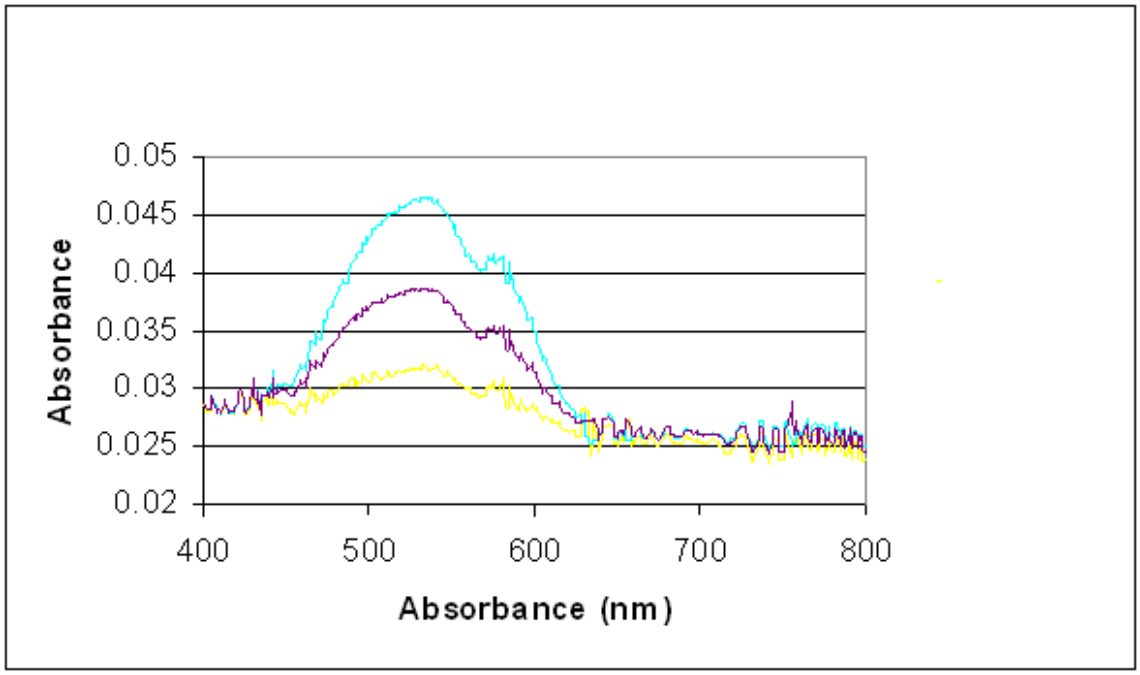

Figure 2.4. UV-Vis absorbance spectra of a cyanine dye adsorbed on APTES: untreated sample after dye adsorption (light blue), sample with one side rubbbed with wet tissue after dye adsorption (purple), and sample with both sides rubbed with the wet tissue after dye adsorption (yellow).

through the sulfonate group, the four-carbon alkyl chain, and the five-membered ring. The length of this chain, assuming the chains are standing, would be on the order of 11 – 14 Å, which is the change in thickness observed for the APTES and APDMES surfaces. If there were only partial coverage of the dye, the change in thickness would be less, *e.g.*, 7Å, as is observed for the APDIPES surface.

2.3.3. Comparison to previous vapor phase work

Table 2.5 provides a comparison of our results to four other APTES surfaces reported in the literature, which were deposited by CVD onto silicon, mica, and alumina. It should be noted that different deposition conditions and substrates would be expected to lead to somewhat different APTES films. For example, Fiorilli and coworkers reported the water contact angles of APTES surfaces prepared on silica wafers without and with water vapor.[2] Their surfaces prepared without water vapor would be closest to ours and show a water contact angle of 38°, which is not far from our result. Crampton[7] reported APTES deposition on mica in the presence of Hünig's base (diisopropylethylamine) under high (60%) and low (7%) humidity conditions. As expected, the thickness of our APTES film is in quite good agreement with their low humidity result (5.4 Å) and not their high humidity result (10.8 Å). Kurth and Bein[10] obtained similar results for deposition on dry surfaces (5 ± 1 Å) *vs*. water-hydrolyzed surfaces (11 ± 1Å). Smith and Chen obtained relatively thin (3.5 Å) films after APTES deposition at 70°C.[16] Interestingly, our APTES films are generally somewhat thicker than all of those reported in Table 2.5. One possible explanation for this difference is that our higher deposition temperature may allow more APTES molecules to deposit on the surface, overcoming some of the steric hindrance around chemisorbed silanes.

Table 2.5. Comparison of our results to other results of silane vapor phase deposition.

Silane	Thickness	Water Contact Angle (θ_a/ θ_r)	Roughness	Comments (All are vapor phase depositions.)
Literature Results				
APTES[2]	----	38° w/o water vapor 50° w/ water vapor	Aggregation <30nm	3 Torr, 10 min, 80°C, silicon substrate.
APTES with Hünig's base[7]	5.4 Å (7% rel. humid) 10.8 Å (60 % rel. humid)	---	----	Room temperature (RT), mica substrate.
APTES[10]	5 Å (dry) 11 Å (wet: pretreated w/ water vapor)	50° (dry) 65° (wet)	----	RT, atm. pressure, Al/Al_2O_3 substrate.
APDMES[16]	3.5 Å	67/42°		Deposition at 70°C on Si/SiO_2.
*Our Results**				Deposition at 150°C on Si/SiO_2.
APTES	6.6 Å	44/31°	0.074 ± 0.010 nm	
APDMES	6.5 Å	58/42°	0.058 ± 0.010 nm	
APDIPES	8.3 Å	64/43°	0.050 ± 0.005 nm	
Related Silane				
APMDES[1]	10 ± 2 Å	60 - 65°	----	RT, 125 – 150 mm Hg

*Note that our receding contact angles were measured after sample storage in the laboratory. However, because the properties of the surfaces hardly changed after storage, the receding water contact angles measured after the stability test are probably very close to the receding water contact angles that would have been measured initially, had this been done.

A higher deposition temperature would be expected to increase mobility of both physisorbed and chemisorbed silanes, ultimately leading to greater surface functionality. By AFM, our aminosilane surfaces are very flat – nearly as flat as bare silicon. Fairly large features were present in Fiorilli's APTES layer.[2] In a study employing a silane related to those we used, Anderson[1] deposited 3-aminopropyl-1-(methyldiethoxysilane) (APMDES), which has only one methyl group instead of the two in our APDMES, at moderately high pressures (125 – 150 mm Hg) in a dessicator. Comparing the thickness of their film to those that Crampton and Bein made under their more humid conditions suggests that Anderson's film has some multilayer character. The overall conclusion that can be drawn from Table 2.5 is that our results, and in particular our APTES results, are in good agreement with those previously reported, and suggest the formation of dense, high quality surfaces.

2.3.4. Discussion

The results of my first stability test (immersion in a pH 10 buffer) should be compared to Smith and Chen's study of APDMES and APTES monolayers (prepared in toluene at 70°C), and an APDMES monolayer prepared by vapor phase deposition at 70°C, which were immersed in water at 40°C for 24 h or 48 h.[16] After these stability experiments, their APTES monolayers were nearly completely removed, while their APDMES films were up to half removed. In contrast, under basic conditions, we found APTES monolayers to be more stable than APDMES films. An noted, films were prepared at a higher temperature (150°C), which probably allowed for greater reagent mobility and reactivity and therefore more complete surface coverages. In addition, this higher temperature might allow APTES to bind more frequently through two Si-O bonds, further increasing its stability.

In the report of Smith and Chen, they found an aminosilane: *N*-(6-aminohexyl)aminomethyltriethoxysilane [$(EtO)_3SiCH_2NH(CH_2)_6NH_2$, AHAMTES], that yielded monolayers with much greater stability against hydrolysis than APTES or APDMES.[16] They attributed this significant improvement in aminosilane monolayer stability to the inability of AHAMTES to form five-membered rings by nucleophilic attack of its amine group on its own silicon atom. Such five-membered rings in APTES or APTMES could, in the presence of water, lead to hydrolysis of the Si-O bond, where an amino group on a given silane molecule could similarly attack and help hydrolyze the Si-O bonds of other aminosilane adsorbates.[19] In any case, this earlier work begs the question regarding the enhanced hydrolytic stability of our APDIPES surfaces. Thus, it is not entirely clear whether the stability of our APDIPES surfaces is due to the hydrophobicity of the isopropyl groups, or perhaps more likely, to a combination of this effect with the steric hindrance they provide their silicon atoms, which would limit both five-member ring formation as well as nucleophilic attack by the nitrogen atom of an adjacent silane.

2.4. Conclusions

Covalently bonded monolayers of two monofunctional aminosilanes (3-aminopropyldimethylethoxysilane (APDMES), and 3-aminopropyldiisopropylethoxysilane APDIPES) and one trifunctional aminosilane (3-aminopropyltriethoxysilane, APTES) were deposited on dehydrated silicon substrates by chemical vapor deposition (CVD) at 150°C and low pressure (a few Torr). XPS data further indicate that the N1s/Si2p ratio is higher after CVD with the trifunctional silane (APTES) compared to the monofunctional ones, with higher N1s/Si2p ratio for APDMES compared to APDIPES. AFM images show an average surface roughness of 0.12 - 0.15 nm among all three aminosilane films. Stability tests indicate that

APDIPES films retain most of their integrity at pH 10 for several hours, and are more stable than APTES or APDMES layers. The films also showed good stability against storage in the laboratory. Optical absorption measurements on adsorbed cyanine dye at the surface of the aminosilane films showed the formation of dimer aggregates on the surface. This was further supported by ellipsometry measurements. The concentration of dye on each surface appears to be consistent with the density of the amines.

These results stand in contrast to those obtained in typical liquid phase depositions of silanes. That is, unless the water concentration in a solution is very tightly controlled, *e.g.*, the reagents are all very dry, the concentration of an aminosilane in the deposition solution would be expected to strongly influence the thickness of the resulting silane films. In our study, because the number of surface sites is limited, silane concentration over a wide range does not affect surface coverage. As a corollary to this statement, the lack of dependence of surface properties on deposition conditions should lead to robustness in an industrial (or other) process, *i.e.*, a small change in silane volume (an important process variable) should have little or no effect on the final film. That is, gas phase silane deposition shows industrial viability.

The wetting of the silane films is clearly a function of molecular structure. The diisopropyl silane shows a higher water contact angle than the dimethyl silane, which in turn is higher than APTES (the triethoxysilane).

The fact that essentially the same films are obtained with either a large or a small volume of any of the three aminosilanes is important because it allows one to use a small volume of the reagent. We assume that the same results will be found with other silanes. Clearly, this will lower the cost of processes and make them more environmentally friendly.

XPS suggests that we can control the density of the amine groups on a silicon oxide surface by changing the structure of the adsorbate, *i.e.*, changing the nature of the groups around the silicon atom in a silane ultimately changes the density of that silane on a surface.

We can control the hydrolytic stability of adsorbed aminosilanes by changing the structure of the adsorbate. Indeed, the hydrolytic stability is substantially improved when bulky side groups are attached to silicon.

We appear to be able to control the amount of dye that adsorbs, and its aggregation, on a surface by changing the density of amine groups on the surface.

This controllable, robust, and clean process provides a straightforward way to make high quality monolayers with active amino groups for semiconductor surface modification, biosurface fabrication, optical material improvement, *etc*. Based on various surface physical properties, this series of amino layers presents multiple choices for practical applications and demonstrates the possibility of producing desirable surface properties by selecting and designing the layer precursors. Properties intermediate between those reported herein could probably be obtained using mixtures of these silanes.

2.5. References

1. Anderson, A. S.; Dattelbaum, A. M.; Montan˜o, G. A.; Price, D. N.; Schmidt, J. G.; Martinez, J. S.; Grace, W. K.; Swanson, B. I., *Langmuir* **2008,** *24*, 2240-2247.
2. Fiorilli, S.; Rivolo, P.; Descrovi, E.; Ricciardi, C.; Pasquardini, L.; Lunelli, L.; Vanzetti, L.; Pederzolli, C.; Onida, B.; Garrone, E., *J. Colloid Interface Sci.* **2008,** *321*, 235-241.
3. Saini, G.; Sautter, K.; Hild, F. E.; Pauley, J.; Linford, M. R., *J. Vac. Sci. Technol. A* **2008,** *26*, 1224-1234.

4. Hozumi, A.; Yokogawa, Y.; Kameyama, T.; Sugimura, H.; Hayashi, K.; Shirayama, H.; Takai, O., *J. Vac. Sci. Technol. A* **2001,** *19*, 1812-1816.

5. Ressier, L.; Grisolia, J.; Peyrade, J. P., *Ultramicroscopy* **2007,** *107*, 980-984.

6. Hozumi, A.; Ushiyama, K.; Sugimura, H.; Takai, O., *Langmuir* **1999,** *15*, 7600-7604.

7. Crampton, N.; Bonass, W. A.; Kirkham, J.; N.H, T., *Langmuir* **2005,** *21*, 7884-7891.

8. Arroyo-Hern´andez, M.; Manso-Silvan, M.; L´opez-Elvira, E.; Mu˜noz, A.; Climent, A.; Mart´ınez Duart , J. M., *Biosens. Bioelectron.* **2007,** *22*, 2786–2789.

9. Du, Y.; George, S. M., *J. Phys. Chem. C* **2007,** *111*, 8509-8517.

10. Kurth, D. G.; Bein, T., *Langmuir* **1995,** *11*, 3061-3067.

11. Vandenberg, E. T.; Information, C.; Bertilsson, L.; Liedberg, B.; Uvdal, K.; Erlandsson, R.; Elwing, H.; Lundström, I., *J. Colloid Interface Sci.* **1991,** *147*, 103-118.

12. Kirkland, J. J.; Glajch, J. L.; Farlee, R. D., *Anal. Chem.* **1989,** *61*, 2-11.

13. Zhang, F.; Sautter, K.; Davis, R. C.; Linford, M. R., *Langmuir* **2009,** *25*, 1289-1291.

14. Howarter, J. A.; Youngblood, J. P., *Langmuir* **2006,** *22*, 11142-11147.

15. Kim, J.; Seidler, P.; Sze Wan, L.; Fill, C., *J. Colloid Interface Sci.* **2009,** *329*, 114-119.

16. Smith, E. A.; Chen, W., *Langmuir* **2008,** *24*, 12405-12409.

17. Saini, G.; Gates, R.; Asplund, M. C.; Blair, S.; Attavar, S.; Linford, M. R., *Lab Chip* **2009,** *9*, 1789-1796.

18. Yao, H.; Isohashi, T.; Kimura, K. J., *Phys. Chem. B* **2007,** *111*, 7176-7183.

19. Etienne, M.; Walcarius, A., *Talanta* **2003,** *59*, 1173-1188.

Chapter 3. Chemical Vapor Deposition of 3-Mercaptopropyltrimethoxysilane as an Adhesion Promoter for Gold Mirrors

3.1. Introduction

3-mercaptopropyltrimethoxysilane (MCPTMS) monolayers have been widely used for surface modification on different materials including semiconductors, polymers, and metals.[1-3] This silane monolayer can bind metal nano particles and metal films because of the strong bond between sulfur and many metals.[4-6] Gray-Munro used this monolayer to improve the corrosion resistance of a magnesium alloy.[7] Zhang explored the structure of MCPTMS monolayers and their influence on oriented deposition of crystalline SnO_2 films.[8] Cabrera investigated Pt electrodeposition on copper surfaces modified with MCPTMS monolayers.[9] MCPTMS monolayers have also been applied in the preparation of gold mirrors. In his patent of adhesion of metals to solid substrates, McGee first discussed the adhesion of gold on MCPTMS monolayers.[10] Goss applied MCPTMS monolayers for fabrication of gold electrodes and illustrated the advantages of thiol monolayers over chromium layers because chromium films can compromise the quality of gold layers.[11] Chung prepared micro and nano gold patterns on glass coated with an MCPTMS layer by transfer printing.[12] Ben Ali enhanced gold adhesion with this silane layer for biosensor applications.[6] Newton investigated the electrical properties of gold films on MCPTMS monolayers.[13] Rubinstein explored the morphology and optical properties of gold films on MCPTMS monolayers.[14] His results showed that roughnesses of these gold mirrors can be up to tens of nanometers.

Clearly, MCPTMS deposition has been important for metal attachment and deposition. However, most of this prior work, including all of the references in the previous paragraph, was

implemented in the solution phase. Nevertheless, there are a few examples of chemical vapor deposition (CVD) of MCPTMS to prepare monolayers. Busca deposited MCPTMS by CVD and studied the IR structure of the resulting monolayers.[15] Janes demonstrated that vapor phase deposition of MCPTMS for gold mirror deposition can improve roughnesses by several Ångstroms.[16] Scott's work confirmed this point on an elastomeric substrate.[17] Our previous work also showed very flat films of silane monolayers with CVD.[18] CVD has other advantages including lower volumes of reagent employed and robust processing.

Here, I prepared MCPTMS monolayers by CVD. This monolayer served as an adhesion promoter for gold mirrors for vibrationally resonant sum-frequency generation (VR-SFG) spectroscopy. The work of my collaborator, Arthur D. Quast, illustrated that gold mirrors on this monolayer have the advantage of not needing the typical chromium adhesion layer between the gold and fused silica, meaning they can be used as either front or back surface mirrors. As a result, there seems to be little or no interference in the nonresonant SFG profile from the adhesion layer. The MCPTMS adhesion layer also provides good long-term stability for the gold mirror.

3.2. Experimental

3.2.1. Materials and Chemicals

All materials and chemicals were used as received unless otherwise specified. 3-Mercaptopropyltrimethoxysilane (95%) was purchased from Gelest Corporation, Morrisville, PA. Sulfuric acid (93%) was obtained from Mallinckrodt, Phillipsburg, NJ. Hydrogen peroxide (30%) was from Fischer Scientific, Waltham, MA. HPLC grade chloroform was obtained from EMD Chemicals, Gibbstown, NJ. Rinsing water was obtained from a Millipore Milli-Q RG water

system with a resistivity of 18 MΩ-cm. Nitrogen and oxygen were obtained from Airgas and used as received. Single polished silicon wafers (100) were from Unisil Corporation, Santa Clara, CA. Fused silica discs (1" diameter and 1/8" thickness) were purchased from Chemglass Life Sciences, Vineland, NJ.

3.2.2. Pretreatment of samples

Fused silica discs and silicon wafers were sonicated in chloroform for 1 min. The samples were then immersed in 120°C piranha solution (70% concentrated sulfuric acid and 30% hydrogen peroxide) for 2 h. Samples were rinsed with copious amounts of water and stored in water. Before coating, the discs were dried under a stream of nitrogen.

3.2.3. CVD of MCPTMS

Coating with MCPTMS took place in a YES 1224P CVD system, which was obtained from Yield Engineering System, Lawrenceville, CA. Before deposition, the chamber was primed with MCPTMS first. Three batches of samples were then made. The first batch was prepared by introduction of 1 mL liquid MCPTMS into an evacuated chamber at 1 torr over 5 min at 150°C. The second batch was prepared by the same method as the first but the samples were left in a nitrogen-purged oven at 150°C for 20 min after coating. The third batch was prepared by the same method as the first but was followed by the introduction of 0.3 mL of liquid water at a chamber temperature of 150°C. After removal of each MCPTMS batch from the oven, all samples were immediately placed in high purity water.

3.2.4. Characterization of MCPTMS surfaces

The MCPTMS coated silicon samples were characterized by contact angle goniometry, TOF-SIMS, XPS, AFM, and spectroscopic ellipsometry.

3.2.5. Gold deposition and peel test (collaborator's work)

Prior to gold deposition, the samples were taken from the water storage bath and dried under a stream of dry nitrogen. Approximately 90 nm layer of gold (99.99% purity) was then thermally evaporated onto the discs, after which they were removed and stored for testing. Samples were tested for gold adhesion with conventional transparent tape using the "Scotch Tape" test; a piece of tape was attached to the gold surface and peeled away.

3.3. Results and discussion

Table 3.1 shows the characterization of MCPTMS monolayers. For three batches, all samples showed consistent contact angles, ratios of sulfur to silicon by XPS, and roughness. These results illustrated that all surfaces have the same or nearly the same sulfur group coverage and morphology. The thicknesses of the second and third batches were different from that of the first batch. This several angstrom difference might be from detection errors of thickness measurements or from surface contamination (these samples were kept in the oven longer than the first). The roughness results indicated that the MCPTMS monolayer is very flat and uniform. PCA analysis of the ToF-SIMS data could not separate any of these samples, also pointing to their similarity.

A peel test was performed to measure the adhesion strength of gold to the silane monolayers. Results showed that the gold layer could be easily peeled off from bare fused silica

Table 3.1. Characterization of MCPTMS monolayers by ellipsometry, contact angle goniometry, XPS, and AFM.

Batch	Thickness	Contact angle	S/Si	Roughness
1	6.4 ± 0.1 Å	60°	0.19 ± 0.01	0.12 ± 0.00 nm
2	10.6 ± 0.9 Å	60°	0.20 ± 0.01	0.10 ± 0.00 nm
3	10.3 ± 2.3 Å	60°	0.19 ± 0.02	0.13 ± 0.03 nm

and silicon surfaces. However, the gold layers cannot be removed from the MCPTMS surfaces. After four weeks, the gold layers still retain their integrity on MCPTMS surfaces.

3.4. Conclusions

Chemical vapor deposition (CVD) of 3-mercaptopropyltrimethoxysilane on silicon and quartz was explored. Several deposition conditions were investigated. Surface characterization showed that there is not any structure or morphological differences between these samples. All deposited surfaces have similar thicknesses, water contact angles, and ratios of sulfur to silicon by XPS. A principal components analysis (PCA) of ToF-SIMS data could not separate the silane monolayers, pointing to their similarity. Peel tests demonstrated the stability of gold on the mercaptosilane layers.

3.5. References

1. Liu, X.; Wang, Q.; Chen, L.-P., *Appl. Surf. Sci.* **2009,** *255*, 3789–3794.
2. Sawada, S.; Masuda, Y.; Zhu, P.; Koumoto, K., *Langmuir* **2006,** *22*, 332-337.
3. Scott, A.; Gray-Munro, J. E., *Thin Solid Films* **2009,** *517*, 6809–6816.
4. Riskin, A.; Dobbelaere, C. D.; Elen, K.; D'Haen, J.; Rul, H. V. d.; Mullens, J.; Hardy, A.; Bael, M. K. V., *Phys. Status Solidi A* **2010,** *207*, 864–871.
5. Park, H.; Kim, A.; Lee, C.; Lee, J.-S.; Leea, J., *Appl. Phys. Lett.* **2009,** *94*, 213508.
6. Ali, M. B.; Bessueille, F.; Chovelon, J. M.; Abdelghani, A.; Jaffrezic-Renault, N.; Maaref, M. A.; Martelet, C., *Mater. Sci. Eng., C* **2008,** *28*, 628–632.
7. Scott, A. F.; Gray-Munro, J. E.; Shepherd, J. L., *J. Colloid Interface Sci.* **2010,** *343*, 474-483.

8. Zhang, J.; Zhang, M.; Li, W.; Zhai, Y., *AIChE J.* **2007,** *53*, 2957-2967.

9. Tremont, R. J.; Cruz, G.; Cabrera, C. R., *J. Electroanal. Chem.* **2003,** *558*, 65-74.

10. Mcgee, J. B. Adhesion of metals to solid substrates, Patent 4315970, United States. 1982.

11. Goss, C. A.; Charych, D. H.; Majda, M., *Anal. Chem.* **1991,** *63*, 85-88.

12. Oleksandrov, S.; Lee, J.; Lee, S.; Lee, M.-G.; Choi, H. Y.; Chung, C.-H., *J. Nanosci. Nanotechnol.* **2009,** *9*, 7481-7484.

13. M I Newton, G. M.; Hooper, P. D., *Vacuum* **1995,** *46*, 315-318.

14. Doron-Mor, I.; Barkay, Z.; Filip-Granit, N.; Vaskevich, A.; Rubinstein, I., *Chem. Mater.* **2004,** *16*, 3476-3483.

15. Finocchio, E.; Macis, E.; Raiteri, R.; Busca, G., *Langmuir* **2007,** *23*, 2505-2509.

16. Mahapatro, A. K.; Scott, A.; Manning, A.; Janes, D. B., *Appl. Phys. Lett.* **2006,** *88*, 151917.

17. Atmaja, B.; Frommer, J.; Scott, J. C., *Langmuir* **2006,** *22*, 4734-4740.

18. Zhang, F.; Sautter, K.; Larsen, A. M.; Findley, D. A.; Davis, R. C.; Samha, H.; Linford, M. R., *Langmuir* **2010,** *26*, 14648-114654.

Chapter 4. Laser Activation Modification of Semiconductor Surfaces (LAMSS)*

4.1. Introduction

Recently, there has been much interest in using light to derivatize surfaces. For example, in their work on machining microchannels, Waddell and co-workers noted that the surface of a substrate, in particular, a polymer, could undergo a chemical change if it were ablated with photons while it was in the presence of a reactive atmosphere.[1-2] Calvert and co-workers first demonstrated the patterning of siloxane monolayers with light; they showed that Si-C bonds in siloxane monolayers could be cleaved by UV photons.[3-4] Surface regions that were exposed in this manner were shown to react subsequently with other silanes. Hartmann and co-workers have studied laser ablation in the air of alkylsiloxane monolayers on oxidized silicon substrates.[5-6] Monolayers on gold have also been patterned with a laser in atmospheres of nitrogen[7] and air.[8] In addition, light has been used to induce monolayer formation on and/or to pattern hydrogen-terminated,[9-14] iodine-terminated,[15] and porous silicon surfaces,[16-17] although these latter procedures required exposure times to light ranging from a few minutes up to a few hours, where 30 min was typical.

The LAMSS technique (laser activation of a semiconductor surface wet with a reactive liquid) requires only a single laser pulse to drive the reaction to completion. Multiple pulses at a single point would probably serve only to ablate, refunctionalize, or even damage an already functionalized region. The LAMSS method also bears some similarity to the chemomechanical modification of silicon surfaces in that in both methods silicon is disrupted or exposed to create a chemically active surface.[18]

---

*Taken from (Feng Zhang, Lei Pei, Eliot Bennion, Guilin Jiang, David Connley, Li Yang, Michael V. Lee, Robert C. Davis, Vincent S. Smentkowski, Greg Strossman, Matthew R. Linford, Matthew C. Asplund) *Langmuir*, **2006**, *22*, 10859–10863. Copyright 2006 American Chemical Society.

4.2. Experimental

4.2.1. Materials and chemicals

All materials and chemicals were used as received unless otherwise specified. Single polished silicon wafers (100) were from Unisil Corporation, Santa Clara, CA. Germanium wafers were purchased from Wafer World Corporation, West Palm Beach, FL. Sodium dodecyl sulphate (98.5%), 1-hexene (99%), 1-decene (97%), 1-tetradecene (97%), octane (99%), 1-iodooctane (98%), 1-octene (98%), 1-dodecene (99%), 1-hexadecene (99%), 1-chlorooctane (99%), 1-bromooctane (99%), 1-octanol (99%), 1,2-epoxyoctane (95%), 1,2,7,8-diepoxyoctane (97%), 1,7-octadiene (97%), hydrochloric acid (ACS reagent, 37%), polylysine solution (0.1 % (w/v) in water), and hexadecane (99%) were purchased from Sigma-Aldrich.

4.2.2. Laser ablation

Laser ablation was induced by pulses from a Nd:YAG (Coherent Infinity) laser. Laser energy was focused by a short focus (50 mm) lens onto the sample. Samples were prepared using 50 mJ of 532 nm light or 25 mJ of 355 nm light. The pulse length was 4 ns. The laser was run at 1 Hz to guarantee that only one laser pulse was incident on each spot of the silicon sample.

4.2.3. LAMSS

LAMSS was performed in an open laboratory with compounds that were not degassed or specially treated in any way. The process can be briefly described as following: 0.05 ml solvent was dropped on surfaces of silicon or germanium, and laser ablation was performed on the solvent area. After ablation, samples were cleaned by agitation with a solution of 2% sodium dodecyl sulphate in water, rinsed with water, and dried with a jet of nitrogen.

4.2.4. Sample characterization

Samples were characterized with X-ray photoelectron spectroscopy (XPS), time-of-flight secondary ion mass spectrometry (ToF-SIMS), and atomic force microscopy (AFM). The XPS instruments had monochromatic Al Kα sources and hemispherical analyzers [SSX-100 spectrometer (Figures 4.3) or a PHI Quantum 2000 instrument (Figure 4.4, Table 4.1, and Table 4.2)]. The PHI instrument employed a small spot size (50, 100, or 200 μm) that fit inside the spots it analyzed. For the SSX-100 instrument a larger area of the surface was functionalized and analyzed. ToF-SIMS was performed with an ION-TOF TOF-SIMS IV instrument with monoisotopic 25 KeV $^{69}Ga^{+}$ primary ions in bunched mode. AFM was performed with a Veeco Dimension 3100 Atomic Force Microscope.

4.3. Results and discussion

LAMSS on clean, native-oxide-terminated silicon and germanium appears to be possible with a number of adsorbates. For example, Figure 4.1 shows representative ToF-SIMS negative ion images of LAMSS spots of Si that was wet with 1-hexene, 1-decene, 1-tetradecene, and octane. Lighter areas represent higher intensities of ions; darker areas represent lower intensities of ions. Figure 4.1e shows ToF-SIMS negative ion images of LAMSS of a clean germanium surface that was wet with 1-iodooctane. The chemical contrast evident in these images is consistent with chemical modification of the silicon and germanium in the spots with the hydrocarbon compounds. These results are quite general. Similar images with similar chemical contrast are found for LAMSS of silicon wet with 1-octene, 1-dodecene, 1-hexadecene, 1-chlorooctane, 1-bromooctane, 1-iodooctane, 1-octanol, 1,2-epoxyoctane, and 1,2,7,8-

diepoxyoctane. ToF-SIMS shows the expected halogen ions from the haloalkanes, as in Figure 4.1e.

ToF-SIMS ion images of LAMSS of germanium wet with 1-hexadecene also show similar chemical contrast between spots and background regions as is found in Figure 4.1.

To better understand the chemical nature of the variation in the spectral images shown in Figure 4.1, a multivariate analysis of the data was performed using the multivariate curve resolution (MCR) feature of the automated expert spectral image analysis (AXSIA) method.[19-20] AXSIA reduces ToF-SIMS images to a limited number of components that sufficiently describe the chemical variation at a surface; AXSIA components better represent the chemical information at a sample surface than individual ToF-SIMS images of single ions.

Figure 4.2 shows a few ion images from a LAMSS spot made on silicon that was wet with 1-decene, images of the AXSIA components in red, green, and blue that were derived from an AXSIA analysis of this ToF-SIMS data, and some AXSIA spectral components from a spot made with 1-hexadecene. These results are quite general. A large number of ToF-SIMS images of LAMSS spots made with different hydrocarbon reagents were analyzed by AXSIA. AXSIA almost always finds three components. One component corresponds to the background, away from the LAMSS spot, that is rich in O^-, OH^-, F^-, and Cl^- and that also contains small SiO_2^- and SiO_3^- ions. The two other AXSIA components are usually quite similar and come from the LAMSS spot. These two components contain larger fractions of H^- and CH^- ions than the background component and fewer oxygen-containing ions and halogen contaminents. Note that ToF-SIMS is very sensitive to trace halogens—XPS suggests that chlorine and fluorine contamination at and around LAMSS spots is at very low levels (*vide infra*). The upshot of these results is that, although the matrix effect of SIMS prevents quantification by direct comparison

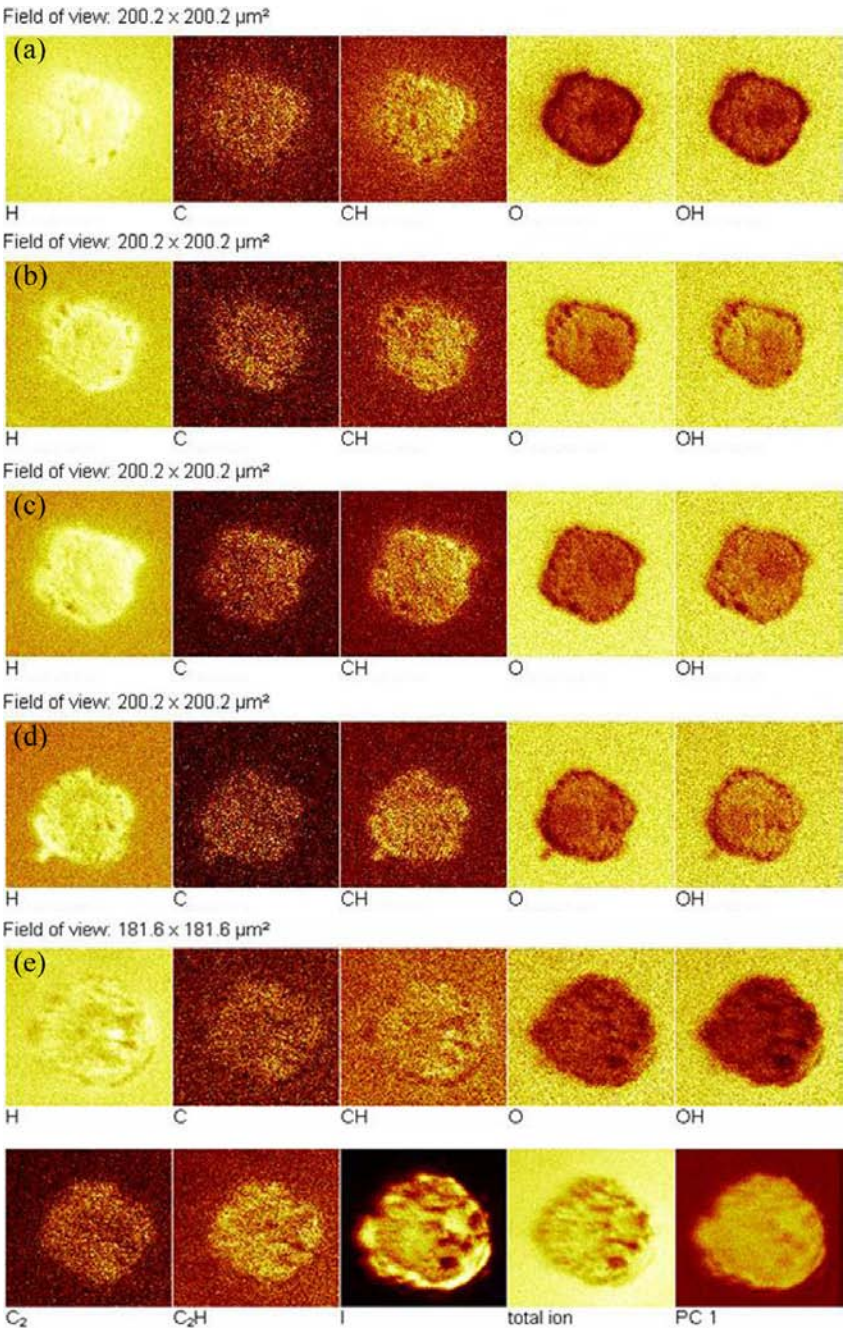

Figure 4.1. ToF-SIMS negative ion images of LAMSS of Si wet with (a) 1-hexene, (b) 1-decene, (c) 1-tetradecene, (d) octane, and (e) Ge under 1-iodooctane. A total ion image and the image of the first principal component from a principal components analysis using the instrument software are shown for the LAMSS spot on Ge.

(a)

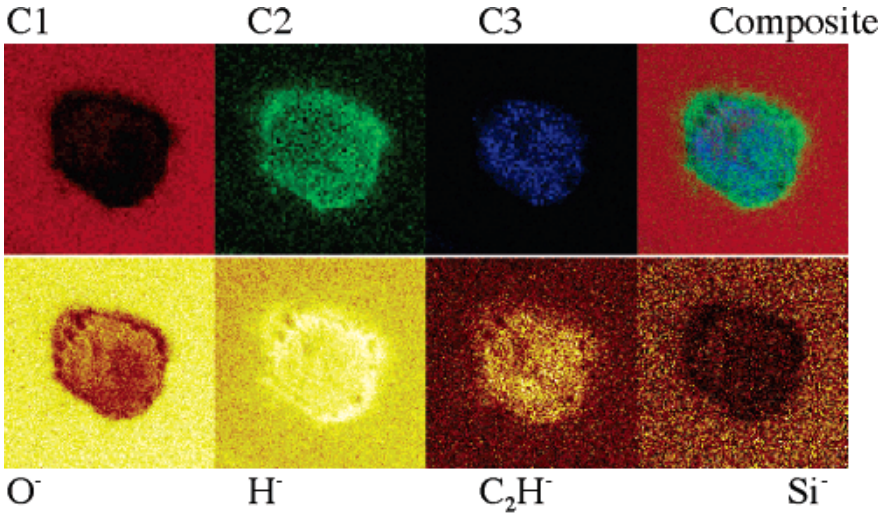

(b)

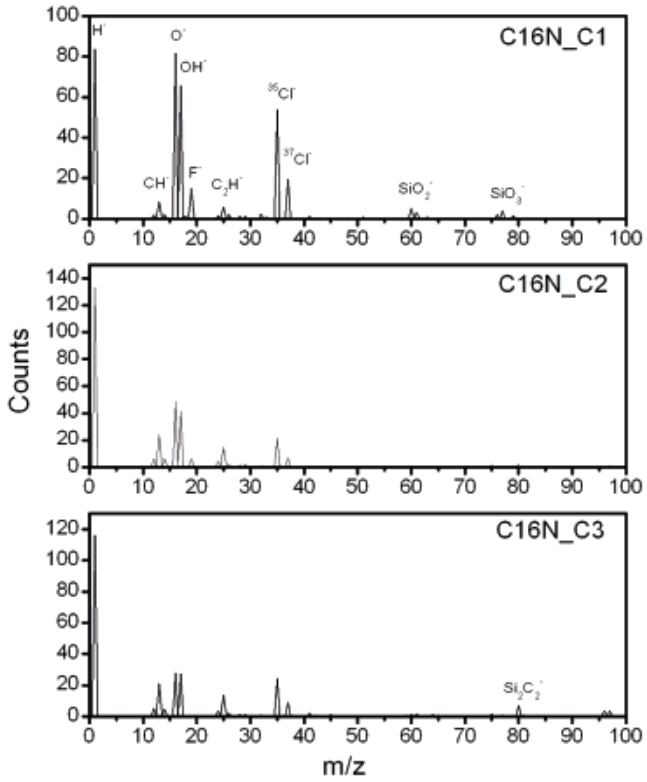

Figure 4.2. (a) Negative ion AXSIA spectral images, a composite image of AXSIA components 1-3 (C1-C3), and single ion images of ToF-SIMS of silicon surfaces modified by LAMSS with 1-decene. (b) Spectra of AXSIA components of silicon modified by LAMSS with 1-hexadecene. [This figure is a modification of Figure VI.1. and VI.3. in Chapter VI of Guilin Jiang's doctoral dissertation. Dr. Jiang was a coauthor on this paper, and has given permission for the use of this figure in my thesis.]

between peaks, ToF-SIMS reveals chemical variation between the LAMSS spots and their backgrounds that is consistent with hydrocarbon functionalization at the LAMSS spots. As noted, this analysis suggests increased levels of hydrogen in the LAMSS spots, which is valuable information that cannot be obtained by XPS.

XPS was also used to probe the elemental composition of LAMSS spots and control regions on silicon. Figure 4.3 shows XPS survey spectra of (a) a blank region on a silicon surface that had been wet with 1-hexadecene but not exposed to a pulse of laser light and (b) a LAMSS spot made with 1-hexadecene. The control region shows strong oxygen, carbon, and silicon signals, where the carbon in this spectrum is presumably due to adventitious material. The survey spectrum from the LAMSS spot in Figure 4.3b also shows primarily oxygen, carbon, and silicon, but the elements appear to exist in different ratios than in the control region; the oxygen signal appears to be somewhat reduced, and the carbon signal, increased. The C 1s/Si 2p and/or O 1s/Si 2p ratios of LAMSS spots made with 1-hexadecene, of 1-hexadecene control regions, of LAMSS spots made with 1-iodooctane, of 1-iodooctane control regions, and of a 1-hexadecene monolayer on hydrogen-terminated silicon are given in Table 4.1. It is noteworthy in these results that the C 1s/Si 2p ratio for the LAMSS spot prepared under 1-hexadecene is similar to the C 1s/Si 2p ratio obtained from a 1-hexadecene monolayer on hydrogen-terminated silicon and that the O 1s/Si 2p ratios for the LAMSS spots are smaller than the ratios found in control regions.

XPS narrow scans provide additional information about control and LAMSS spots. Figure 4.4 shows XPS narrow scans of the C 1s and Si 2p regions that correspond to the survey spectra shown in Figure 4.3 and that indicate the oxidation states of the carbon and silicon atoms at the surfaces. The C 1s narrow scan of the control region (Figure 4.4b) suggests mostly carbon

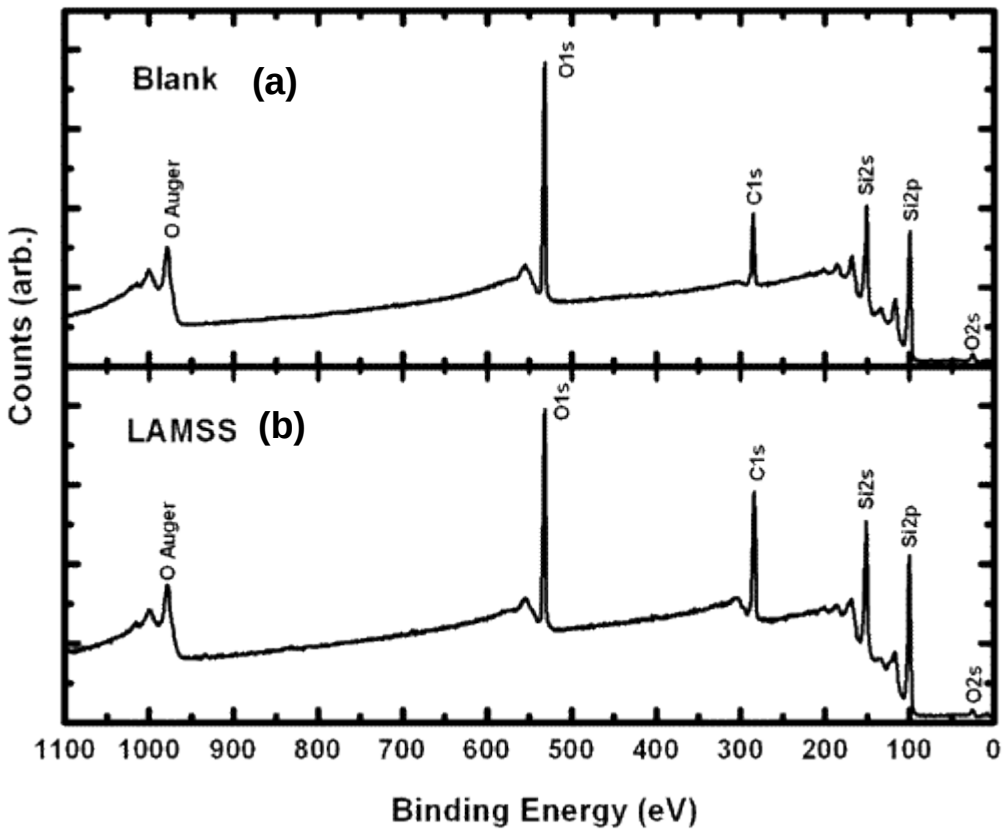

Figure 4.3. XPS survey spectra of a silicon surface that had been wet with 1-hexadecene. (a) Blank region that was not exposed to a pulse of laser light. (b) LAMSS spot.

Table 4.1. C 1s/Si 2p and O 1s/Si 2p XPS ratios of LAMSS spots and control regions

Surface composition	C 1s/Si 2p ratio	O 1s/Si 2p ratio
1-hexadecene	1.12 ± 0.05	0.66 ± 0.02
1-hexadecene control	0.67 ± 0.03	0.87 ± 0.01
1-iodooctane	0.66 ± 0.05	0.64 ± 0.03
1-iodooctane control	0.23 ± 0.02	0.84 ± 0.01
1-hexadecene on hydrogen terminated silicon.[18] 16 Å. (Literature control)	1.27 ± 0.03	

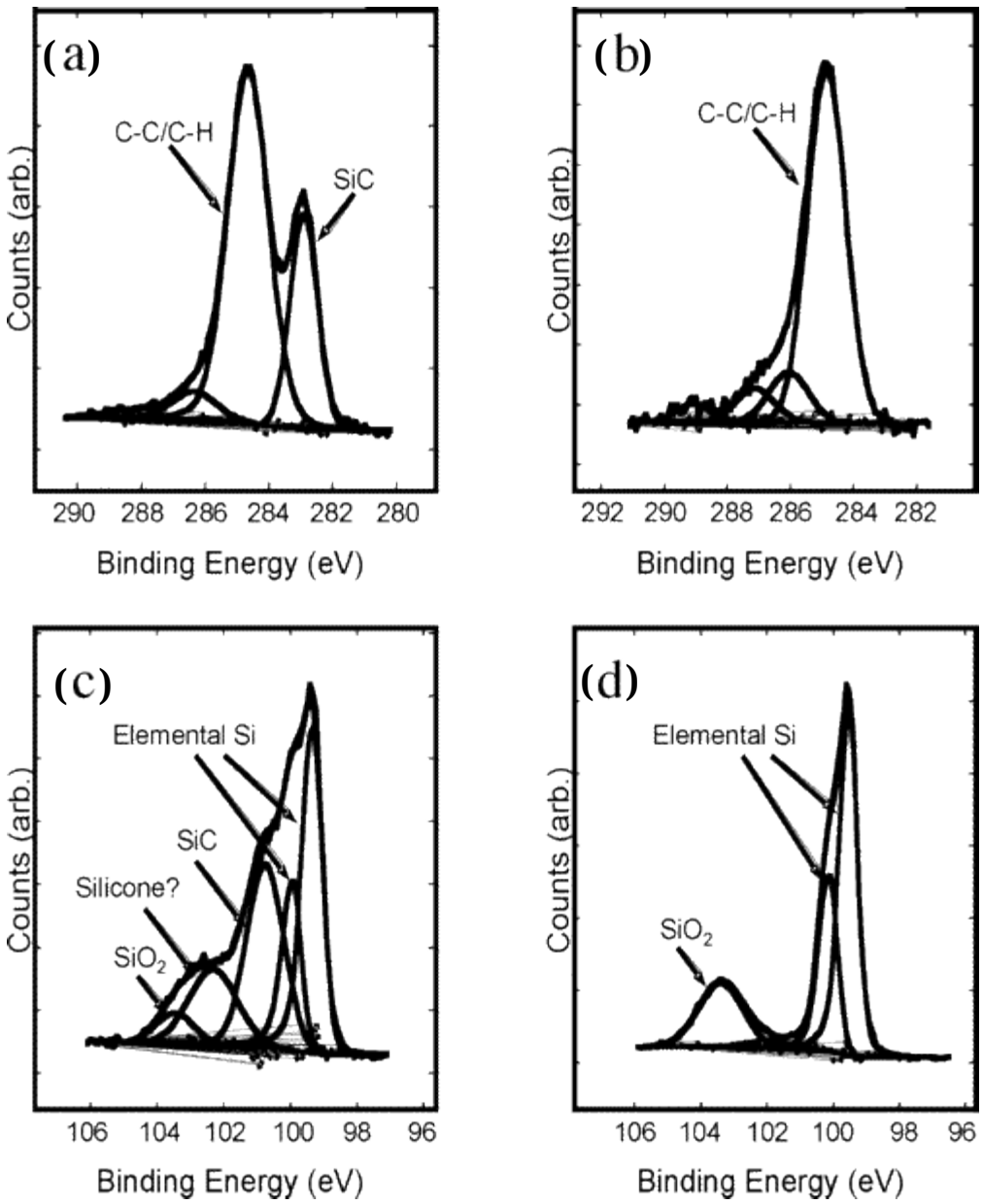

Figure 4.4. XPS scans of LAMSS of Si under 1-hexadecene and control (unfunctionalized) regions near the LAMSS spots. (a) C 1s LAMSS, (b) C 1s control, (c) Si 2p LAMSS, and (d) Si 2p control. [This figure is a modification of Figure V.3. in Chapter V of Guilin Jiang's doctoral dissertation. Dr. Jiang was a coauthor on this paper, and has given permission for the use of this figure in my thesis.]

bonded to carbon and hydrogen. In contrast, the C 1s narrow scan of the LAMSS spot (Figure 4.4a) consists primarily of two peaks: a larger signal that corresponds to carbon bonded to carbon and hydrogen and a smaller but still very significant peak that we identify as silicon carbide. The Si 2p narrow scans are consistent with the C 1s results. The control region is almost entirely composed of signals from bulk silicon and oxide. In contrast, the Si 2p narrow scan of the LAMSS spot shows many oxidation states for silicon, including silicon carbide and a silicone-like species (i.e., silicon bonded to both oxygen and carbon atoms). The basis for the peak assignments included binding energy reference data for silicon. Table 4.2 contains a deconvolution of the C 1s and Si 2p regions for LAMSS spots made with 1-hexadecene and 1-iodooctane and corresponding controls. It is significant that strong hydrocarbon and silicon carbide signals are observed in the LAMSS spots, but only hydrocarbon signals are present in the controls.

These XPS and ToF-SIMS results make it clear that high energy laser pulses can drive surface reactions that would not be possible at room temperature. Despite this, it appears that some chemical functionality is preserved in the LAMSS process. For example, LAMSS spots were made in the air and on silicon surfaces wet with octane, 1-octene, and 1,7-octadiene. After the formation of these LAMSS spots, the surfaces were exposed to HCl vapor because HCl readily reacts with carbon-carbon double bonds. The following ToF-SIMS Cl/Si ratios [The Cl/Si ratio is the ratio of peak areas from the negative ion spectra as follows: $[(^{35}Cl + {}^{37}Cl)/(SiO_2 + SiHO_2 + SiO_3 + SiHO_3 + SiHO + Si + SiH)]$ were calculated for the resulting LAMSS spots: 0.23 ± 0.04 (air), 6.4 ± 1.8 (octane), 5.8 ± 2.3 (1-octene), and 14.7 ± 1.4 (1,7-octadiene). A priori we would have expected that the Cl/Si ratio for octane would have been less than that for 1-octene. We believe that these results are a reflection of the well-known and ready reaction

Table 4.2. Deconvolutions of C 1s and Si 2p narrow scans from LAMSS spots and control regions.

Sample		1-Hexadecene	1-Hexadecene control	1-Iodooctane	1-Iodooctane control
% Carbon seen as	Si-C (carbide)	26.4 ± 1. 9	---	47.7 ± 1.2	---
	C-C, C-H	67.7 ± 2.4	83.7 ± 1.8	46.3 ± 2.1	78.2 ± 1.3
	C-O	4.4 ± 1.3	8.3 ± 0.1	4.0 ± 0.6	10.3 ± 1.4
	C=O	--	1.7 ± 0.4	---	7.3 ± 0.9
	O-C=O	1.5 ± 0.4	6.4 ± 1. 6	1.9 ± 0.4	4.2 ± 0.9
% Silicon seen as	Elemental Si	47.7 ± 2.0	75.3 ± 0.4	47.9 ± 3.0	75.7 ± 0.6
	Si-C (carbide)	30.6 ± 1.5	---	28.3 ± 2.9	----
	Silicone (?)	16 ± 0.3	3.3 ± 0.1	10.3 ± 0.3	3.3 ± 0.9
	SiO_2	5.7 ± 1.2	21.5 ± 0.5	13.6 ± 0.3	21.1 ± 0.2

between exposed silicon surfaces and carbon-carbon double bonds. In addition, these results are consistent with the retention of functionality from the diene and the creation of double bonds by thermal cracking of the alkane and alkenes.

In many applications, it would be advantageous to have smaller spots than the *ca.* 150 µm spots shown in Figure 4.1. Figure 4.5 shows a LAMSS feature made with a 25 mm focal length achromat doublet lens. The spots were produced with 5 µJ of energy per pulse, which corresponds to a peak laser power of 5×10^9 W/cm^2. The diameter of the feature is 6 µm, with a noticeable raised ring around a 4-µm-diameter, 500-nm-deep spot. An AFM analysis of sub-10-µm LAMSS spots made in this manner suggests that the volume of material above the plane of the substrate is roughly equal to the volume of the recessed region below the plane. In other words, the focused, low-power laser shots primarily appear to cause surface melting (the mp of Si is 1414 °C) rather than ablation, although ablation is clearly seen in LAMSS at higher laser powers. The high temperatures that must be present at the point of the LAMSS spot during activation is well above that needed to crack hydrocarbons (350-750 °C).[21-22] This would help explain the reactivity of an alkane (octane) in LAMSS and carbide/silicone formation at the surface.

We have also used the LAMSS reaction of an alkane to show an application of this new method to surface patterning. A silicon surface was wet with hexadecane, and LAMSS spots were made. This surface was then immersed in a dilute solution of polylysine. The adsorption of polylysine onto oxide surfaces has been used for many years as an important coupling layer for DNA to surfaces.[23-24] Figure 4.6 shows a ToF-SIMS negative ion image of the LAMSS spot made in hexadecane and the surrounding background. It is clear that the C_2H^- peak, which is typical of a hydrocarbon, is more abundant in the spot whereas the CN peak, which comes from

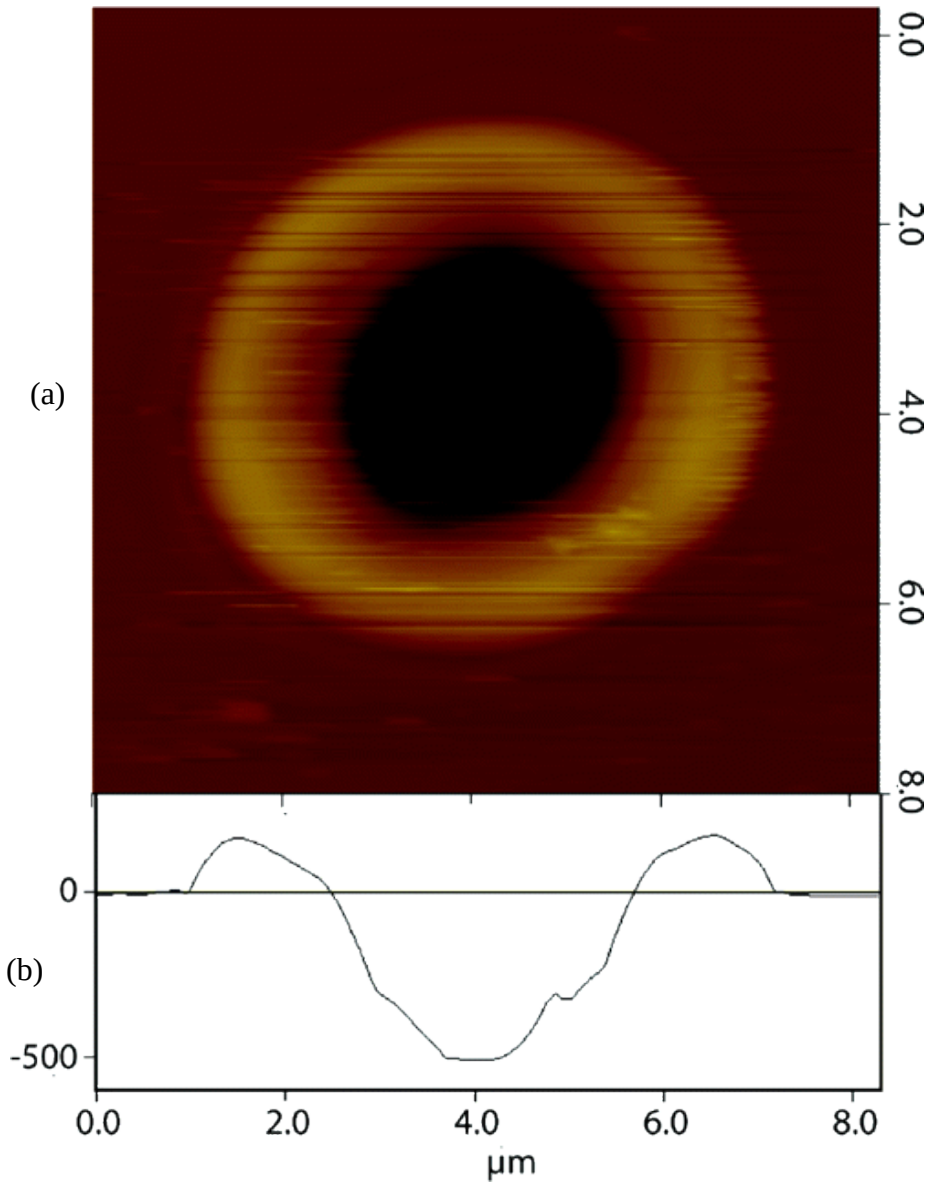

Figure 4.5. (a) AFM height image of a small LAMSS spot. (b) Trace through the middle of the spot.

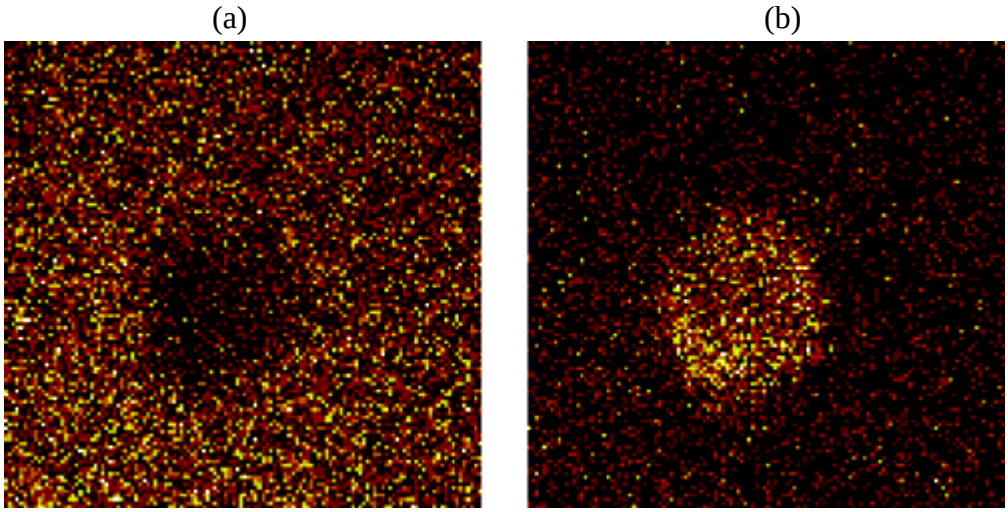

Figure 4.6. ToF-SIMS images of a LAMSS spot made in hexadecane followed by the adsorption of polylysine from an aqueous solution on a Si/SiO2 surface around the spot showing (a) the CN- fragment from polylysine adsorption and (b) the C2H- fragment from hexadecane in the LAMSS spot.

the polylysine, is more abundant in the background. Thus we show a method for controlling/patterning the deposition of polylysine, and presumably other amine containing polymers, in the plane.

4.4. Conclusions

I demonstrated a new method for simultaneously patterning and functionalizing surfaces. This functionalization requires only a single laser pulse and no special preparation of either the surface or the reactive liquid. This method consists of wetting a semiconductor surface (e.g., silicon or germanium) with a reactive compound and then firing a highly focused nanosecond pulse of laser light through the transparent liquid onto the surface. The high peak power of the pulse at the surface activates the surface so that it reacts with the liquid with which it is in contact.

4.5. References

1. Waddell, E. A.; Johnson, T. J.; Kramer, G. W.; Locascio, L. E. Chemical Modification of Substrates by Photo-ablation Under Different Local Atmospheres and Chemical Environments for the Fabrication of Microstructures. U.S. Patent 6,703,189 B2, 2004.
2. Waddell, E. A.; Locascio, L. E.; Kramer, G. W., *J. Assoc. Lab. Automat.* **2002,** *7*, 78-82.
3. Dulcey, C. S.; Georger, J. H., Jr; Krauthamer, V.; Stenger, D. A.; Fare, T. L.; Calvert, J. M., *Science* **1991,** *252*, 551-554.
4. Calvert, J. M.; Georger, J. H.; Peckerar, M. C.; Pehrsson, P. E.; Schnur, J. M.; Schoen, P. E., *Thin Solid Films* **1992,** *210/211*, 359-363.
5. Balgar, T.; Franzka, S.; Hasselbrink, E.; Hartmann, N., *Appl. Phys. A* **2006,** *82*, 15-18.

6. Balgar, T.; Franzka, S.; Hartmann, N., *Appl. Phys. A* **2006,** *82*, 689-695.

7. Shadnam, M. R.; Kirkwood, S. E.; Fedosejevs, R.; Amirfazli, A., *Langmuir* **2004,** *20*, 2667-2676.

8. Chang, W.-S.; Choi, M.-J.; Kim, J.-G.; Cho, S.-H.; Whang, K.-H., *Int. J. Precis. Eng. Manuf.* **2006,** *7*, 13-17.

9. Linford, M. R. Chemical Functionalization of Hydrogen-Terminated Silicon Surfaces: The First Self-Assembled Monolayers on Silicon. Ph.D. Thesis. Stanford University, Stanford, CA, 1996.

10. Cicero, R. L.; Linford, M. R.; Chidsey, C. E. D., *Langmuir* **2000,** *16*, 5688−5695.

11. Effenberger, F.; Götz, G.; Bidlingmaier, B.; Wezstein, M., *Angew. Chem., Int. Ed.* **1998,** *37*, 2462−2464.

12. Wojtyk, J. T. C.; Tomietto, M.; Boukherroub, R.; Wayner, D. D. M., *J. Am. Chem. Soc.* **2001,** *123*, 1535−1536.

13. Sieval, A. B.; Linke, R.; Zuilhof, H.; Sudhölter, E. J. R., *Adv. Mater.* **2000,** *12*, 1457−1460.

14. Eves, B. J.; Sun, Q.-Y.; Lopinski, G. P.; Zuilhof, H., *J. Am. Chem. Soc.* **2004,** *126*, 14318−14319.

15. Cai, W.; Lin, Z.; Strother, T.; Smith, L. M.; Hamers, R. J., *J. Phys. Chem. B* **2002,** *106*, 2656−2664.

16. Lee, E. J.; Ha, J. S.; Sailor, M. J., *J. Am. Chem. Soc.* **1995,** *117*, 8295−8296.

17. Lee, E. J.; Bitner, T. W.; Ha, J. S.; Shane, M. J.; Sailor, M. J., *J. Am. Chem. Soc.* **1996,** *118*, 5375−5382.

18. Yang, L.; Lua, Y.-Y.; Lee, M. V.; Linford, M. R., *Acc. Chem. Res.* **2005,** *38*, 933−942.

19. Ohlhausen, J. A.; Keenan, M. R.; Kotula, P. G.; Peebles, D. E., *Appl. Surf. Sci.* **2004,** *231-232*, 230-234.

20. Smentkowski, V. S.; Ohlhausen, J. A.; Kotula, P. G.; Keenan, M. R., *Appl. Surf. Sci.* **2004,** *231-232*, 230-234.

21. Archibald, R. C.; Greensfelder, B. S.; Holzman, G.; Rowe, D. H., *Ind. Eng. Chem.* **1960,** *52*, 747-750.

22. Khorasheh, F.; Gray, M. R., *Ind. Eng. Chem. Res.* **1993,** *32*, 1853−1863.

23. Shi, X. Y.; Sanedrin, R. J.; Zhou, F. M., *J. Phys. Chem. B* **2002,** *106*, 1173−1180.

24. Ren, K. F.; Ji, J.; Shen, J. C., *Bioconjugate Chem.* **2006,** *17*, 77-83.

Chapter 5. Direct Adsorption and Detection of Proteins, Including Ferritin, onto Microlens Array Patterned Bioarrays*

5.1. Introduction

Protein arrays emerged five yeas after the announcement of the DNA array. Macbeath published the first paper on protein arrays in Science in 2000.[1] Protein arrays have several applications, such as identifying the substrates of protein kinases and screening for protein-protein interactions.[1] Because of considerably smaller quantities of reagents/samples needed and also the higher throughput of protein arrays compared to many other tests, protein arrays should be valuable for the miniaturization of numerous assays.[2] For protein interactions, protein arrays have been used to analyze the Src Homology 2 and 3, pleckstriin homology, forkhead, and different enzymes.[3-8] Bulyk used microarrays of distinct dsDNA sequences to assay protein-DNA interactions.[9] Protein arrays were also used to study protein expression.[10]

Obviously, protein arrays are prepared by selectively attaching proteins to solid substrates, including silicon, polymer, and glass. There are several means for such attachment, such as covalent bonding, affinity interaction, and physical adsorption. Covalent bonding is a strong interaction, but it is generally not specific. Affinity binding is specific, and it can also be strong, such as in the binding of avidin to biotinylated proteins.[11] Physical binding is a result of electrostatic or hydrophobic forces. This binding lacks specificity and the resulting forces are generally not as strong as those of covalent or affinity binding.

A variety of protein methods have been explored, for example, microcontact printing,[12] ink-jet printing,[13] mechanical pin-tool deposition,[14] microspotting,[15] and microfluidics.[16] These

*Taken from (Feng Zhang, Richard J. Gates, Vincent S. Smentkowski, Sriram Natarajan, Bruce K. Gale, Richard K. Watt, Matthew C. Asplund, and Matthew R. Linford) *J. Am. Chem. Soc*. **2007**, *129*, 9252-9253. Copyright 2007 American Chemical Society.

methods use different attachment chemistries.[17] However, not all of these methods can be applied on an industrial scale because of problems associated with cost, automation, and throughput.

Here, I present a technique to make industrially viable protein arrays. An ultrathin polyethylene glycol silane layer that resists protein adsorption is prepared on silicon oxide surfaces.[18] Then, micro spots are rapidly created on these surfaces by microlens array patterning. These spots have excellent affinity for the adsorption of various proteins, and the PEG layer around them maintains good resistance to protein adsorption.

5.2. Experimental

5.2.1 Materials

Silicon wafers (100), single polished, were obtained from Unisil, Santa Clara, CA. Toluene (≥ 99.9%, Sigma, USA), ethanol (100%, AaperAlcohol, USA), sodium phosphate dibasic, heptahydrate, (≥ 99%, Fluka, USA), HCl (concentrated, 37%, Mallinckrodt, USA), 2-[methoxy(polyethylenoxy)propyl]trimethoxysilane, $[(CH_3O)_3Si(CH_2)_3(OCH_2CH_2]_{6\text{-}9}OCH_3$ (≥ 90%, MW 460-590, 6-9 PEG units, Gelest, Tullytown, USA), and sodium phosphate monobasic, anhydrous (≥ 99%, Sigma) were used as received. The phosphate buffer (0.02 M) was prepared with anhydrous sodium phosphate (monobasic), and sodium phosphate dibasic, heptahydrate. Albumin (from bovine serum, IgG-free, cell culture tested, Sigma, USA), myoglobin (from equine skeletal muscle, 95-100%, Sigma), lysozyme (95 %, ~50,000 units/mg protein, Sigma, USA), Immunopure Avidin (Pierce Biotechnology, USA), streptavidin (AnaSpec, USA), Cy3 tagged Protein A (Invitrogen, USA), biotin-4-fluorescein (Invitrogen, USA) (the "fluorescein-biotin conjugate"), fluorescein (free acid, Fluka), Protein A (essentially salt-free, Sigma), and

ferritin (from horse spleen, 99.5%, Sigma) were also used as received. The aqueous buffer (pH 7.5) used to dissolve ferritin consisted of 0.05 M NaCl and 0.05 M MOPS (3-(N-Morpholino) propanesulfonic acid, sodium salt).

5.2.2. PEG monolayer preparation

Following a literature procedure,[19] a silane with 6-9 polyethylene glycol (PEG) units [$(CH_3O)_3Si(CH_2)_3(OCH_2CH_2)_{6\text{-}9}OCH_3$] was dissolved in toluene to form a 4-5 mM solution that also contained 0.8 mL/L HCl (conc). Silicon wafers were plasma cleaned for 5 min at high power (18 W applied to the RF coil) with a plasma cleaner (model PDC-32G) from Harrick Plasma (Ithaca, NY), and then immersed into the PEG silane solution for 18h at room temperature. The wafers were washed with toluene, ethanol, and water, and finally dried with a jet of nitrogen. The resulting films had uniform ellipsometric thicknesses (15.2 ± 0.3 Å) and advancing water contact angles (29.8° ± 2.2°). These values are the average of eight measurements from four surfaces.

5.2.3. Surface patterning with the microlens array

A microlens array (MA) with 100 μm spacing between microlenses (SUSS MicroOptics, Neuchatel, Switzerland) was placed approximately 200 μm over the PEG monolayer coated silicon oxide substrate. A single, short (few ns) pulse of 15 mJ 532 nm laser light from an Infinity Nd:YAG laser (Coherent, Santa Clara, CA, USA) was then shot through this optical element to pattern the surface. The surface was not cleaned or rinsed in any way after MA patterning.

5.2.4. Protein adsorption

Proteins, except ferritin, were dissolved in phosphate buffered saline (PBS) to form 10^{-5} M solutions. The concentration of ferritin was also 10^{-5} M, but it was dissolved in the MOPS buffer described above. A microlens array patterned PEG monolayer on silicon oxide was then immersed into a protein solution overnight at 2–8°C. The surfaces, including those with ferritin adsorbed on them, were then rinsed with PBS buffer followed by Millipore water, and dried with a jet of N_2.

5.2.5. Surface characterization

Planar surfaces described in this chapter were characterized with spectroscopic ellipsometry (J.A. Woollam M-2000**,** Lincoln, NE, USA), contact angle goniometry (Ramé-Hart model 100-00 contact angle goniometer, Netcong, NJ), X-ray photoelectron spectroscopy (XPS) (Surface Science SSX-100 instrument with a monochromatized Al Kα source and a hemispherical analyzer, Surface Science Laboratories, Mountain view, CA, USA), and time-of-flight secondary ion mass spectrometry (ToF-SIMS) (ION-TOF TOF-SIMS IV instrument with a two-lens $^{69}Ga^{+}$ gun).

5.2.6. Fluorescence system

Our imaging system employs a TE 2000-U inverted microscope (Nikon, Tokyo, Japan). The laser light was generated with an air-cooled 35-LAP-321-120 Ar ion laser (Melles Griot, Carlsbad, CA) and directed into the microscope via an optical path consisting of an excitation filter (D488/10, Chroma, Brattleboro, VT), a homemade periscope, a homemade quartz diffuser, which was used to homogenize images, and a light-gathering lens. Fluorescence was collected

through a 10×/0.30 NA objective (Nikon) and passed through a Z488LP long-pass filter set (Chroma). All images were recorded with a Coolpix 5400 digital camera (Nikon).[20]

5.2.7. Microfluidics spotting

Spotting on MA patterned surfaces was performed with a Continuous Flow Microspotter (CFM) from Wasatch Microfluidics (Salt Lake City, UT, USA). The concentration of the Cy3 tagged Protein A solution was 50 μM S1 in PBS buffer (pH 7.4), and the flow time was 15 minutes. After this deposition, the surfaces were washed with PBS buffer using the spotter. After removal of the spotter the surfaces were washed with water.

5.2.8. Data analysis

Multivariate curve resolution (MCR) of ToF-SIMS images was performed using the AXSIA toolbox that was written at Sandia National Laboratories. Details of data binning and preprocessing have been described previously.[21] The data shown here were binned to 1 amu in the mass range of 0 to 1000 amu.

5.3. Results and discussion

The PEG terminated monolayers used for MA patterning exhibit the expected resistance to protein adsorption (see Figure 5.1). To within experimental error, spectroscopic ellipsometry showed no change in PEG monolayer thickness after immersion in dilute protein solutions. The protein resistance of these films was further confirmed by XPS (see Figure 5.2), which showed no N 1s signal from PEG monolayers that were immersed in solutions of proteins, but strong N

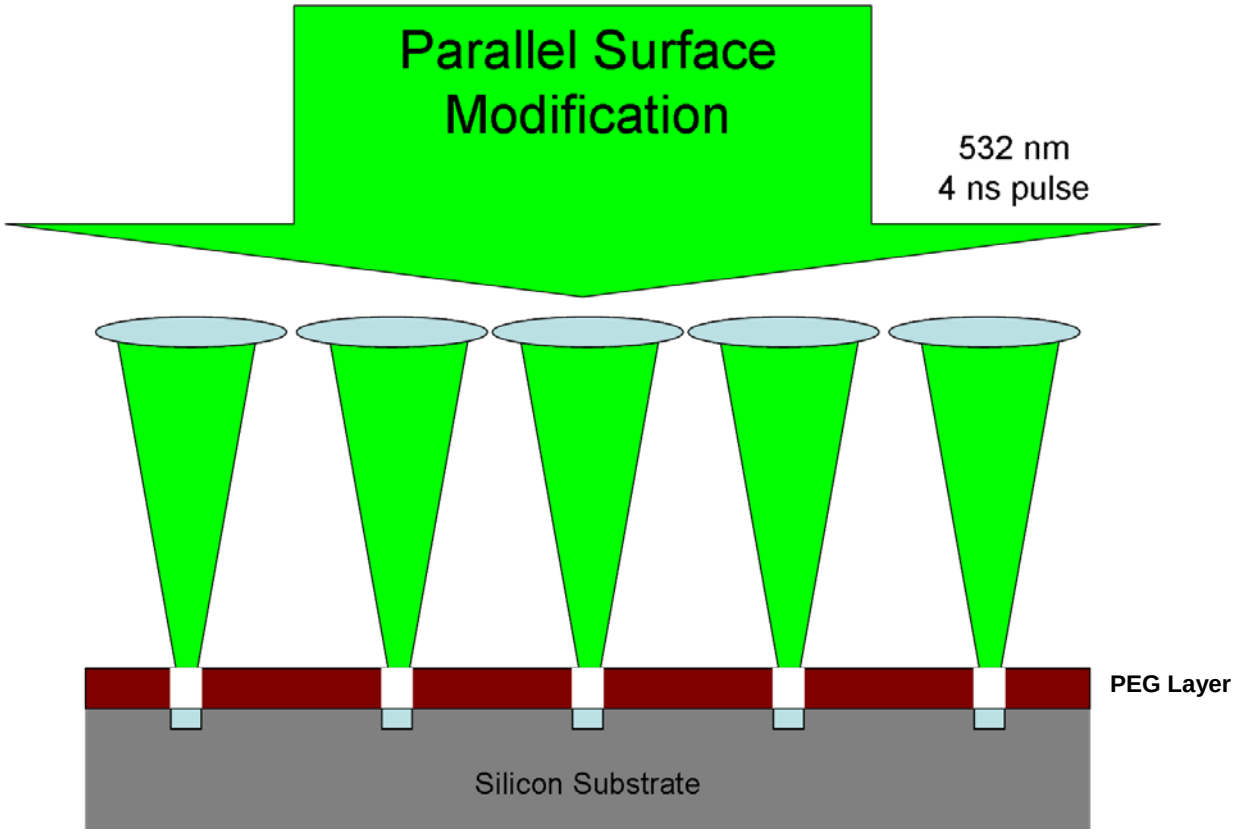

Figure 5.1. Microlens array patterning. A 4 ns pulse of 532 nm laser light passes through a microlens array, ablates the PEG layer, and thereby creates spots (wells) on silicon surfaces. Proteins could be attached on the spot areas.

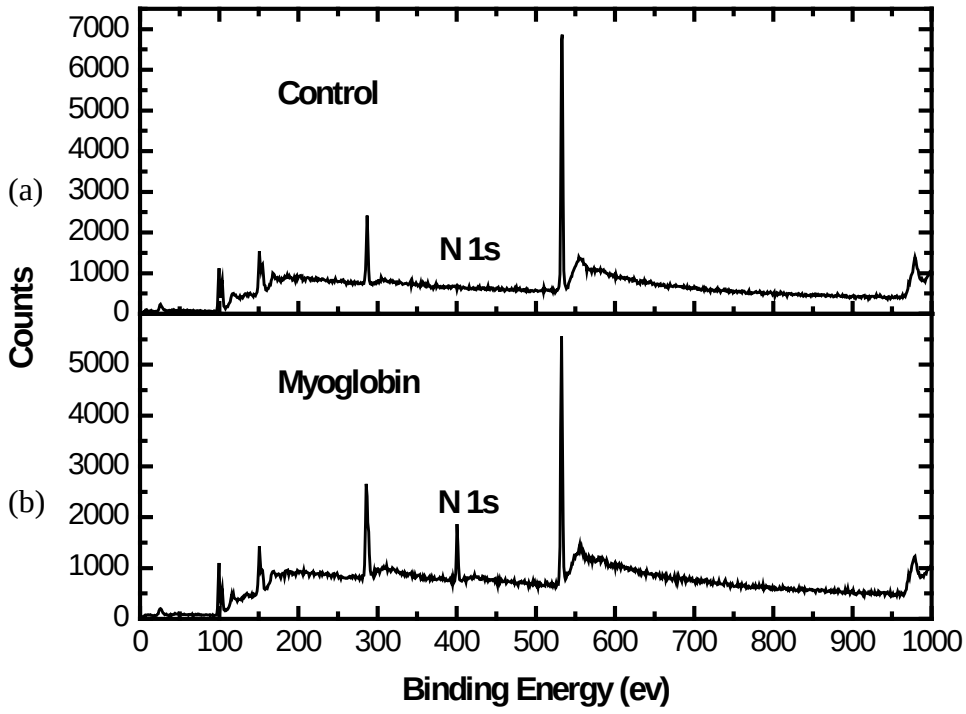

Figure 5.2. X-ray photoelectron spectroscopy survey scans of (a) an Si/SiO2 surface and (b) a PEG silane monolayer coated Si/SiO2 surface after immersion in a pH 5.6 solution of myoglobin in PBS buffer. The N1s signal is indicative of protein adsorption.

1s signals from clean, bare silicon oxide control surfaces.

PEG monolayer coated Si/SiO_2 slides were patterned with an MA by placing it over the substrate and firing a 4 ns pulse of 532 nm laser light through the optic. TOF-SIMS ion images of H^-, CH^-, CH_2^-, OH^-, C_2H^-, and the total ion image showed good contrast between the spots and the background, that is, the spots and the background were chemically distinct. Almost no contrast and little signal was found for the CN^- (see Figure 5.3 (a)) and CNO^- ions on this surface, which are characteristic of proteins.[22] MA patterned PEG monolayers were then immersed in solutions of various proteins chosen to have a wide range of pI values and molecular weights. All of the proteins studied adsorbed to the spots with strong preference over the background, as shown by the CN^- (see Figure 5.3) and CNO^- ions in TOF-SIMS imaging of these surfaces. This adsorption appears to be general and nonspecific and based on van der Waals and electrostatic interactions with the exposed substrate. As suggested in the figure, the size of the spots could be controlled by changing the laser power and the focus of the MA. The S^- ion image also showed good contrast in a number of the protein array images. Among the proteins studied were some with useful function in bioconjugate chemistry. For example, avidin and streptavidin have a well-known and high affinity for biotin. Protein A binds IgG antibodies, and BSA is employed as a blocking agent in enzyme-linked immunosorbent assays **(**ELISA).

Multivariate curve resolution (MCR) of the TOF-SIMS images further confirmed protein adsorption in the spots and not in the backgrounds of the arrays. MCR, which has been shown to be a valuable tool for TOF-SIMS image analysis,[23] was possible because an entire mass spectrum was saved at each pixel in the raw data file. MCR was performed on all of the spectral images of all of the adsorbed proteins in MA patterned protein arrays. A representative example of these results is shown in Figures 5.4 a and b and demonstrates that the surfaces are primarily

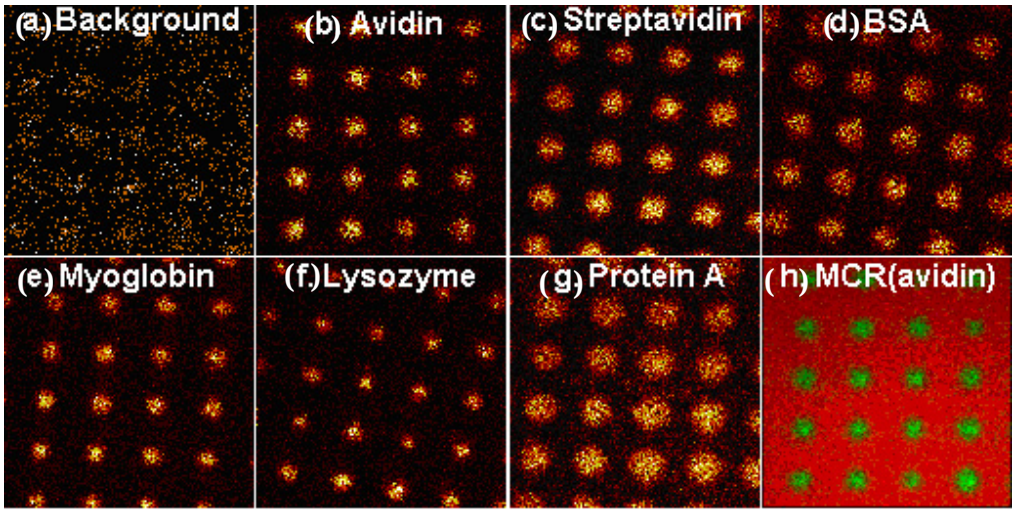

Figure 5.3. ToF-SIMS negative ion, CN^-, images (500 µm x 500 µm) of (a) a PEG silane monolayer patterned with a microlens array, and (b – g) a PEG silane monolayer patterned with a microlens array after immersion in a solution of the protein indicated in each panel. Panel (h) shows an AXSIA multivariate curve resolution (MCR) analysis of the negative ion spectra from the avidin image.

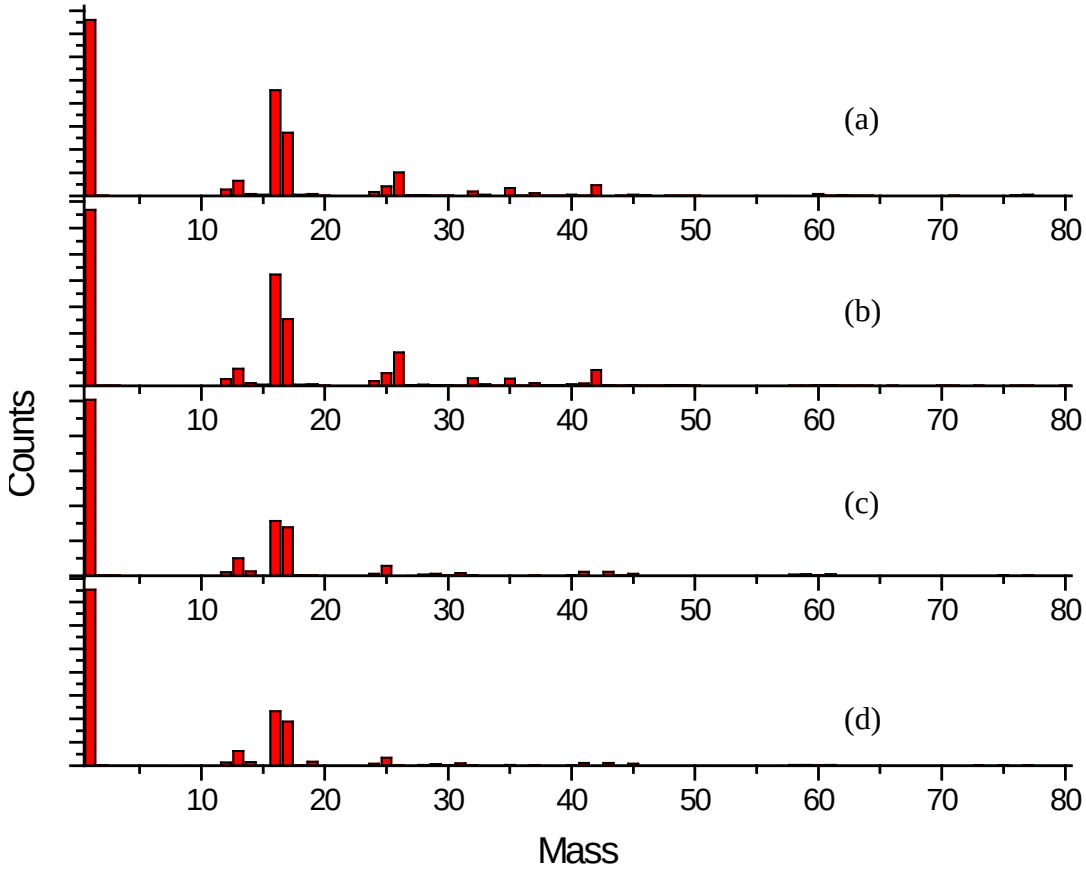

Figure 5.4. ToF-SIMS spectra of (a) the MCR component corresponding to the avidin spot in a protein array, (b) an avidin-coated, planar, native oxide terminated silicon surface, (c) the MCR component corresponding to the background area in a protein array, (d) a PEG silane coated surface. Only the low mass region of the spectra is shown.

composed of two surface species: a spectrum corresponding to the PEG background, and a spectrum corresponding to the adsorbed protein. These assignments were confirmed for avidin arrays (see Figure 5.4) by comparing these two MCR components to the TOF-SIMS spectra of planar Si/SiO_2 that was coated with the PEG silane monolayer and avidin adsorbed onto planar Si/SiO_2.

I next determined whether or not the proteins were stably bonded to the spots in the arrays and I assayed their activity after binding. Table 5.1 showed the molecular weights and pI values of the proteins that were studied. TOF-SIMS imaging of bioarrays containing lysozyme and myoglobin both deposited at two different pH values (5.6 and 8.0) showed that little change occurred in the protein spots after immersion in PBS buffer for 1 or 3 days. To assay the activity of an avidin array, a control experiment was performed. The surface was incubated in a dilute solution of fluorescein and rinsed. As expected, no array was detected by fluorescence microscopy. However, when the array was incubated with a fluorescein-biotin conjugate and rinsed, the array was seen by fluorescence microscopy (see Figure 5.5). The solution pH did not appear to strongly alter protein adsorption, as measured on model, planar, silicon oxide surfaces. For BSA, only a small decrease in protein layer thickness was observed as the pH of the deposition solution increased; solutions at pH 5.6, 6.6, and 7.4 gave ellipsometric thicknesses of 21.4 ± 0.1 Å, 18.23 ± 0.02 Å, and 18.6 ± 0.3 Å, respectively. These thickness measurements were consistent with XPS results for these pH values; by XPS, the percentages of nitrogen at the surfaces were 8.6, 7.2, and 6.0. For myoglobin deposited from PBS buffer at pH 5.6 and 8.0, the film thicknesses were 39.5 ± 0.2 Å and 17.69 ± 0.03 Å, respectively, and the percentages of nitrogen by XPS were 5.5 and 4.3, respectively.

Table 5.1. Molecular weights and pI values of the proteins that were studied.

Protein	pI	MW (Da)
BSA	4.9	66,000
Avidin	10.5	66,000
Streptavidin	5.5	60,000
Lysozyme	11.35	14,700
Myoglobin	7	16,951
Protein A	6.8	42,000
Ferritin	4.4	440,000

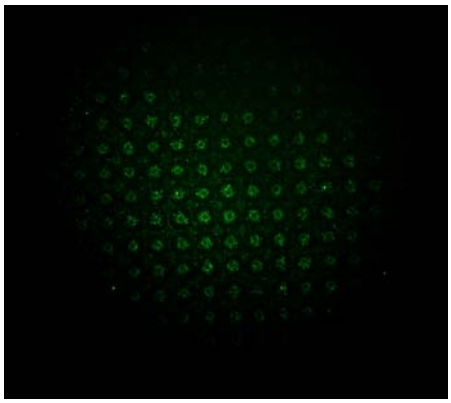

Figure 5.5. Fluorescence microscopy images of an avidin array after exposure to a fluorescein-biotin conjugate.

Localized protein deposition was demonstrated using a microfluidic spotter at multiple points on the surface.[16] This polydimethylsiloxane device was pressed against an MA patterned surface, which allowed a dilute solution of Cy3 tagged protein A to be circulated over selective regions (about 500 μm in diameter) on the surface. Selective adsorption of protein A at the MA patterned spots was confirmed by fluorescence microscopy (see Figure 5.6).

Ferritin also adsorbs directly onto spots on PEG monolayer substrates after MA patterning. Ferritin is an iron storage protein found in most biological systems.[24] Ferritin molecules are hollow protein shells that can store 2500-4000 iron atoms. Apoferritin is the protein shell, which is ca. 2 nm thick. The cavity inside apoferritin is ca. 8 nm in diameter.

After ferritin binds to the patterned substrates, TOF-SIMS, using a Ga^+ primary ion beam, shows the presence of the protein in the spots, but no iron can be detected (see Figure 5.7, (c) #1 Fe^+). This is consistent with the extremely shallow information depth of TOF-SIMS (*ca.* 2 nm).[25] These results also suggest that, like avidin, ferritin does not denature upon adsorption. After heating to 500°C in an inert atmosphere to remove ferritin's protein shell, TOF-SIMS reveals iron at the surface (Figure 5.7, (d) #2 Fe^+). Recently, there has been interest in replacing the iron in ferritin with other metals.[26-28] The results from analytical methods used to determine whether the new metal is deposited within the ferritin shell, or whether it remains outside, are sometimes ambiguous. This new approach should shed light on this problem.

5.4. Conclusions

I developed a new method for preparing protein arrays that is compatible with high throughput manufacturing. Time-of-flight secondary ion mass spectrometry (ToF-SIMS) shows that all of the proteins studied, including avidin, BSA, ferritin, lysozyme, myoglobin, Protein A,

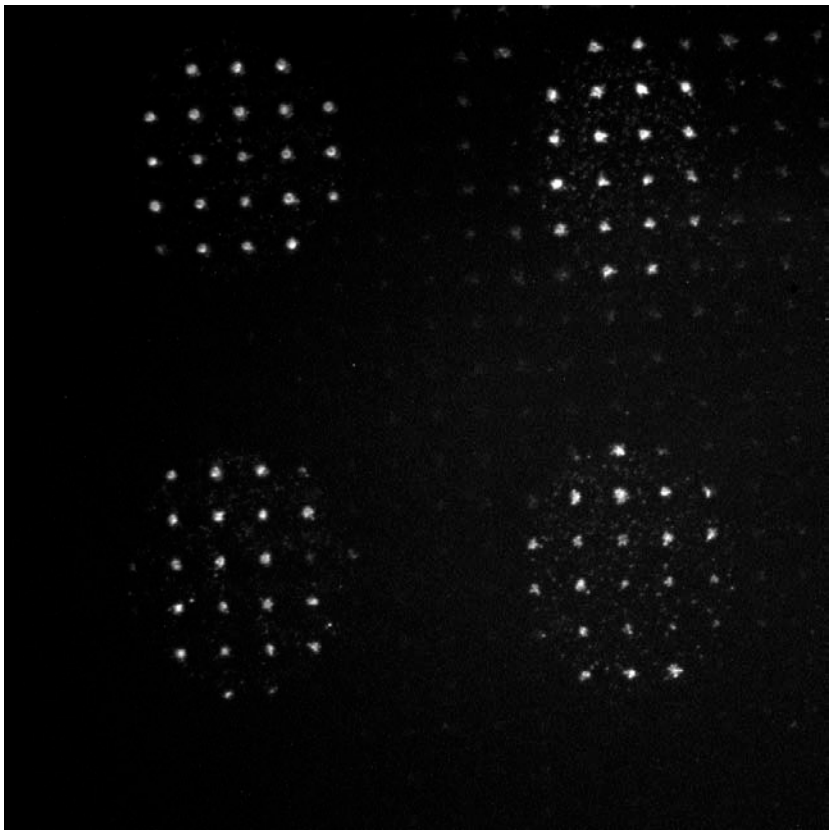

Figure 5.6. Fluroescence microscopy image of Cy3 tagged Protein A selectively deposited onto an MA patterned substrate using a continuous flow microspotter. The excitation wavelength was *ca.* 540 nm and the emission wavelength was *ca.* 600 nm. This particular experiment differed from all others reported in this work in that the spacing between the microlenses in the MA was 83 μm and the spaces between the microlenses were masked by chromium.

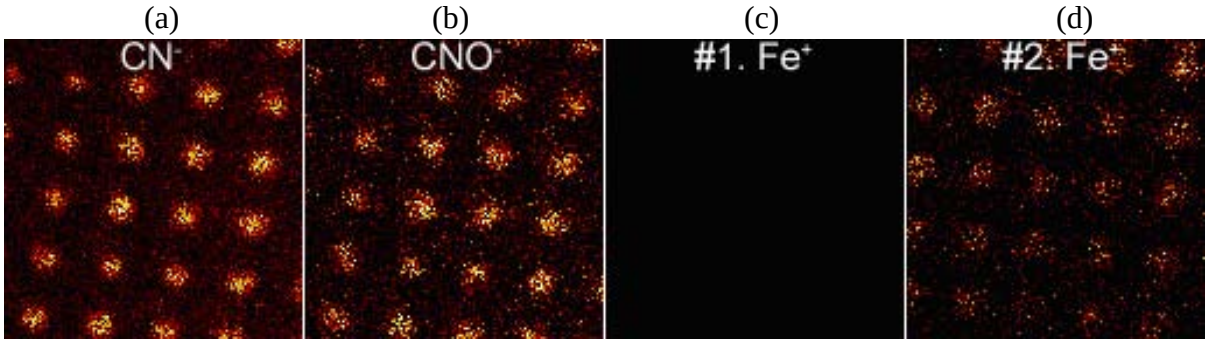

Figure 5.7. ToF-SIMS negative ion CN^- (a) and CNO^- (b) images and positive ion Fe^+ image (c) after ferritin deposition. The rightmost panel shows the Fe^+ image (d) after the array was heated to 500°C under Ar for 1 h. Images are 500 µm x 500 µm.

and streptavidin, adsorb selectively into the spots in the array. The stability of these adsorbed proteins is shown. The retention of activity of avidin after adsorption is demonstrated. Additionally, it is shown that this method can be used to confirm the location of the metal (iron) in ferritin. It should be possible to generalize this analytical method to other metals that are loaded into ferritin.

5.5. References

1. MacBeath, G.; Schreiber, S. L., *Science* **2000,** *289*, 1760.
2. Templin, M. F.; Stoll, D.; Schwenk, J. M.; Pötz, O.; Kramer, S.; Joos, T. O., *Proteomics* **2003,** (3), 2155.
3. Espejo, A.; Cote, J.; Bednarek, A.; Richard, S., *Biochem. J.* **2002,** *367*, 697.
4. Ge, H., *Nucleic Acids Res.* **2000,** *28*, e3.
5. Zhu, H.; Klemic, J. F.; Chang, S.; Bertone, P.; Casamayor, A.; Klemic, K. G.; Smith, D.; Gerstein, M.; Reed, M. A.; Snyder, M., *Nat Genet* **2000,** *26*, 283.
6. Arenkova, P.; Kukhtina, A.; Gemmellb, A.; Voloshchuka, S.; Chupeevaa, V.; Mirzabekov, A., *Anal. Biochem.* **2000,** *278*, 123.
7. Houseman, B. T.; Huh, J. H.; Kron, S. J.; Mrksich, M., *Nat Biotechnol* **2002,** *20*, 270.
8. LizcanoDagger, J. M.; DeakDagger, M.; MorriceDagger, N.; KielochDagger, A.; Hastie, C. J.; Dong, L.; Reimer, U.; Alessi, D. R., *J. Biol. Chem.* **2002,** *277*, 27839.
9. Bulyk, M. L.; Gentalen, E.; Lockhart, D. J.; Church, G. M., *Nat Biotechnol* **1999,** *17*, 573.
10. Ziauddin, J.; Sabatini, D. M., *Nature* **2001,** *411*, 107.
11. Pavlickova, P.; Knappik, A.; Kambhampat, D.; Ortigao, F.; H. Hug, *Biotechniques* **2003,** *34* (1), 124.

12. Kumar, A.; Whitesides, G. M., *Appl. Phys. Lett.* **1993,** *63* (14), 2002.

13. Newman, J. D.; Turner, A. P. E.; Marrazza, G., *Anal. Chim. Acta* **1992,** *262* (1), 13.

14. Schena, M.; Shalon, D.; Davis, R. W.; Brown, P. O., *Science* **1995,** *270*, 467.

15. Shumaker-Parry, J. S.; Zareie, M. H.; Aebersold, R. T.; Campbell, C. T., *Anal. Chem.* **2004,** *76*, 918-929.

16. Chang-Yen, D. A.; Myszka, D. G.; Gale, B. K., *J. Microelectromech. Syst.* **2006,** *15*, 1145-1151.

17. Hermanson, G. T., *Bioconjugate Tech*. Academic Press: SanDiego, CA, 1996.

18. Prime, K. L.; Whitesides, G. M., *J. Am. Chem. Soc.* **1993,** *115*, 10714-10721.

19. Papra, A.; Gadegaard, N.; Larsen, N. B., *Langmuir* **2001,** *17*, 1457.

20. Liu, J.; Sun, X.; Farnsworth, P. B.; Lee, M. L., *Anal. Chem* **2006,** *78*, 4654.

21. Ohlhausen, J. A. T.; Keenan, M. R.; Kotula, P. G.; Peebles, D. E., *Appl. Surf. Sci.* **2004,** *231-232*, 230-234.

22. Wagner, M. S.; Castner, D. G., *Langmuir* **2001,** *17* (15), 4649.

23. Smentkowski, V. S.; Ohlhausen, J. A.; Kotula, P. G.; Keenan, M. R., *Appl. Surf. Sci.* **2004,** *231-232*, 245-249.

24. Harrison, P. M.; Arosio, P., *Biochim. Biophys. Acta* **1996,** *1275*, 161-203.

25. Michel, R.; Luginbu¨hl, R.; Graham, D. J.; Ratner, B. D., *Langmuir* **2000,** *16*, 6503-6509.

26. Wardeska, J. G.; Viglione, B.; Chasteen, N. D., *J. Biol. Chem.* **1986,** *261*, 6677-6683.

27. Pead, S.; Durrant, E.; Webb, B.; Larsen, C.; Heaton, D.; Johnson, J.; Watt, G. D., *J. Inorg. Biochem.* **1995,** *59*, 15-27.

28. Okuda, M.; Iwahori, K.; Yamashita, I.; Yoshimura, H., *Biotechnol. Bioeng.* **2003,** *84*, 187-194.

Chapter 6. Subsurface Oxidation for Micropatterning Silicon (SOMS)*

6.1. Introduction

Surface patterning on silicon is important in silicon semiconductor manufacturing and microchip fabrication. Accordingly, many techniques have been applied, where the most popular is photolithography.[1] There are several other methods that have been used in laboratories and industry such as plasma polymerization,[2] microcontact printing,[3] and the chemomechanical method.[4]

Plasma processing has also been used to effect patterning on surfaces by etching and polymerization.[2, 5] However, plasma methods typically require expensive equipment and costly reaction gases. In addition, plasma methods can be complicated. Here, I use a relatively simple and inexpensive method for surface patterning with a plasma to overcome these drawbacks. In this work, a TEM grid was used as stencil mask. The plasma oxidizes the silicon surfaces through the holes of the stencil mask. The area covered/obscured on the surfaces by the mask is protected from oxidation by the plasma. Therefore, a silicon dioxide pattern is formed on the surface by plasma oxidation. Consequently, etching can be performed after the formation of the silicon pattern. HF removes the silicon dioxide pattern and leaves a silicon pattern with shallow features. KOH etching produces much deeper features with faster etching rates through silicon compared to silicon dioxide. This surface patterning technique can be performed in many chemistry laboratories under normal conditions. Because it is simple, straightforward, and could potentially be automated, SOMS is industrially viable.

---

*Taken from (Feng Zhang, Ken Sautter, Robert C. Davis, and Matthew R. Linford) *Langmuir,* **2009**, *25(3),* 1289-1291. Copyright 2009 American Chemical Society.

6.2. Experimental

6.2.1. Instrumentation

YES 1224P (Yield Engineering Systems, Livermore, CA, USA) was used for plasma generator for subsurface oxidation. PDC-32G (Harrick Plasma, Ithaca, NY, USA) was used for for surface cleaning. Surfaces were characterized by spectroscopic ellipsometer (M-2000D, J.A. Woollam, Lincoln, NE, USA), X-ray photoelectron spectrometer (XPS) (Surface Science SSX-100, Surface Science Laboratories, Mountain View, CA, USA), scanning electron microscope (Philips XL30 S-FEG, Philips, Eindhoven, Netherlands), atomic force microscope (Veeco Dimension V scanning probe microscope, Veeco, Plainview, NY, USA), and optical microscope (Leica DM2000, Leica Microsystems, Bannockburn, IL, USA).

6.2.2. Materials

Silicon wafers (100), single polished, were obtained from Montco Silicon Technologies, Spring City, PA. 2-Propanol (99.9%, Sigma), acetone (>99.5%, Sigma), potassium hydroxide (>90%, Sigma), hydrofluoric acid (49%, Ashland, Norwood, NJ, USA), and oxygen gas (99.5 and 99.994%, Airgas, Denver, CO, USA) were used as received.

6.2.3. Surface cleaning

Native oxide terminated silicon wafers were washed with soap and water, 2-propanol, and acetone and dried under nitrogen. They were then cleaned in the Harrick plasma cleaner for *ca.* 3 min using an air plasma.

6.2.4. Surface oxidation and patterning

A stencil mask was placed onto the silicon surfaces, and samples were transferred to the plasma chamber. Plasma conditions for SOMS were 300 W, 0.5 Torr O_2, and 10 min. The 1224P can be configured with multiple shelves, including the three parallel active, ground, and float shelves (in this order) employed in this study. The distance between the plates in our study was 2 cm. The radio frequency in the 1224P was 40 KHz. Although the temperature in the 1224P can be raised to 200°C, we worked near room temperature, *i.e.*, the only heating came from the plasma itself, where the temperature in the chamber would typically rise to *ca.* 40°C during oxidation studies.

6.2.5. Surface etching

After surface patterning, samples were immersed in 5% aqueous HF or 35% w/w aqueous KOH for 30 min.

6.2.6. Surface characterization

Surfaces were characterized by spectroscopic ellipsometry, AFM, and XPS. In the XPS measurement, a decontaminator (Evactron C RF plasma cleaner, XEI Scientific, Redwood City, CA, USA) was used for in situ cleaning in the XPS antechamber.

6.3. Results and discussion

I first explored basic reaction conditions for oxide growth (effects of pressure and reagent purity). The effect of pressure was studied by performing oxidation at both 2 Torr and 0.5 Torr, where the degree of surface oxidation was evaluated on each of the active, ground, and float

plates. Reagent purity was also studied. The second part of this chapter describes the use of SOMS as a surface-patterning tool.

Surface oxidation at 2 Torr oxygen was performed from 100 to 250 W plasma power in 50 W increments, inclusively (see Table 6.1). In general, no increase in silicon oxide thickness was observed by spectroscopic ellipsometry from shards on the active, ground, or float plates in 14 experiments, where one silicon shard was present on each shelf in each experiment. However, in a few cases, film increases of up to 10Å were found. This higher (2 Torr) pressure was eliminated as a viable reaction condition based on the irreproducibility of these results and/or lack of surface oxidation. After the treatments at 2 Torr O_2 and at lower pressure (*vide infra*), all surfaces were wetted by water.

A pressure of 2 Torr did not yield stable and reproducible oxidation. To better understand this result, I went back to the equation for the mean free path of a gas:

$$\lambda = \frac{kT}{\sqrt{2}\pi\sigma p} \tag{6.1}$$

where λ represents the mean free path, k is Boltzmann's constant, T is the absolute temperature, σ is the collision cross section, and p is the gas pressure:

Also, in an electric field, the kinetic energy of a particle is given by:

$$E_k = qE\lambda \qquad (v_0 = 0) \tag{6.2}$$

Therefore, if the mean free path is too small, the electrons or ions initially formed in a plasma are unable to act under the influence of the high voltage long enough to gain sufficient energy to ionize surrounding neutral species. As a result, reasonable plasma cannot be maintained. To increase the mean free path, the pressure can be lowered. Upon going from 2 to 0.5 Torr, λ

Table 6.1. Changes in ellipsometric thickness after oxygen plasma treatment of silicon wafers at 2 Torr O_2 (99.5% O_2). Either no oxidation or irreproducible oxidation is observed.

Power (W)	Δt (Å) (active plate)	Δt (Å) (ground plate)	Δt (Å) (float plate)
250	-0.11	0.08	-0.1
250	0.02	0.07	0.24
200	0.71	0.53	0.31
200	0.52	0.23	0.11
200	0.06	-0.03	0.05
150	0.12	-0.01	0.17
150	7.91	10.43	1.44
150	-0.07	-0.08	-0.35
150	2.15	5.05	1.05
150	0.25	0.28	1.46
100	0.19	0.11	-0.09
100	0.96	2.54	0
100	-0.32	-0.43	0.09
100	-1.63	-1.81	-0.84

increases by a factor of 4, *i.e.*, $\lambda \propto 1/p$, and therefore stable, reproducible plasma oxidation should be more easily obtainable. However, if pressure is too low, plasma cannot be retained. For example, when we decreased pressure to 0.2 torr, plasma was not stable and cannot happen continuously. Indeed, linear increases in SiO_2 film thickness on the active and ground plates were observed as the plasma power increased from 50 to 400 W for a fixed time (Figure 6.1). Essentially no increase in film thickness took place on the float plate and, as expected, the film thickness increase on the active plate was somewhat higher than on the ground plate.

Si 2p narrow scans in X-ray photoelectron spectroscopy (XPS) confirmed silicon oxide growth by the increase in the silicon oxide peak at *ca*. 103 eV compared to the bulk silicon signal at *ca*. 99 eV (see Figure 6.2). Oxidation was also confirmed by the increasing ratio of oxygen to silicon, *i.e.*, with an increase in oxidation, the silicon dioxide layer thickness increased and the ration of oxygen to silicon increased (see Table 6.2). Steady increases in oxide thickness were also observed as oxidation times were increased from 4 to 20 min at fixed power (250 W) (see Figure 6.3). Atomic force microscopy (AFM) confirmed surface flatness. For example, after plasma oxidation at 250 W for 5 min, the rms surface roughness was 1.59 Å compared to 1.51 Å rms roughness prior to plasma oxidation.

A mathematical model was empirically derived to fit the change in oxide thickness on the active and ground plates. The thickness of the native oxide, which had been measured for each surface and then subtracted from the total ellipsometric thickness to give the values in this table, was 18.19 ± 0.72 Å. The data were fit by multiple linear regression from the model:

$$\Delta t_{oxide} = b_0 + b_1 * P + b_2 * t \qquad (6.3)$$

where P is power in Watts and t is time in min. Sets of experimental results (t_{oxide}, p, t) were used to create data matrices, as shown for the data from the active plate:

(a)

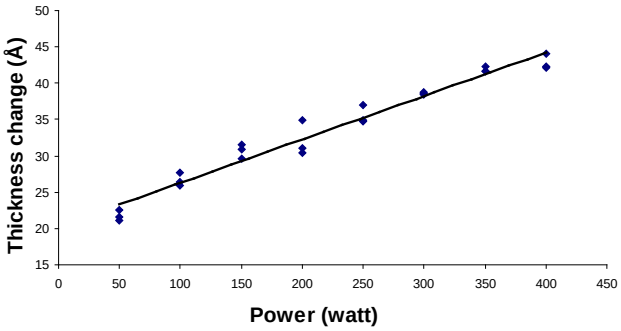

(b)

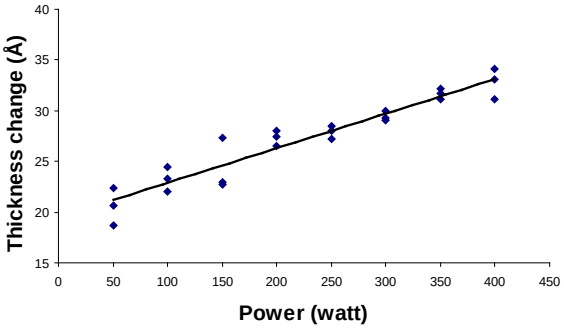

(c)

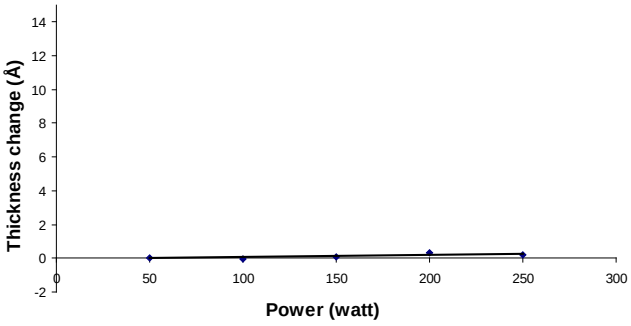

Figure 6.1. Spectroscopic ellipsometry after plasma oxidation (99.994% O_2) at 0.5 torr as a function of power. By "Thickness change" we mean that the native oxide thickness of 18-20 Å was subtracted from the total thickness obtained after oxidation. (a) active plate, (b) ground plate, (c) float plate.

(a)

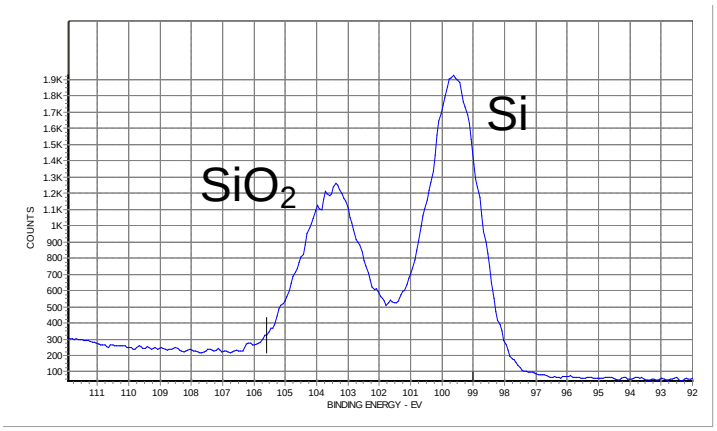

(b)

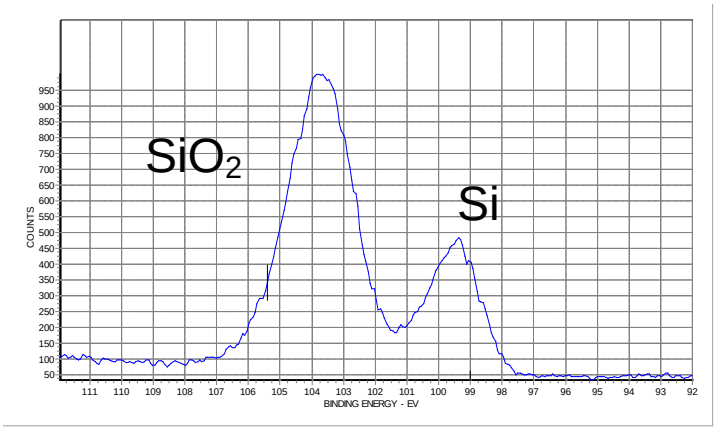

(c)

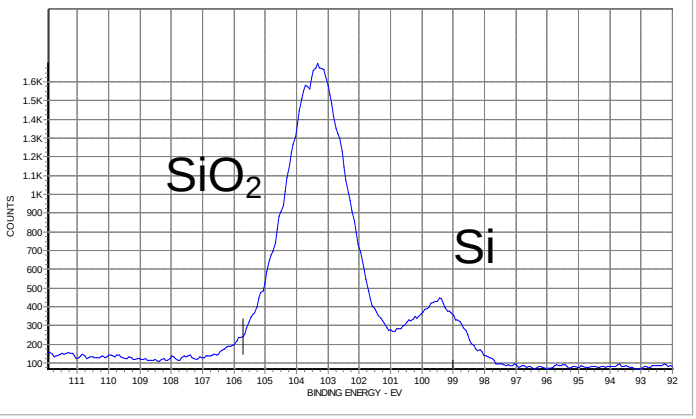

Figure 6.2. XPS narrow scans of silicon before and after plasma oxidation using 99.5% O_2. (a) Untreated Si wafers after cleaning, (b) after 5 min of plasma oxidation at 50 W on active plate, (c) after 5 min of plasma oxidation at 250 W on active plate.

Table 6.2. O1s/Si2p ratio after plasma oxidation on the active plate for 5 min as measured by XPS.

Samples	O/Si	Total oxide thickness (Å)
Control (no oxidation)	1.32	17.9
Plasma power: 50 W	2.32	38.3
Plasma power: 250 W	2.57	51.0

(a)

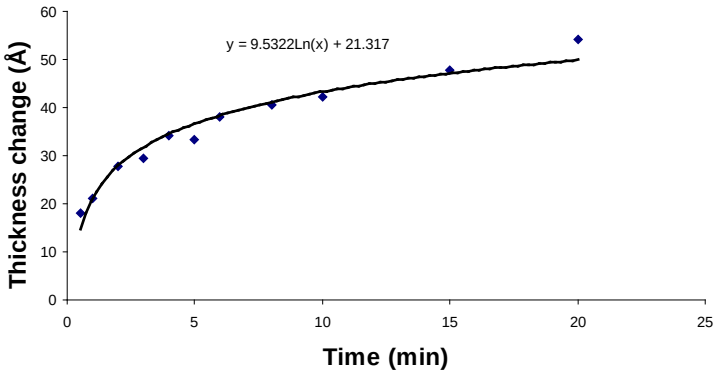

(b)

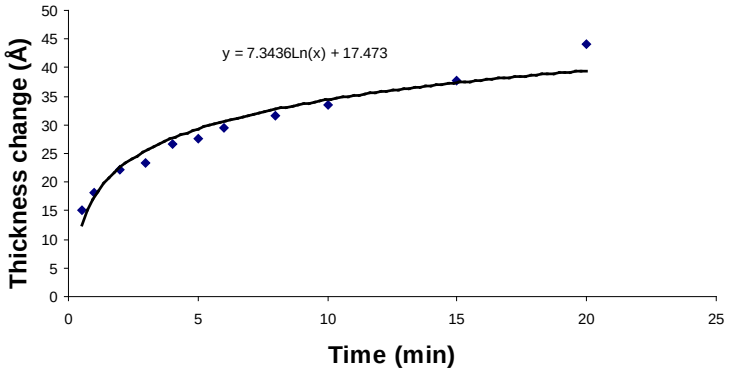

Figure 6.3. Spectroscopic ellipsometry after plasma oxidation (99.994% O_2) at 0.5 Torr and 250 W as a function of time, (a) samples on active plate, and (b) samples on ground plate. "Thickness change" means that the native oxide thickness of 18-20 Å was subtracted from the total thicknesses before these numbers were plotted. These oxide thicknesses were individually measured and then subtracted for each surface.

$$\begin{bmatrix} 42.78 \\ 41.90 \\ 38.60 \\ 35.55 \\ 32.16 \\ 30.68 \\ 26.62 \\ 21.75 \\ 54.26 \\ 47.77 \\ 42.26 \\ 40.69 \\ 38.03 \\ 33.32 \\ 34.13 \end{bmatrix} = \begin{bmatrix} 1 & 1 & 0.25 \\ 1 & 0.875 & 0.25 \\ 1 & 0.75 & 0.25 \\ 1 & 0.625 & 0.25 \\ 1 & 0.5 & 0.25 \\ 1 & 0.375 & 0.25 \\ 1 & 0.25 & 0.25 \\ 1 & 0.125 & 0.25 \\ 1 & 0.625 & 1 \\ 1 & 0.625 & 0.75 \\ 1 & 0.625 & 0.5 \\ 1 & 0.625 & 0.4 \\ 1 & 0.625 & 0.3 \\ 1 & 0.625 & 0.25 \\ 1 & 0.625 & 0.2 \end{bmatrix} \begin{bmatrix} b_0 \\ b_1 \\ b_2 \end{bmatrix}$$

The two vectors and matrix are denoted **a = V * b**, respectively. The parameters to be fit to the linear model (B) were obtained by basic matrix algebra:

$$\mathbf{a = V * b} \tag{6.4}$$

$$\mathbf{V^T a = V^T V * b\ b} \tag{6.5}$$

$$\mathbf{b = (V^T V)^{-1} V^T a} \tag{6.6}$$

Increases in oxide thickness (Δt_{oxide}) (from 4 to 20 min and from 50 to 400 W) could be well fit to an empirical model, giving

active plate:

$$\Delta t_{oxide}(\text{Å}) = 13.97\ (\text{Å}) + 0.05988\ (\text{Å/W}) \times \text{power (W)} + 1.281\ (\text{Å/min}) \times \text{time (min)} \tag{6.7}$$

ground plate:

$$\Delta t_{oxide}(\text{Å}) = 14.22\ (\text{Å}) + 0.03415\ (\text{Å/W}) \times \text{power (W)} + 1.0515\ (\text{Å/min}) \times \text{time (min)}. \tag{6.8}$$

The average absolute values of the errors from these models were 0.81 and 0.40Å with

$$\frac{\sum \left| t_{oxide(real)} - t_{oxide(predicted)} \right|}{n} \qquad (6.9)$$

mean square errors of 1.08 and 0.21 on the active and ground plates, respectively (see Table 6.3).

Reagent purity was studied using 99.5 or 99.994% O_2. After oxidizing silicon at 250W for 5 min at 0.5 Torr with both O_2 sources on the active and ground plates, the carbon content of the resulting films was evaluated by XPS, where this analysis included a gentle *in situ* cleaning of the surface to remove carbon contamination at the SiO_2-vacuum interface using an Evactron CDe-Contaminator from XEI Scientific. Although the carbon content is low on all of the surfaces, it is higher on surfaces made with the less pure reagent gas (see Table 6.4). It is clear that higher-purity oxygen is preferred for silicon oxidation. The oxidation experiments in Figure 6.1 were repeated with the more pure O_2 gas, and the change in film thickness was essentially the same as before.

I wondered if it would be possible to use room-temperature plasma oxidation of silicon as a patterning method. A first proof of principle experiment involved plasma oxidation of a silicon shard that was half-covered with another silicon shard. After plasma oxidation, the ellipsometric thickness of the covered area did not change, but the thickness of the exposed area did increase. A TEM grid (a square pattern of 5 μm open squares separated by 7.5 μm bars) was then employed as a more sophisticated stencil mask. A cartoon of this process (Scheme 6.1) illustrates the placement of the mask, oxygen plasma treatment of the surface, mask removal, and then etching in HF to reveal/create a three dimensional pattern. As suggested in this Scheme, HF etching results in oxide removal. HF can etch silicon dioxide very quickly, about 20 Å/s. However, for silicon, the etching rate of HF is extremely slow. Therefore, after HF etching on this silicon dioxide pattern, a physical pattern of silicon can be obtained. Because the silicon dioxide pattern is shallow, about 1 nm, the same shallow silicon pattern is obtained. Optical

Table 6.3. Data fit with linear models.

Time (min)	Power (W)	Δt (Å) (Active)	Δt (Å) (Ground)
5	400	42.78	32.8
5	350	41.9	31.69
5	300	38.6	29.43
5	250	35.55	27.88
5	200	32.16	27.3
5	150	30.68	24.36
5	100	26.62	23.27
5	50	21.75	20.58
20	250	54.26	44.05
15	250	47.77	37.84
10	250	42.26	33.54
8	250	40.69	31.54
6	250	38.03	29.59
5	250	33.32	27.56
4	250	34.13	26.76

Table 6.4. Carbon content of surfaces as measured by XPS after surface oxidation using higher and lower purity O_2 gas.

Samples	99.5%O_2	99.994%O_2
Active plate	1.41% C	0.21% C
Ground plate	2.12% C	0.56% C

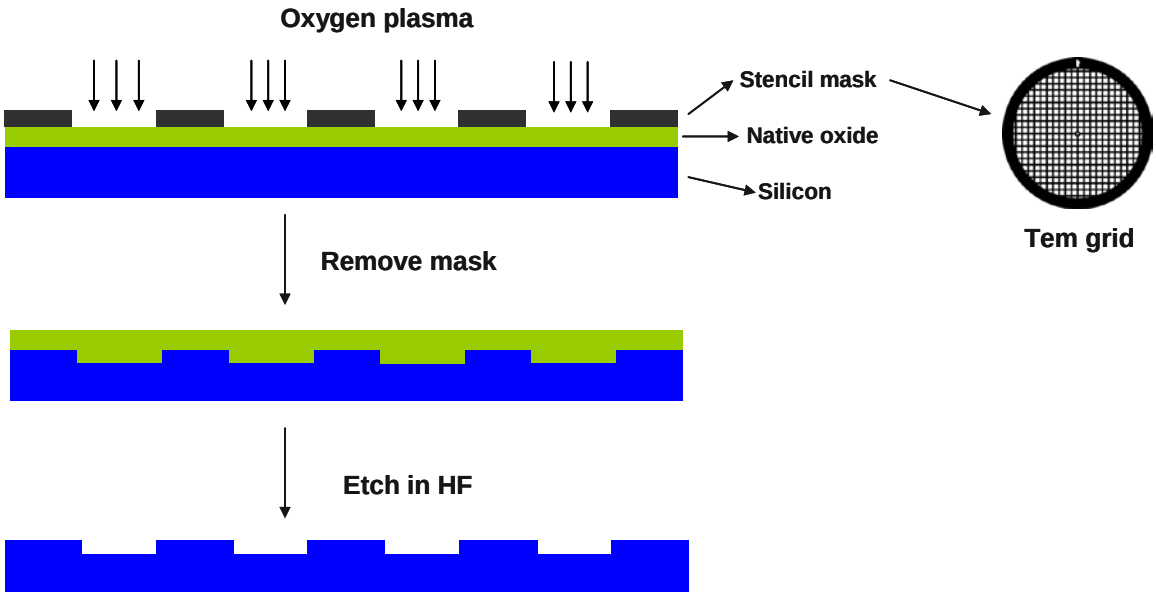

Scheme 6.1. HF etching process.

microscopy and SEM offered clean pictures of this physical silicon pattern (see Figure 6.4). AFM confirmed the form of the pattern and gave the aspect ratio of this pattern (see Figure 6.5)

Deep etching can be performed with KOH, which etches SiO_2 much more slowly than Si (1.44 nm/h *vs.* 1.32 μm/h, respectively, 20°C) (see Figure 6.6).[6] Accordingly, the plasma-patterned surface was immersed in a KOH solution that slowly etches the oxide until it breaks through the thinner regions of the oxide layer (the masked regions). The thicker layers of oxide produced by plasma oxidation remain to mask regions of the substrate from deep etching (see scheme 4.2). AFM confirmed the patterning/etching process (Figure 6.7). SEM and optical micrographs showed the expected pattern after plasma treatment. After KOH etching, AFM reveals a pattern of squares *ca.* 500 nm higher than the background lines (Figure 6.8). Other stencil masks are available that should allow the creation of lines, dots, and other shapes with our method.

Plasma oxidation at *ca*. room temperature has been investigated as a function of plasma power, pressure, and time. Surface patterning using stencil masks is demonstrated. Patterns are revealed by HF or KOH etching.

6.4. Conclusions

I explored a straightforward patterning technique for silicon: subsurface oxidation for micropatterning silicon (SOMS). Plasma oxidation is used to create a pattern of thicker oxide in the exposed regions. Etching with HF or KOH produces very shallow or much higher aspect ratio features on silicon, respectively, where patterning is confirmed by atomic force microscopy, scanning electron microscopy, and optical microscopy. The oxidation process itself is studied under a variety of reaction conditions, including higher and lower oxygen pressures (2 and 0.5

(a)

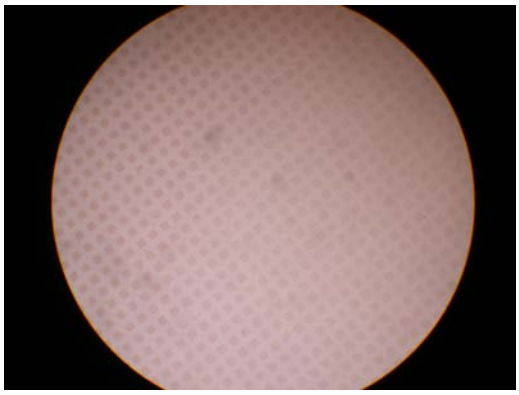

(b)

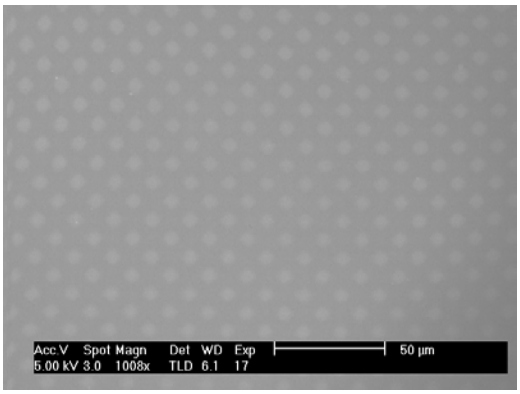

Figure 6.4. Silicon subsurface patterning by oxidation through a TEM grid. (a) Optical micrographs after etching. (b) SEM micrographs after etching. Each small square is 5 µm × 5 µm.

(a) (b)

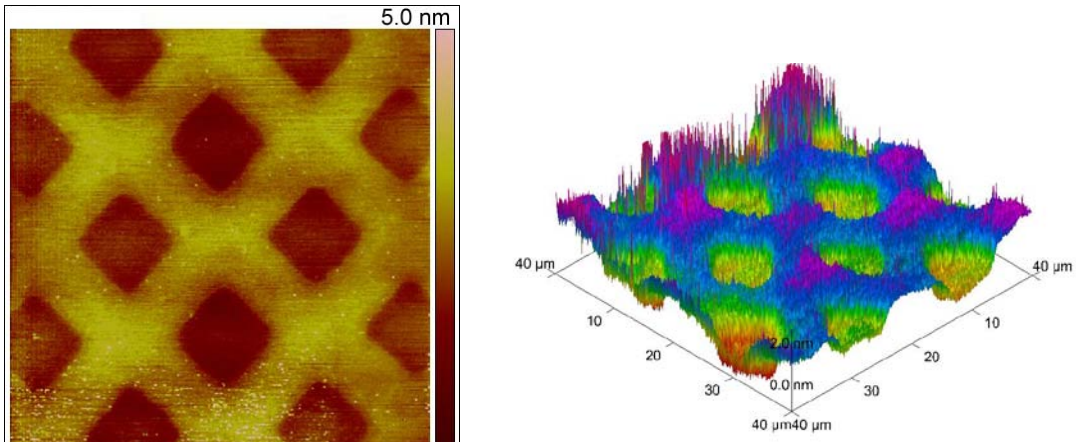

(c) (d)

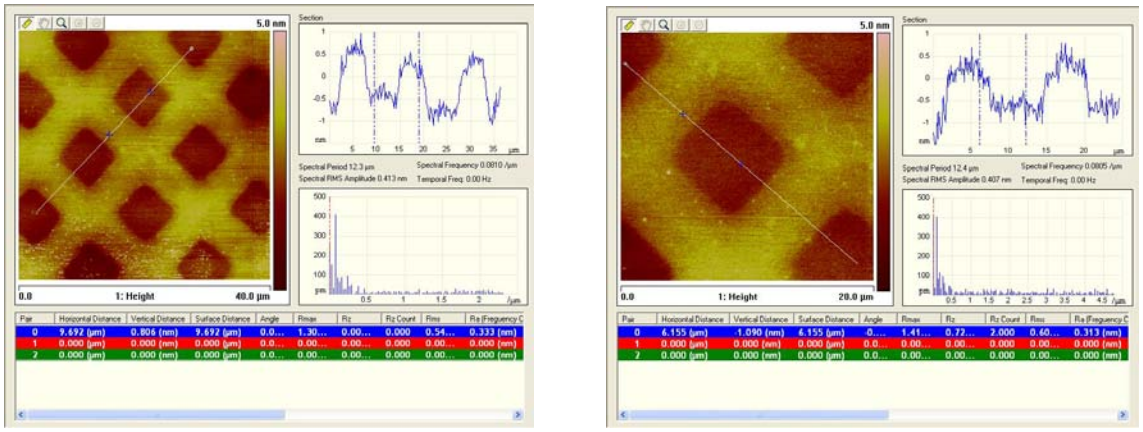

Figure 6.5. AFM images following HF etching (*ca.* 1 nm vertical features are observed). (a) 40 µm × 40 µm image, (b) 3D image, (c) height measurement of 40 µm × 40 µm image, (d) height measurement of 20 µm × 20 µm image.

(a)

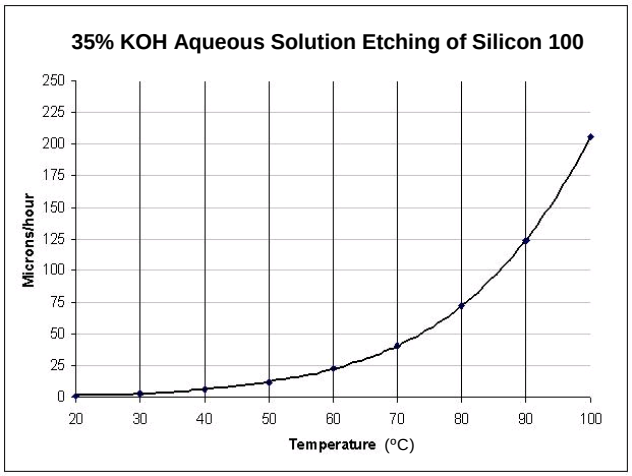

(b)

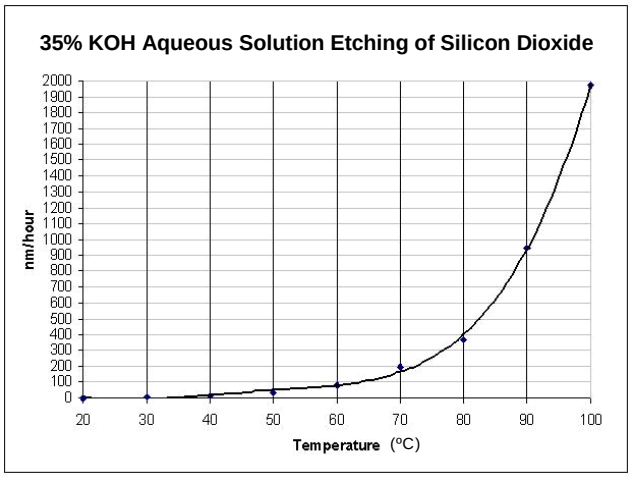

Figure 6.6. KOH etching rate on silicon (a) and silicon dioxide (b).[6]

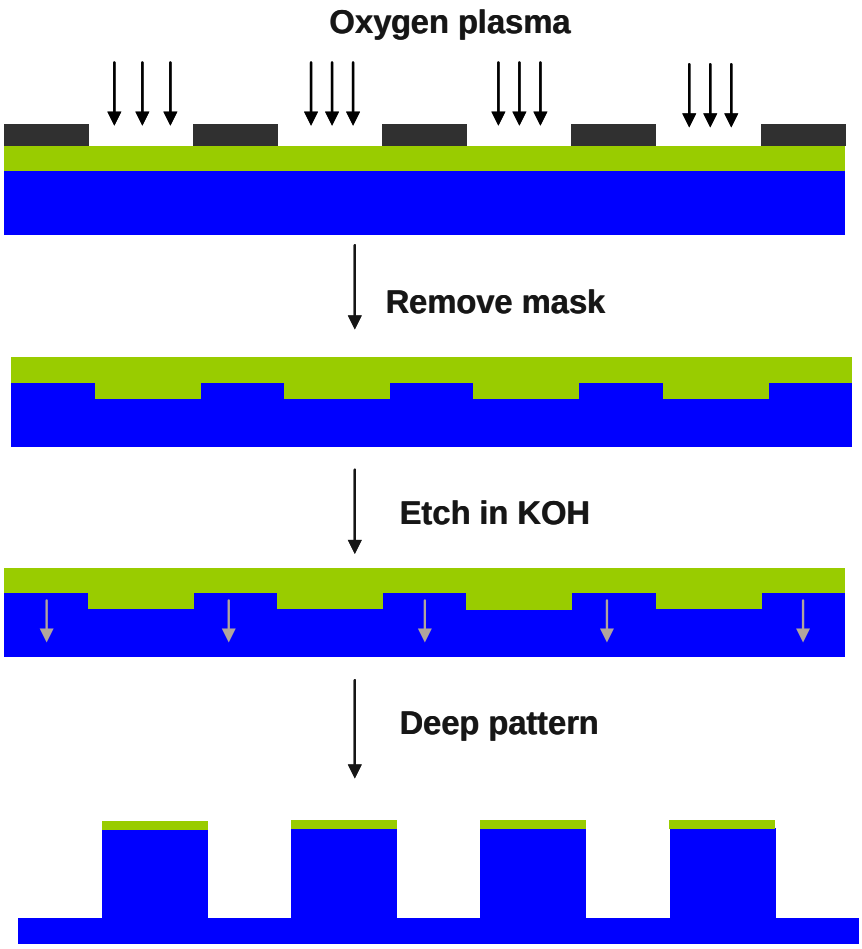

Scheme 6.2. KOH etching process showing formation of deep features.

(a)

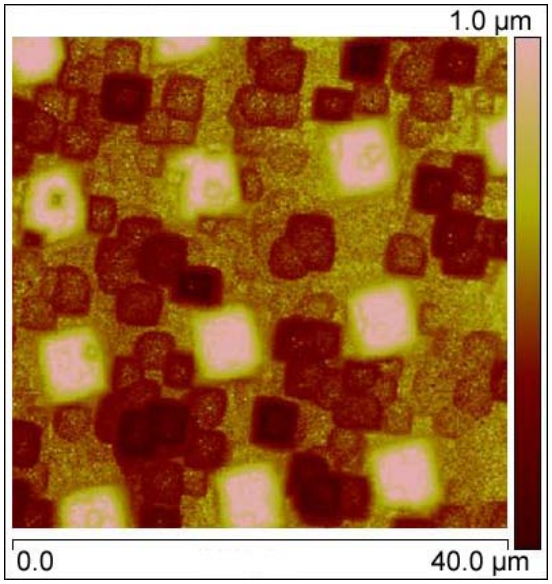

(b)

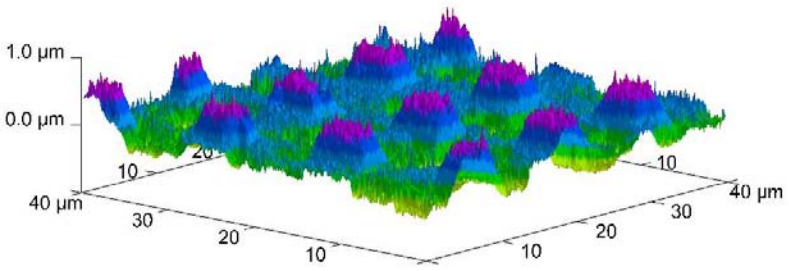

Figure 6.7. Silicon subsurface patterning by oxidation through a TEM grid. (a) AFM 2D and (b) 3D images after etching with KOH.

(a)

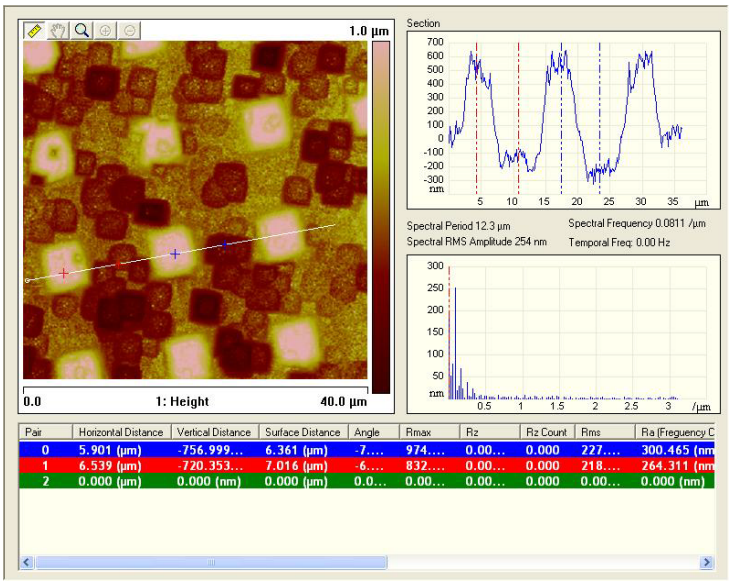

(b)

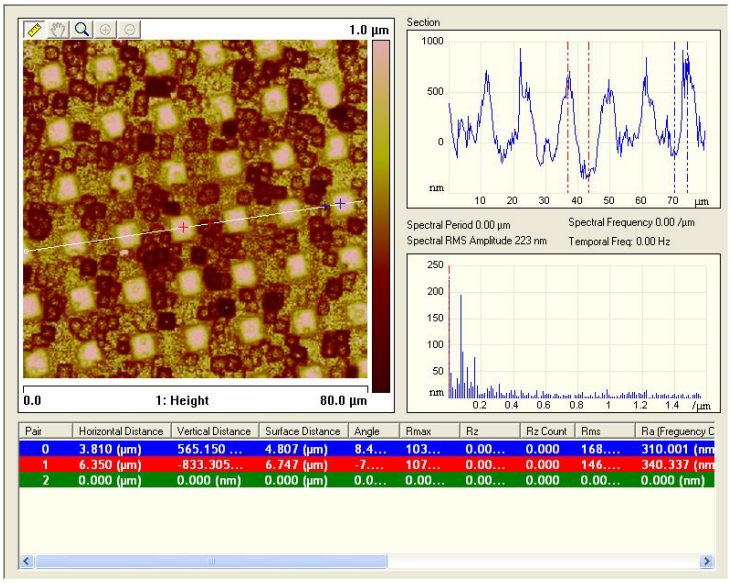

Figure 6.8. AFM images after KOH etching. (a) 40 µm × 40 µm image, (b) 80 µm × 80 µm image.

Torr), a variety of powers (50-400 W), different times, and as a function of reagent purity (99.5 or 99.994% oxygen). SOMS can be easily executed in any normal chemistry laboratory with a plasma generator. Because of its simplicity, it may have industrial viability.

6.5. References

1. Madou, M. J., *Fundamentals of Microfabrication, 2nd ed.* CRC Press: Boca Raton, FL, 2002.
2. Bullett, N. A.; Short, R. D.; O'Leary, T.; Beck, A. J.; Douglas, C. W. I.; Cambray-Deakin, M.; Fletcher, W.; Roberts, A.; Blomfield, C., *Surf. Interface Anal.* **2001,** *31*, 1074-1076.
3. Khademhosseini, A.; Suh, K. Y.; Jon, S.; Eng, G.; Yeh, J.; Chen, G.-J.; Langer, R., *Anal. Chem.* **2004,** *76*, 3675-3681.
4. Yang, L.; Lua, Y.-Y.; Lee, M. V.; Linford, M. R., *Acc. Chem. Res.* **2005,** *38*, 933-942.
5. Abe, H.; Yoneda, M.; Fujiwara, N., *Jpn. J. Appl. Phys.* **2008,** *47*, 1435-1455.
6. Seidel, H.; Csepregi, L.; Heuberger, A.; BaumgSrtel, H., *J. Electrochem. Soc.* **1990,** *137*, 3612–3626.

Chapter 7. Wet Spinning of Pre-doped Polyaniline into an Aqueous Solution of a Polyelectrolyte*

7.1. Introduction

Polyaniline (PANi) has several advantages over other conductive polymers because it is stable, highly conductive, and has good mechanical properties.[1-4] Originally, high molecular weight PANi could only be processed in the non-conductive form or in the low conductivity, low molecular weight emeraldine salt form. However, Cao *et al*. found that the emeraldine base of polyaniline (PANi EB) could be doped in such a way that its counter ion induces solubility.[5] In addition, this form of doping was more uniform than before, because the bulkier dopant molecules employed could not easily diffuse within the polymer. In another important advance, Monkman and coworkers used 2-acrylamido-2-methyl-1-propanesulfonic acid (AMPSA) or camphor sulfonic acid as the dopant and dichloroacetic acid (DCA) as the solvent to wet-spin fibers with good mechanical and electrical properties. However, in the wet spinning of this material, only flammable and somewhat toxic organic solvents were used as coagulation solvents.[6-7] Also, star poly(styrenesulfonate) has previously been used as a template for making an electroactive polymer complex with polyaniline.[8]

Here I show that an aqueous solution of a polyanion facilitates the formation of fibers compared to other aqueous solutions, including those containing different salts, polycations, and other small molecules. I then show a more extensive study on the formation and characterization of PANi fibers spun into a solution of a common polyanion: poly(styrene sulfonic acid), sodium salt (PSS). Scanning electron microscopy (SEM) and X-ray photoelectron spectroscopy (XPS) analyses suggest that PSS stabilizes the fibers by forming a thin polymer film on their surfaces.

---

*Taken from (Feng Zhang, Peter A. Halverson, Barry Lunt, and Matthew R. Linford) *Synthetic Metals*, **2006**, *156*, 932-937.

7.2. Experimental

PANi (MW 55,000) obtained from Panipol (Porvoo, Finland)) was mixed with AMPSA (Sigma Aldrich, 99%) using a mortar and pestle at a molar ratio of 1:0.6. Previous work has suggested this to be a good doping ratio for films and fibers.[9] The mixture was then dissolved in DCA (Sigma Aldrich) to form a 9 wt.% solution, which is reported to be the optimal concentration for fiber spinning.[6] The solution was stirred for 45 min and filtered through a 90 µm inline filter. The solution was then pushed through a single 150 µm orifice at a pressure between 690 and 760 KPa into a coagulation solvent. No air gap was present, and no take up mechanism was used. The fiber was later removed from the coagulation solvent. Once removed, the fiber was washed with copious quantities of distilled water and dried at 50°C for 12 h. Electrical conductivity measurements were made via the four-probe method. All reagents were used as received including: PSS (MW 70,000, 30 wt.% solution in water, Sigma, USA), poly(methacrylic acid) sodium salt (PMAA, MW 9500, 30 wt.% solution in water, Sigma, USA), sodium propionate (≥ 99%, Sigma, USA), sodium dodecyl sulfate (SDS, ≥ 99%, Fisher, USA), sodium benzenesulfonate (≥ 99%, Spectrum Quality Products, New Brunswick, NJ, USA), Na_2SO_4 (≥ 99%, Fisher), Na_2CO_3 (≥ 99%, EM Science, Gibbstown, NJ, USA), NaCl (≥ 99%, Fisher, USA) propylamine hydrochloride (≥ 99%, Sigma, USA), hexadecyltrimethylammonium bromide (≥ 99%, Sigma, USA), poly(allylamine hydrochloride) (PAH, ≥ 99%, Sigma, USA), poly(diallyldimethylammonium chloride) (PDADMAC, MW 400,000–500,000, 30 wt.% solution in water, Sigma, USA), acetone (≥ 99%, Fisher, USA). Scanning electron microscopy (SEM) was performed with a Philips XL30 ESEM FEG (Philips, MX Amsterdam, Netherlands). X-ray photoelectron spectroscopy (XPS) was performed with an SSX-100 ESCA Spectrometer from Surface Science Laboratories, Mountain View, CA, USA.

7.3. Results and discussion

7.3.1. Different coagulation solutions

It has been shown in the literature that acetone,[6-7] but not water,[6] can be used as a coagulation bath for spinning PANi fibers. We repeated these results in attempts to make thick PANi fibers. As noted in Table 7.1, infinitely long fibers can be made when PANi is spun into acetone, but only very short fibers, which break apart quickly in the coagulation bath, are obtained when PANi is spun into water.

In this study, I show that aqueous solutions of two different polyanions facilitate PANi spinning. However, to better explore this topic and to understand the generality of our results, I also attempted to spin PANi into aqueous coagulation baths that contained different salts, small cationic molecules, polycations, and small anionic molecules (see Figure. 7.1). In general, poor results were obtained with all of these other materials. For example, Table 7.1 shows that spinning into aqueous solutions of sodium sulfate (Na_2SO_4), sodium carbonate (Na_2CO_3), and sodium chloride (NaCl) produces very short fibers (0.5-1 cm). Clearly, dianions like SO_4^{2-} and CO_3^{2-} do not stabilize the polymer as it is extruded to allow fiber formation. Low quality fibers were also produced when PANi is spun into aqueous solutions of small cationic molecules, such as propylamine hydrochloride ($CH_3CH_2CH_2NH_2 \cdot HCl$), a primary amine, and hexadecyl-trimethylammonium bromide ($C_{16}H_{33}N(CH_3)_3Br$), a quaternary amine. Slightly longer fibers, but still of very low quality, were obtained when PANi was spun into aqueous solutions of polycations such as poly(allylamine hydrochloride) (PAH), a polymer containing primary amines, or poly(diallyldimethylammonium chloride), (PDADMAC), a polymer containing quaternary amines. I also attempted to spin into aqueous solutions of three small, anionic molecules including sodium benzenesulfonate ($C_6H_5SO_3Na$), sodium dodecylsulfate ($C_{12}H_{25}OSO_3Na$)

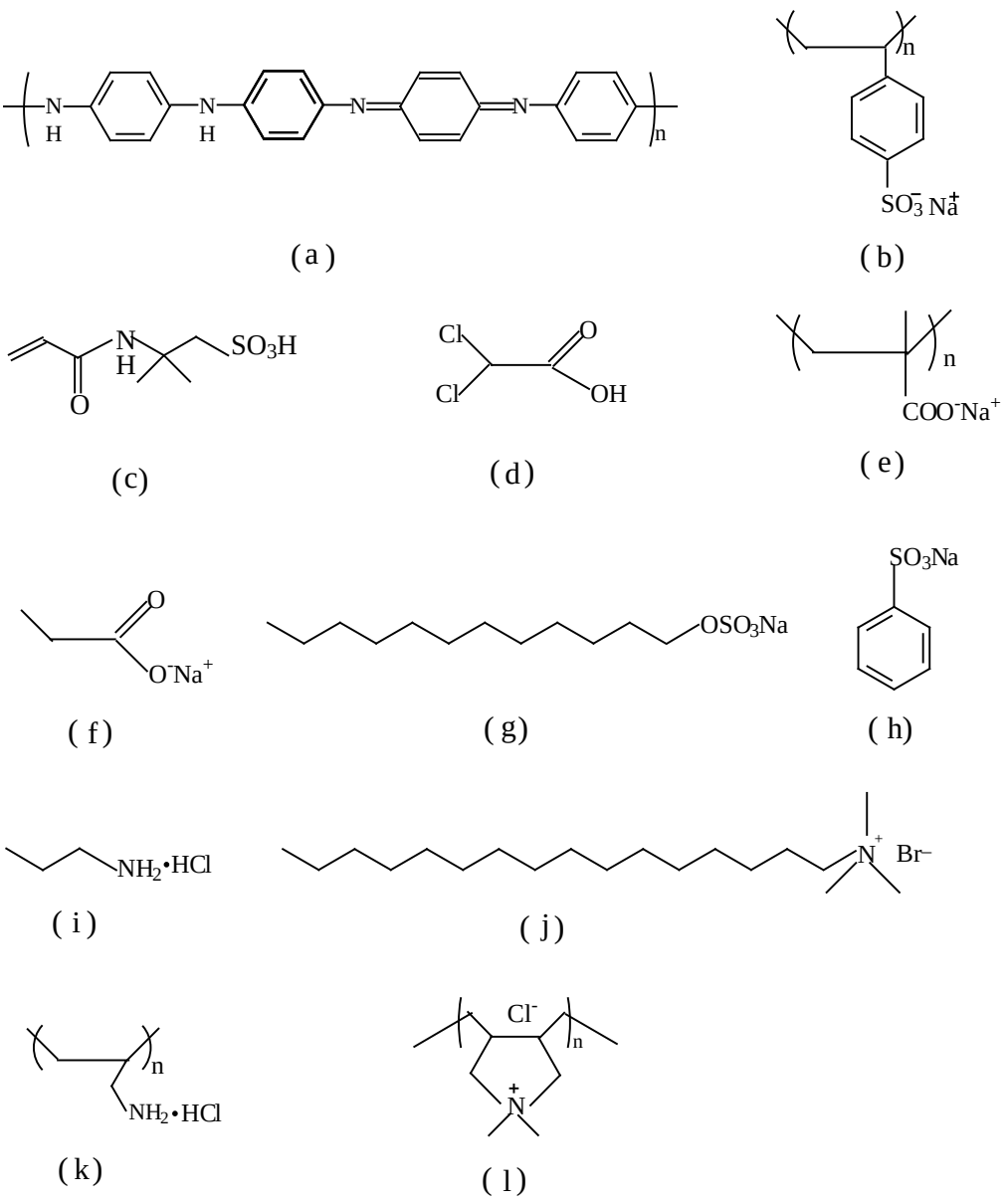

Figure 7.1. Structures of compounds used in this study. (a) polyaniline (PANi), (b) poly(sodium 4-styrenesulfonate) (PSS), (c) 2-acrylamido-2-methyl-1-propanesulfonic acid (AMPSA), (d) dichloroacetic acid (DCA), (e) poly(methacrylic acid) sodium salt (PMAA), (f) sodium propionate, (g) sodium dodecyl sulfate (SDS), (h) sodium benzenesulfonate, (i) propylamine hydrochloride, (j) hexadecyltrimethylammonium bromide, (k) poly(allylamine hydrochloride) (PAH), (l) poly(diallyldimethylammonium chloride) (PDADMAC).

Table 7.1. Results of spinning PANi into different coagulation solvents.

Coagulation solvent[a]	Length (cm)	Extruding velocity	Fiber thickness (μm)	Fiber shape/ description
acetone	infinite	medium	70-90	uniform diameter, smooth
water	0.5 - 1	fast	50-70	short, cylindrical
Na_2SO_4	0.5 - 1	fast	50-70	short, cylindrical
Na_2CO_3	0.5 - 1	fast	50-70	short, cylindrical
NaCl	0.5 - 1	fast	50-70	short, cylindrical
propylamine hydrochloride	< 0.5	fastest	50-70	very short, cylindrical
hexadecyltrimethyl ammonium bromide	< 0.5	faster	50-70	twisted, irregular fibers
PAH[b]	1 – 2	lowest	irregular diameter	short, twisted ribbon
PDADMAC[b]	1 – 2	lowest	irregular diameter	soft, short highly twisted ribbon
sodium benzenesulfonate	0.5 - 1	medium	50-70	short, cylindrical
SDS	0.5 - 1	a little slower than medium	50-70	short, cylindrical
sodium propionate	2 - 3	medium	50-70	smoothly cylindrical
PSS	4 - 5	medium	70-90	smoothly cylindrical, uniform
poly(methacrylic acid) sodium salt	4 - 5	medium	70-90	smoothly cylindrical, uniform

[a] All solutions of the species given in this column were 5 wt.% in water, except the first two entries: pure water and pure acetone.

[b] These solutions had high viscosities.

(SDS), and sodium propionate (CH_3CH_2COONa), where the first two of these molecules are conjugate bases of strong acids, and sodium propionate is the conjugate base of a weak acid. Aqueous solutions of sodium benzenesulfonate and SDS led to the formation of very poor quality fibers. The fibers produced by spinning into the solution of sodium propionate were slightly longer, but still too short to be useful. Finally, Table 7.1 shows the result of spinning into aqueous solutions of two different polyanions. The first, poly(styrene sulfonic acid), sodium salt, contains anionic groups (sulfonates), which are the conjugate bases of strong acid groups, and the second, poly(methacrylic acid) sodium salt, contains anionic groups (caboxylates), which are the conjugate bases of weakly acidic groups. At 5% by weight, solutions of PSS and PMAA produce the longest fibers of the aqueous solutions shown in Table 7.1. It is believed that when these polyanions adsorb onto the PANi surface during spinning, the anionic groups of the polyanion take the place of the mobile anions on the surface of the PANi.

7.3.2 PSS coagulation solutions and physical properties of the resulting fibers

In Section 7.3.1, I showed that aqueous solutions of polyanions can be used as coagulation baths to produce PANi fibers. In this section, I present the effect of the concentration of one of these polyanions (PSS) on fiber morphology, conductivity, and surface chemistry.

In order to investigate the effects of PSS concentration on fiber formation, the PANi–AMPSA–DCA solution was wet spun into aqueous solutions that contained between 0 and 20 wt.% PSS. At 0% PSS (pure water), only very short fibers were obtained (see Table 7.2). However, when a low percentage of PSS was present in water (0.5–5.0%) a longer fiber would form. The length of the fibers that could be extruded without breaking increased as the concentration of PSS increased. Finally, at and above 10% PSS, infinitely long fibers (filaments)

Table 7.2. Fiber properties as a function of wt. percent PSS in the coagulation bath.[a]

% PSS	Length	Fiber Properties
0	0.5-1	Did not form
0.5	*ca.* 2 cm	Very rough, irregular
1.0	*ca.* 2 cm	Very rough, irregular
1.5	*ca.* 2 cm	Very rough, irregular
2.0	*ca.* 2 cm	Very rough, irregular
2.5	4-5 cm	Rough cylindrical
5.0	4-5 cm	Rough cylindrical
10	Infinite	Smooth cylindrical
15	Infinite	Smooth cylindrical
20	Infinite	Smooth cylindrical

[a] Lengths given for the fibers spun into 0.5 – 5% PSS are approximate.

would form.

Fiber morphologies were studied by scanning electron microscopy, and were observed to vary smoothly with PSS concentration in the coagulation bath. At lower PSS concentrations, the fiber surfaces were rough and irregular. As the PSS concentration increased, the fibers became smoother. Finally, at the highest concentrations of PSS studied (10–20 wt.%), the fibers were smooth (see Figure 7.2. and Table 7.2.). It is significant that the PSS was not visible on the fiber surfaces by SEM.

SEM micrographs taken of the fiber ends showed no significant macro-voids in any of the fibers regardless of the concentration of PSS into which they were spun (see Figure. 7.3). X-ray photoelectron spectroscopy is used to obtain elemental compositions of the upper *ca.* 10 nm of surfaces, and XPS was used to verify that PSS had adsorbed onto the surface of PANi fibers in the spinning process. Figures. 7.4. and 7.5. show the percent sulfur, nitrogen, chlorine, carbon, and oxygen on PANi fibers (or the powder) that were extruded into different concentrations of PSS. It is significant that at 0 wt.% PSS there is very little sulfur on the surface, which is presumably due to the dopant, but that this amount rises abruptly as the percent PSS in the coagulation bath increases. The sulfur and oxygen contents of the PANi surfaces also appear to be well correlated, which is consistent with a material such as PSS that contains both sulfur and oxygen adsorbing to the surface. Also consistent with this adsorption is a decreasing nitrogen signal. In addition, the gradually decreasing carbon signal is consistent with PSS adsorption: polyaniline has six carbon atoms per heteroatom (nitrogen), while PSS has only three carbon atoms per heteroatom, excluding sodium. The small chlorine signal is probably due to deprotonated dichloroacetic acid acting as a counter ion for the PANi. Chlorine is also a common

(a)

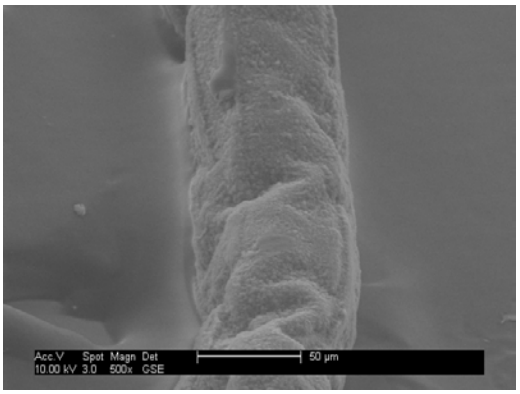

(b)

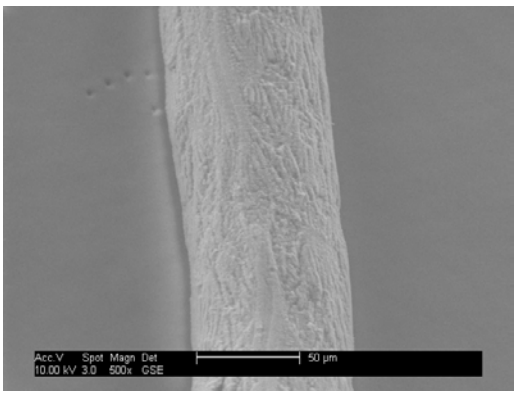

(c)

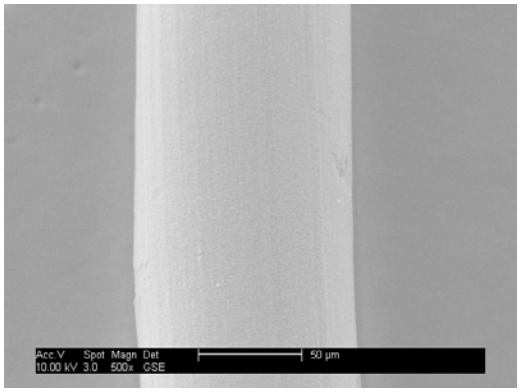

Figure 7.2. Fiber morphology; (a) very rough, irregular (spun into 1.5% PSS), (b) rough, cylindrical (spun into 5% PSS) and (c) smooth, cylindrical (spun into 15% PSS).

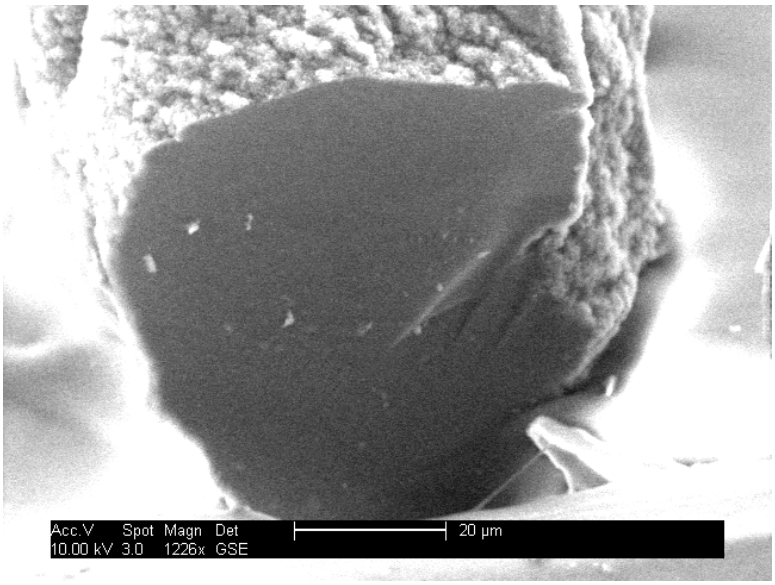

Figure 7.3. Cross section of a PANi fiber (spun into 2% PSS solution).

(a)

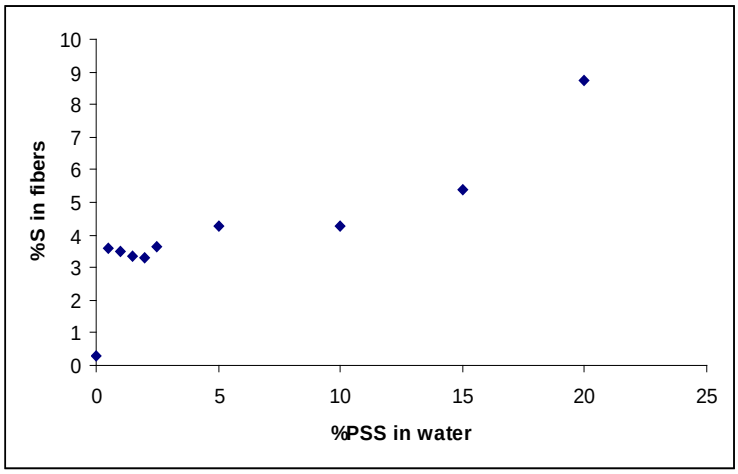

(b)

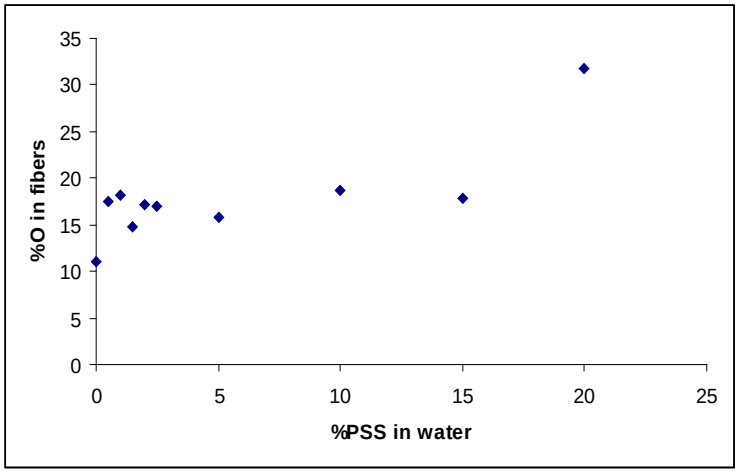

(c)

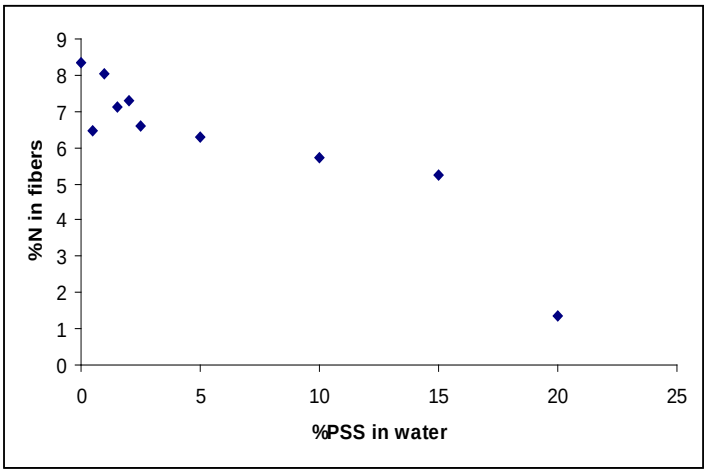

Figure 7.4. XPS data giving percentages of (a) sulfur, (b) oxygen, and (c) nitrogen on the surfaces of the PANi fibers spun into aqueous solutions of PSS.

(a)

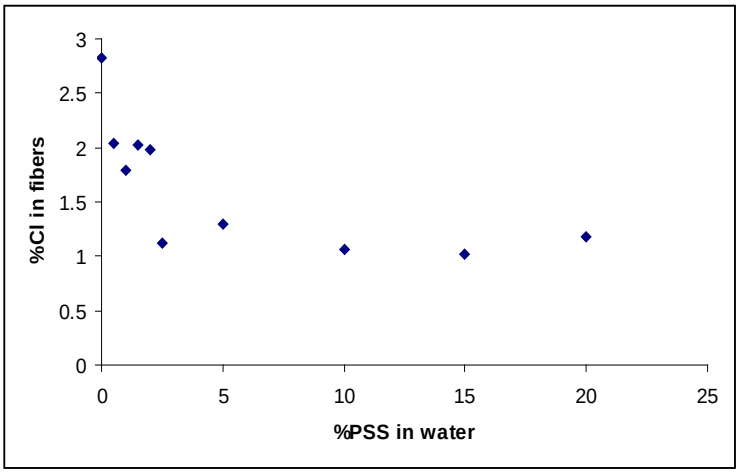

(b)

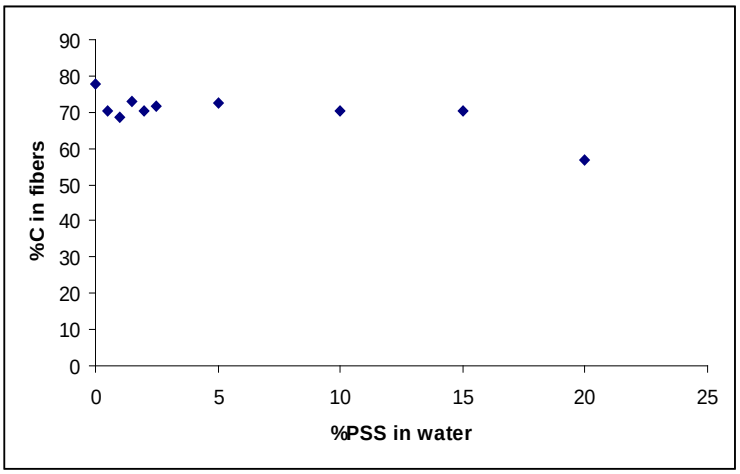

Figure 7.5. XPS results giving percentages of (a) chlorine and (b) carbon on the surfaces of fibers spun into aqueous solutions of PSS.

contaminant of many materials. Based on the known mean-free paths of photoelectrons in polymers these XPS results suggest that the PSS film is not more than 100–150 Å thick for the 20% PSS concentration.[10]

The presence of PSS in water undoubtedly lowers the solubility parameter of water thus slowing the rate of diffusion of DCA out of the fiber. However, this cannot be the only contributing factor to the formation of fibers. If there were lower concentrations of PSS, one would expect to see an increase in the formation of macro-voids in the PANi fiber due to the rapid formation of a fiber skin. As the inner core solidifies, the density would increase causing increased stress and, possibly, fissures on the shell along with larger macro-voids in the interior. As previously mentioned, an SEM inspection of the cross-section showed no change from one sample to another. Finally, I note that one of the most important properties of a conductive fiber is its electrical conductivity. I found reasonable conductivities for all of the fibers spun at different PSS concentrations (see Table 7.3.).

7.4. Conclusions

I prepared highly conductive polyaniline (PANi) fibers via a wet-spinning process into different coagulation solvents or solutions. To the best of my knowledge, this is the first successful spinning of PANi fibers into an aqueous environment where no post-doping of the fiber is needed. Aqueous solutions of different salts, small anionic molecules, small cationic molecules, polycations, and polyanions were studied. Best results were obtained using an aqueous solution of a polyanion as a coagulation bath. The resulting fibers exhibited good length, stability, and morphology. An in depth study of the relationship between the fiber properties and the concentration of a polyanion in the aqueous bath [poly(sodium 4-styrenesulfonate), PSS] was

Table 7.3. Effect of PSS concentration on the electrical properties of the fibers.

% PSS	Electrical Conductivity (s cm^{-1})[a]
20	22.7 ± 3.92
15	23.54 ± 5.45
10	15.22 ± 2.56
5	37.3 ± 6.41
2.5	35.2 ± 6.10

[a]Errors are the standard deviations of two or three measurements.

performed. It was shown that PSS solutions stabilize the PANi fibers without dramatically changing the conductivity of the fibers. It is believed that this stabilization is a result of numerous ionic interactions between cationic centers on the PANi and anionic groups on the polyanion. These results are promising for the production of PANi fibers on a commercial scale because they dramatically reduce the number of toxins used in the wet-spinning process.

7.5. References

1. Kohlman, R. S.; Zibold, A.; Tanner, D. B.; Ihas, G. G.; Ishiguro, T.; Min, Y. G.; MacDiarmid, A. G.; Epstein, A. J., *Phys. Rev. Lett.* **1997,** *78*, 3915-3918.
2. Pratt, F. L.; Blundell, S. J.; Hayes, W. A.; Nagamine, K.; Ishida, K.; Monkman, A. P., *Phys. Rev. Lett.* **1997,** *79*, 2855–2858.
3. Shimano, J. Y.; MacDiarmid, A. G., *Synth. Met.* **2001,** *123*, 251-262.
4. Jang, S.-Y.; Seshadri, V.; Khil, M.-S.; Kumar, A.; Marquez, M.; Mather, P. T.; Sotzing, G. A., *Adv. Mater.* **2005,** *17*, 2177–2180.
5. Cao, Y.; Smith, P.; Heeger, A. J., *Synth. Met.* **1992,** *48*, 91-97.
6. Pomfret, S. J.; Adams, P. N.; Comfort, N. P.; Monkman, A. P., *Adv. Mater.* **1998,** *10*, 1351–1353.
7. Pomfret, S. J.; Adams, P. N.; Comfort, N. P.; Monkman, A. P., *Polymer* **2000,** *41*, 2265–2269.
8. Chua, C.-C.; Wangb, Y.-W.; Wangb, L., *Synth. Met.* **2005,** *153*, 321–324.
9. Holland, E. R.; Pomfret, S. J.; Adams, P. N.; Monkman, A. P., *J. Phys. Condens. Matter* **1996,** *8*, 2991-3002.

10. Moulder, J. F.; Stickle, W. F.; Sobol, P. E.; Bomben, K. D., *Handbook of X-ray Photoelectron Spectroscopy*. Physical Electronics Inc.: Eden Prairie, MN, 1995.

Chapter 8. Conclusions and Future Work

8.1. Conclusions

Self-assembled monolayers play an important role in surface modification. The preparation and modification of alkylsilane monolayers has been one of the most important parts of self-assembled monolayer research. From my work on silane deposition and patterning, I obtained the following conclusions.

Aminosilanes are among the most widely applied of the silanes because of their use as adhesion promoters and for biomolecule attachment. Most of the work on aminosilane deposition is from the solution phase, which easily leads to aggregates. Also, as mentioned in the introduction, silane monolayers are easily damaged in basic solutions. I investigated the chemical vapor deposition of three aminosilanes with different structures. I used three different aminosilanes to find an effective way to improve the stability of silane monolayers. This chemical vapor deposition method showed several advantages over liquid phase deposition, including the production of smooth surfaces, good film uniformity, lower quantities of reagents needed, and process robustness. These results also showed that alkyl groups on the silanes greatly affect the stability of the resulting monolayers. The two isopropyl groups of APDIPES stabilize the monolayer in basic solution so that only 6% of it is lost after 4 h in a pH 10 buffer. Comparatively, 31% of the APTES monolayer is lost under the same conditions. Moreover, storage of APDIPES functionalized surfaces in the atmosphere for 6 months does not change the monolayer thickness or surface hydrophobicity. These results indicate that APDIPES monolayers are more resistant to contamination and change over time than those prepared from APTES. XPS results show that APDIPES surfaces have somewhat less amine coverage than those made from

APTES. For many applications, stability is the most important property, and the minimal difference in amine coverage between the different aminosilanes should not have a significant effect on surface reactivity. For example, for biological applications, some particles are very large, such as proteins or cells. They do not require high densities of amine groups, but rather need good stability in basic solutions. In addition, as adhesion promoters of metals, a relatively small number of attachment points between a metal film and the monolayer may suffice for good adhesion. Therefore, APDIPES should be a better aminosilane under these conditions than APTES. Along with providing a better choice for possible aminosilane monolayers, this work also suggests that by selecting the proper precursor, one can design an amine monolayer to have specific properties.

Aside from the aminosilanes, 3-mercaptopropyltrimethoxysilane (MCPTMS) is another widely used silane for metal attachment on semiconductor surfaces and in optical devices. For these applications, uniformity is the major concern because aggregates or particles on a plate or mirror will greatly affect its function. In addition, many patterned or textured materials cannot be functionalized well with a uniform monolayer from solution because they cannot disperse deep into some patterns or features. Chemical vapor deposition of 3-mercaptopropyltrimethoxysilane eliminates these problems. There are few reports regarding this deposition. However, most of the vapor phase depositions in the literature use laboratory desiccators. Some aggregates are still found using this method. Using CVD in the YES 1224P, a commercial system, which employs high temperatures under vacuum conditions, no aggregates were present. Since this process is implemented with industrial equipment, this technique should be transferrable into an industrial setting. Film thicknesses of several Ångstroms guarantee that the film really is a monolayer, not a multilayer. Ultra thin monolayers will have the lowest possible effects on optical properties

without the loss of adhesion. The monolayer prepared with the CVD system onto which gold mirrors were deposited illustrated these points.

Most surface patterning techniques involve physical or chemical treatments, which might damage or contaminate monolayers. Here, I investigated three clean processes for making chemical or physical patterns. First, laser direct patterning was used as a very fast tool for changing surfaces physically and chemically at the same time. Characterization of alkenes deposited in this way showed the adsorption of carbon chains to surfaces. The halogens from haloalkanes were also observed. Modified areas have similar surface properties to monolayers deposited on hydrogen terminated silicon surfaces. This clean laser direct patterning method is relatively low cost with few requirements on deposition conditions. It only requires a common laser. Therefore, this method could be applied widely for semiconductor and biochip modification. Second, with a microlens array (MLA), we can pattern thousands of spots simultaneously onto silicon, or other, surfaces. For this process, a surface was first coated with a PEG silane monolayer so that it would resist protein adsorption. Subsequent patterning with an MLA ablated the PEG monolayer and created 10,000 spots/cm^2 for protein deposition. Compared to commercial protein chips that have 2,000-4,000 spots/cm^2, this technique could provide a higher throughput substrate for biochips. Results showed that the activity of proteins is maintained after deposition. Combined with microfludic deposition, I was able to deposit different proteins on different areas of the patterned substrate so that this technique could be used to potentially test thousands of proteins on one chip. I found another application for this MLA patterning: detection of iron atoms in ferritin. Because iron is located inside the protein shell of ferritin, it is hard to see directly. Using ToF-SIMS, we were able to detect iron in ferritin and confirm that it was located inside the protein, and not exterior to it. This capability is important

for current ferritin research in which new metals are placed inside the protein. Third, I explored another clean patterning technique: stencil lithography. MLA pattering has limitations for patterning shapes; MLA patterning cannot make high aspect ratio features. Stencil lithography offers a solution. Accordingly, I investigated physical patterning of silicon surfaces using stencil lithography. Results indicate that plasma activation through a stencil mask leads to patterns of silicon dioxide on silicon substrates. After wet etching, physical patterns can be obtained. This method offers a simple way to make both deep and shallow features on silicon. The advantages are obvious: this technique is simple and low-cost, no cleanroom is needed, and no expensive instrumentation is required.

Finally, I used polyelectrolyte coatings to stabilize conductive polymer fibers during their formation (wet spinning). Although this work differs from the monolayer depositions and patterning methods explored in this thesis, it is based on deposition of a monolayer or multilayer, which changes surface properties. Here a PSS coating was used as an electrostatic stabilizer for fibers spun into water. With a higher concentration of PSS in the coagulation bath, the length of the fiber becomes unlimited and surface morphology becomes smoother. At the same time, the conductivity of the fibers does not change substantially, meaning that the PSS coating does not penetrate into the fibers. This point was confirmed by XPS and SEM. A number of aqueous solutions were investigated and only polyanions in solution produced long, stable fibers. This indicates that electrostatic forces can play a major role in stabilizing these fibers. All previous methods used organic solvents as coagulation solvents to spin conductive polymers. Our work is the first to employ aqueous solutions to make conductive polymers without an obvious loss of material conductivity. This new method is also much more environmentally friendly and could, therefore, be industrially viable.

In summary, my work primarily explored various monolayer depositions and related pattering techniques. Results showed that chemical vapor deposition at high temperatures and under vacuum is an effective way to make high quality monolayers with amino and mercapto groups on surfaces. These monolayers present different surface properties and provide different levels of surface functionalization for adhesion to metals or for biological applications. The monolayer patterning work showed new functionalization tools for the preparation of high throughput substrates for protein chips. Stencil lithography allowed the creation of physical patterns up to micrometers in size. Electrostatic layer deposition produced conductive polymer fibers of unlimited length in a safer and more environmentally friendly way. This work points to improved surface modification choices for a variety of applications.

8.2. Future work

There are several important developments that might follow from my work. First, in the semiconductor industry, thick aminosilane layers have been considered as barrier films. However, these thicker aminosilane films would need to be at least tens of nanometers thick. And, of course, the film should also maintain its stability. Different, new multilayer methods could be considered as well for this purpose. Such thicker films might be deposited from solution, but such solution phase depositions generally require many washings to remove carryover between adsorptions. In addition, exposure to the laboratory environment after each deposition might damage the activity of groups for subsequent adsorptions. Therefore, solution phase deposition is not ideally suited for this task. Our CVD method shows significant advantages for multilayer deposition. For example, vacuum conditions guarantee that reactions occur under clean conditions so that reactions can occur with higher yields. A subsequent nitrogen purge then

removes carryover for the next reaction. High temperature and low pressure guarantee that chemicals can be vaporized completely to react quickly and efficiently with surfaces. The vacuum environment also allows vaporized chemicals to enter in and around small surface features to deposit uniform layers.

Two possible chemicals might be used for multilayer deposition by CVD: a diisocyanate and a triamine. The reaction process would be the following. First, an aminosilane would be deposited on a silicon surface to create a monolayer with active amine groups. After this, a diisocyanate would be deposited on this amino surface. Some of the isocyanate groups would bond with the surface amino groups to form strong urea linkages. Then, a triamine would be deposited. A fraction of the amino groups on the triamine would react with isocynate groups remaining on the second layer. The deposition of the diisocyanate and triamine would be repeated until films of desired thicknesses are obtained. This method should provide uniform and high quality films because each reaction should be self-terminating and there would be little or no carryover to form aggregates.

There might also be another method for preparing thick films with these two compounds. The two compounds could be injected simultaneously. Accordingly, diisocyanates and triamines could form a cross-linked polymer. This polymer could be deposited onto surfaces to prepare thick films. By controlling the amounts of these two chemicals as they are injected, films of different thickness could be achieved in single step depositions. This method would be much faster than the first method, but the first method may lead to higher quality films because it eliminates the possibility of aggregate formation.

Second, for surface and monolayer patterning, single point patterning with a laser or multpoint patterning with an MLA might not meet all industrial requirements. In addition, while

stencil lithography may employ masks with complicated patterns, it is expensive to design and create such masks. There may be another way to make complicated patterns on monolayer surfaces that has the advantages of both of these methods. This would require combining laser patterning and dynamic stencil lithography. A monolayer could be deposited first. It would then be covered with a mask containing one or more holes. The mask would be attached to a machine that can move the mask precisely. By allowing the laser to shine through the hole, only the area that the laser hits would be affected. It may even be possible to beat the diffraction limit of light in this manner. The remaining parts of the monolayer would be unaffected by this process. After a desired pattern is achieved, by moving the mask over the surface, the mask would be removed. The ablated regions should have chemistries characteristic of the bulk material in the substrate, and the unablated areas would be still covered by the monolayer. Each of the regions could then be modified with another chemical group. For example, an aminosilane layer could be deposited onto a silicon substrate first, after which it could be patterned. A pattern consisting of silicon dioxide lines on an amino surface would then be achieved. Next, one might deposit the MCPTMS silane onto these silicon dioxide lines so the line would be changed to contain active SH groups. The patterned substrate might then be immersed in a solution containing gold ions. Gold ions would deposit on the SH groups in the lines. Finally, a pattern with nanometer or perhaps even micrometer gold lines might be obtained. Alternatively, one might also fix the laser and mask, and move the substrate. Indeed, this seems like the simplest approach to this problem. Because the substrate could be moved significant distances with appropriate stages, this method could be used to create patterns on large samples.

With regard to applications of monolayer patterning, work on protein arrays should be continued so that each spot has better and more controlled affinity for specific proteins.

Currently, adsorption is nonspecific, employing silicon dioxide to capture proteins. In the future, amino or epoxy silanes should be deposited onto these silicon dioxide spots. Then, using ink-jet printing, small droplets of solutions containing biomolecules should be placed to more selectively bind these species onto active amino or epoxy groups. Another possibility is to bind more specific molecules, such as biotin, to the amino or epoxy silane monolayer in a spot. One could then use specific interactions between a protein and the species in the spots for more selective biomolecule adsorption. This process would create strong binding sites for specific proteins with a protein-resistant background.